This is to certify that the

dissertation entitled

THEORETICAL AND EXPERIMENTAL STUDIES OF SECOND ORDER BRAGG DIFFRACTION OF AN ACOUSTO-OPTIC INTERACTION

presented by

Bing-Chuan Hsu

has been accepted towards fulfillment of the requirements for

Ph.D. degree in Electrical Eng.

Major professor

Date 8/29/94

THEORETICAL AND EXPERIMENTAL STUDIES OF SECOND ORDER BRAGG DIFFRACTION OF AN ACOUSTO-OPTIC INTERACTION

By

Bing-Chuan Hsu

A DISSERTATION

Submitted to
Michigan State University
in partial fulfillment of the requirements
for the degree of

DOCTOR OF PHILOSOPHY

Department of Electrical Engineering

1994

ABSTRACT

THEORETICAL AND EXPERIMENTAL STUDIES OF SECOND ORDER BRAGG DIFFRACTION OF AN ACOUSTO-OPTIC INTERACTION

By

Bing-Chuan Hsu

Bragg diffraction of an acousto-optic interaction could be used to modulate light or to obtain information about a number of characteristics of an acoustic wave. In this thesis, the theoretical and experimental studies are focused on the second order Bragg diffraction. A partial wave approach is used to investigate the acousto-optic interaction of the Bragg diffraction.

The numerical simulations which provide a better understanding of the interaction of Bragg diffraction were carried out for various acoustic frequencies, acoustic pressures, and incident angle of the light beam. The criteria of the optimum system parameter sets which provide a maximum second order Bragg diffraction were established. In addition, experiments were designed and performed to verify the theory developed. These experiments include the intensity distribution of the diffraction mode with various acoustic amplitudes,

acoustic frequencies, and incident angles of the light. The experimental results agreed well with the theory developed.

Furthermore, acoustic Bragg imaging using first and second order modes were obtained. The image resolution of the first and second order modes were compared, and the images with various acoustic frequencies were analyzed. The image results indicate that the second order Bragg image provides better image resolution than that of the first order mode. It is also observed that the Bragg image resolution is directly proportional to the acoustic frequency and acoustic beam width. The results of this investigation could be applied to areas of nondestructive evaluation of materials as well as in noninvasive clinical diagnostics.

ACKNOWLEDGMENTS

The author is sincerely grateful to his academic advisor Dr. Bong Ho who provided much of the guidance, counsel and encouragement throughout the course of this research. Gratitude must also be expressed to Dr. Timothy A. Grotjohn, Dr. Robert O. Barr and Dr. Wayne W. Repko for their sincere interest and encouraging advice.

Furthermore, I would like to thank my parents, Mr. and Mrs. Hsing-Chang and Chueh Kim Hsu, and my wife Chun-Mei Kuo for their encouragement and support.

TABLE OF CONTENTS

LIST OF FIGURES

Chapter 1

Introduction

1.1 Introduction

The interaction of light and acoustic waves gives rise to light diffraction patterns whose intensity distribution in the various orders can be used to obtain information about a number of characteristics of the acoustic wave. The interaction displays different characteristics depending on the width of the interaction region, the light and acoustic wavelengths, and the amplitude of the acoustic wave. Roughly speaking, if the width and amplitude of the acoustic beam are sufficiently small, and the operating frequency is low, the diffraction phenomenon was explained by Raman and Nath and frequently referred to as Raman-Nath diffraction. Conversely, Bragg diffraction is observed if the width, frequency, and amplitude of the acoustic beam are sufficiently large.

In this thesis, effort has been focused in investigating the Bragg diffraction. The analysis of Bragg diffraction closely parallels the earlier treatment by Klein and Cook but is extended to the second order Bragg diffraction which includes a greater number of experimental conditions. Moreover, the procedure described in this thesis leads directly to equations which can be solved numerically. The interaction of light and acoustic waves is analyzed for various experimental conditions. The optical wave equation is solved by resolving the light traveling through the acoustic beam into a system of plane waves whose amplitudes are described by a set of difference-differential equations. These equations provide a large extent of physical insight into the nature of light diffraction by acoustic waves even though analytic solutions are obtained for several special cases.

Numerical results are obtained by converting the set of difference-differential equations into a set of difference equations which can be solved by computer simulation. For analyzing the acousto-optic system in various experimental conditions, it will be shown that the solution of these difference-differential equations can depend only on a small number of dimensionless combinations of experimental parameters. Since the actual choice of these parameters is somewhat arbitrary, the equations are written in terms of parameters corresponding most directly with typical experimental variables. It will be shown that the intensities of the second order Bragg diffraction can be greatly enhanced if certain system parameter sets are chosen, and that the second order Bragg diffraction gives a finer angular resolution than the first order interaction.

The criteria of the Bragg diffraction and optimum second order Bragg diffraction are also investigated. The results show that even if the criteria for the Bragg diffraction are met, the mode intensities in the second order are still comparatively weak. Therefore, the requirement for optimum second order Bragg diffraction becomes a critical issue. In addition, the criteria indicate that the second order Bragg diffraction requires only half the acoustic frequency of the first order to provide the same degree of sharpness of diffraction (i.e. light intensity versus incident angle) with first order. This makes the second order Bragg diffraction much more feasible in practical acousto-optic systems.

The acoustic waves can modulate the amplitude and phase of a coherent light beam. Furthermore, it can deflect, focus, and even shift the frequency of the light beam. As a result, the light beam can reconstruct an acoustic imaging or provide detailed information on the thermal vibration in solids and liquids. Diffraction of light waves by acoustic waves takes several different forms, depending on their wavelengths and the dimensions of the interaction region. In the industry, acousto-optic modulation has been widely used in laser ranging, optical signal-processing systems, optical communication, high-speed optical deflectors, acoustic traveling-wave lens devices, Q switching, amplitude and frequency modulation, and mode-locking. Acousto-optic modulators can in general be used for similar applications to electro-optic modulators, though they are not so fast as electro-optic modulators. On the other hand, because the electro-optic effect usually requires voltages in the kilovolt range, the drive circuitry for modulators based on this effect is much more expensive than for acousto-optic modulators, which operate at low voltages. The advantage by using the second order Bragg diffraction in acousto-optic system is that this system provides not only larger deflection angle and frequency shift in light beam, but high efficiency and double resolution in beam deflector and imaging reconstruction. In recent years, acoustical imaging has been widely applied in the areas of clinical diagnostics and non-destruction evaluation of materials. One major drawback of this type of imaging system is that it requires either a mechanical or electronic scanning mechanism. Such a system involves complex design and hardware implementation. As a result, the system becomes very bulky and costly. Acousto-optical imaging could add some attractive features to the conventional acoustic imaging techniques. In view of the Bragg diffraction, we see that there is a possibility of providing a real-time imaging system without using a mechanical or electronic array scanner. In addition, high power solid-state laser sources have become available in recent years due to the advancement of laser technology. By using such diodes as laser beam sources, the proposed method of acousto-optical interaction could lead to a way of providing the possibility of low-cost, portable and real-time imaging system.

1.2 Outline of the Thesis

Chapter 2 provides theoretical background to the interaction of the light and acoustic wave. The problem of light diffraction by an acoustic field will be treated by solving the optical wave equation which resolves the light into a system of plane waves. The amplitudes of these waves passing through the acoustic field are given by a set of difference-differential equations. The analytic solutions of the difference-differential equation are found for cases when the frequencies of the acoustic wave is either low or very high. The reason is that for low frequencies the acoustic wave produces an optical phase grating effect, and at high frequencies light diffraction occurs when the light is incident on the acoustic waves at angles associated with Bragg diffraction. With a double incident Bragg angle between the light and acoustic wave, a closed-form expression of the second order Bragg diffraction is derived by applying the Laplace transform technique to the difference equations. Several experimental parameters which lead to a deeper understanding of the Bragg diffraction are defined, and those parameters correspond most directly to the practical experimental variables.

The numerical analysis in acousto-optic system is carried out in chapter 3. Before the experimental setup are designed to verify the theory developed, numerical simulation can readily be implemented to see the mode amplitude variations for a given set of system parameters (Q, V, α). The advance analysis for the second order Bragg diffraction is analyzed in details. After going through the general analysis of acousto-optic interaction, it appears that we can adjust the system parameters to obtain a significant strength of the second order Bragg diffraction. Furthermore, it appears that the second order Bragg diffraction provides a sharper resolution than the first order.

Chapter 4 studies the criteria for Bragg diffraction effects in the acousto-optic system. In this chapter, two types of criteria are discussed. One criterion analyzes the minimum requirement for satisfying the Bragg diffraction. Another criterion relates to the conditions for maximum second order Bragg diffraction. The result indicates that Bragg diffraction is to be associated not only with high acoustic frequency F (unit in MHz) but also with wide widths L of the acoustic beam. More precisely, it depends strongly on the values of "LF^2 ". The sharpness of the Bragg diffraction will increase with increasing the LF^2 values. However, in order to maximize the second order Bragg diffraction other system parameters such as acoustic pressure, dielectric constant of the medium, temperature, ... etc. have to be considered as well. Trade off among parameters have to be made for optimum operation.

In chapter 5, the experimental system setup and the measurement procedures are described. The experimental results for verifying the Bragg diffraction are presented. The experimental verifications include the intensity distribution of the diffraction mode with various acoustic amplitude, acoustic frequency and incident angle of the light beam. The results show that when the incident angle equals to twice of the Bragg angle, the second order diffraction can be driven to its peak intensity under a certain system parameter sets. Comparing the angular sensitivity of the diffraction modes, the second order diffraction provides a sharper angular resolution than first order mode. In general, the experimental results agreed with the theory quantitatively.

An acoustic imaging application by using Bragg diffraction has been mentioned in chapter 6. A brief description of Bragg imaging theory will be given here. The imaging system setup and the measurement procedures will be described in detail. Imaging resolution using different acoustic frequencies and beam width will be examined. The experimental result shows that the final Bragg image resolution is directly proportional to the acoustic frequency. In addition, the imaging resolution for the first and second order are compared, and the result indicates that the second Bragg diffraction imaging provides a sharper image resolution than the first order. This could be very useful in medical diagnostic applications. Since biological materials have higher attenuation for higher acoustic frequency, there will be a trade off between depth of penetration and image resolution. However, from the results of this research we noticed that one can preserve image quantity by using second order diffraction.

Chapter 2

THEORY OF LIGHT DIFFRACTION BY SOUND WAVES

2.1 Introduction

In this chapter, a very brief historical survey of the field of light diffraction by sound waves will be given. Then, the acousto-optical interaction will be analyzed by the partial wave approach. The second order Bragg diffraction will be derived in detail and solved for the special case that the incident angle of the light approaches two times of the Bragg angle. Several experimental parameters which lead to a deeper understanding of the Bragg diffraction are defined, and those parameters correspond most directly to the practical experimental variables.

2.2 Review of Light Diffraction by Sound Wave

Diffraction of light by high-frequency sound waves, often called Brillouin Scattering,[1] was first observed by Debye and Sears[2] in the United States and by Lucas and Biquard[3] in France. Brillouin's original theory[1] predicted a phenomenon closely analogous to X-ray diffraction in crystals: plane waves of light striking the acoustically induced planes of compression and rarefaction at a certain critical angle would be partially reflected. There would be only one critical angle(i.e. Bragg angle), since the spatial structure of acoustically induced density variations is essentially sinusoidal and hence contains no space harmonic components. Brillouin predicted that the reflected light would be Doppler shifted by an amount equal to the sound frequency because the reflecting layers themselves move with sound velocity.

A fundamental theory for light distribution in the diffraction orders was first proposed by Raman and Nath[4]-[9]. They assumed that the sound column would act essentially as a two-dimensional phase grating which was not too thick in the direction of light propagation. Their theory correctly predicted the Bessel function dependence of the intensity of the various orders as a function of sound pressure when the light beam is perpendicular to the sound column. For the case of oblique incidence, it was treated later[5]. The frequency change in the diffracted light was also investigated[6]. Next[7], they departed from the simple phase grating model and formulated a wave equation of the incident light in the acoustically perturbed medium. Then they went on to obtain an infinite set of coupled differential equations which described the spatial behavior of the various modes traversing the sound beam. Finally, they extended their theory to arbitral angles of incidence of the light[8].

Although the fundamental theory of the acousto-optics diffraction was derived by Raman and Nath, the results of that theory are not in a form which can provide a easy way for the numerical evaluation of experimental situations. In 1969, Klien and Cook[10][11] developed an unified approach for acousto-optical diffraction. In their papers, they extended to include a greater number of experimental conditions in the infinite set of differential equations, and those equations can be solved numerically. The results by using those equations confirmed with those given by Parisean.[12][13] However, their discussion was restricted to only first order Bragg diffraction with different acoustic wave frequencies at various incidence angles. There were others[14]-[17] who discussed the first-order Bragg diffraction from alternate approaches and applications but the second order Bragg diffraction has been generally ignored.

In 1981, Poon and Korpel[18] give a brief discussion on the efficiency of second order Bragg diffraction. A similar result has been given by Alferness[19] in the study of holograms. These results described the interaction when the incident angle is precisely at twice the Bragg angle. The physical setups for these two separate investigations are quite different in nature. Consequently, there were some discrepancies from their analyses. In this research, partial wave approach is used to analyze the acousto-optical interaction. The condition of the interaction in terms of system parameters such as incident angle, acoustic and laser frequencies, and the size of the interaction region are investigated.

2.3 Theory of Light Diffraction by Sound Wave

The interaction between the acoustic wave and the light can be treated by resolving the diffracted light into a series of plane waves. Consider a monochromatic light beam incident at an angle θ upon an acoustic beam of width L as shows in Fig. 2.1.

The electric field intensity E is being polarized along the y-direction. For simplicity, let us assume the medium is non-magnetic, non-conducting and source free. The scattered field is described by the following set of Maxwell's equations.

$$\nabla \cdot \vec{D} = \rho \tag{2-1}$$

$$\nabla \times \vec{E} = -\mu_0 \frac{\partial}{\partial t} \vec{H} \tag{2-2}$$

$$\nabla \times \vec{H} = \frac{\partial}{\partial t} \vec{D} \tag{2-3}$$

$$\nabla \cdot \vec{H} = 0 \tag{2-4}$$

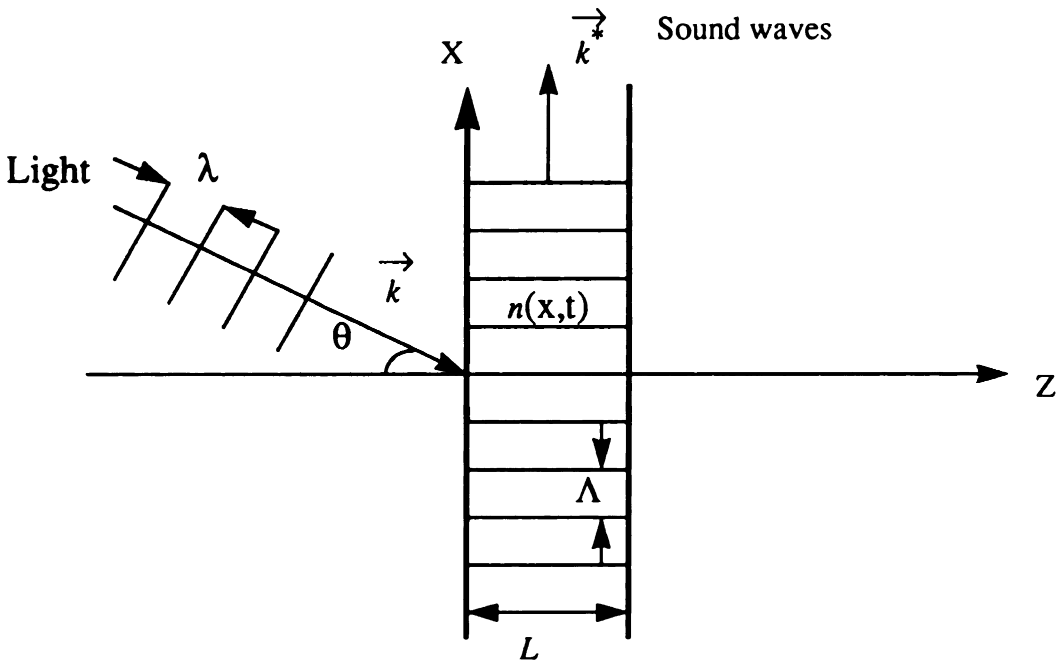

Figure 2.1 Diagram of the acoustic diffraction grating.

where $D = \varepsilon E_y$, and the permittivity ε can be put in terms of the refraction index n as $\varepsilon = n^2 \varepsilon_0$.

For source free $\rho = 0$, Eq. (2-1) becomes

$$\nabla \cdot \left(n^2 \varepsilon_0 E_y\right) = 0$$

$$n^2 \nabla \cdot E_y + \nabla n^2 \cdot E_y = 0 \tag{2-5}$$

where $\nabla n^2 = 2n\nabla n = \hat{x} 2n \frac{dn}{dx}$ (n is only function of x, see Fig. 2.1)

Since the electric field is uniform in the Y direction and $\nabla n^2 = 0$ in Y direction, Eq. (2-5) becomes $\nabla \cdot \vec{E} = 0$. To obtain the scattered E field, we proceed to take curl of Eq. (2-2)

$$\nabla \times \nabla \times \vec{E} = -\mu_0 \frac{\partial}{\partial t} \nabla \times \vec{H} \tag{2-6}$$

$$\nabla (\nabla \cdot \vec{E}) - \nabla^2 \vec{E} = -\mu_0 \frac{\partial}{\partial t}\left[\frac{\partial}{\partial t} n^2 \varepsilon_0 \vec{E}_y\right] \tag{2-7}$$

$$\nabla (\nabla \cdot \vec{E}) - \nabla^2 \vec{E} = -\mu_0 \varepsilon_0 \left[n^2 \frac{\partial^2 \vec{E}_y}{\partial t^2} + 2\left(\frac{\partial \vec{E}_y}{\partial t} \cdot \frac{\partial n^2}{\partial t}\right) + \vec{E}_y \frac{\partial^2 n^2}{\partial t^2} \right] \tag{2-8}$$

Since the radian frequency of acoustic wave is small compared with the radian frequency of the light wave, the last two terms in Eq. (2-8) can be ignored. Then, Eq. (2-8) becomes

$$\nabla (\nabla \cdot \vec{E}) - \nabla^2 \vec{E} = -\mu_0 \varepsilon_0 n^2 \frac{\partial^2 \vec{E}_y}{\partial t^2} \tag{2-9}$$

Because $\nabla \cdot \vec{E} = 0$, the optical wave equation which describes the propagation of the electric field intensity can be written as

$$\nabla^2 \vec{E}(x, z, t) = \left[\frac{n}{C}\right]^2 \frac{\partial}{\partial t^2} \vec{E}(x, z, t) \tag{2-10}$$

where $C = \dfrac{1}{\sqrt{\mu_0 \varepsilon_0}}$.

2.3.1 Solution of the Optical Wave Equation

The acoustic field is assumed to be composed of plane waves. All frequency components of the sound field are assumed to be measurable. Further, the medium is assumed to be nondispersive and nonabsorbable so that the frequency components retain a constant phase relationship and remain constant in magnitude. It is also assumed that the medium is not birefringent, i.e. the refractive index distribution is independent of the polarization of the incident light beam. For acoustic waves with arbitrary periodic waveform, the refractive index in the region of the sound field ($0 < z < L$) can be expressed as

$$n(x, t) = n_0 + \sum_{j=1}^{\infty} n_j \sin\left[j(\omega^* t - k^* x) + \delta_j\right]$$

where ω^* and k^* are the radian frequency and wave number of the sound wave respectively, n_j is the amplitude of the jth Fourier component and δ_j is its relative phase. The coefficients n_j are assumed to be directly proportional to the harmonic coefficients describing the density change and consequently may be considered to be directly proportional to the various harmonic coefficients of the acoustic pressure. For the $n^2(x,t)$, we have

$$n^2(x, t) = n_0^2 + 2n_0\left(\sum_{j=1}^{\infty} n_j \sin\left[j(\omega^* t - k^* x) + \delta_j\right]\right) + \text{higher order terms}$$

The quantity of the higher order terms can be neglected because compared to the magnitude of the n_0 terms the perturbation of n is small. Then n^2 becomes

$$n^2(x,t) = n_0^2 + 2n_0 \sum_{j=1}^{\infty} n_j \sin\left[j(\omega^* t - k^* x) + \delta_j\right] \tag{2-11}$$

In the region of the sound field the electric field intensity of the light beam can be expressed as

$$E = A(x,z,t)\, e^{j\left(\omega t - n_0 \vec{k} \cdot \vec{r}\right)} \tag{2-12}$$

Since $A(x,z,t)$ is a periodic function with the variable k^*x, it can be expended into a complex Fourier series as follows

$$A(x,z,t) = \sum_{m=-\infty}^{\infty} \phi_m(z)\, e^{im(\omega^* t - k^* x)}$$

Then, the electric field intensity becomes

$$E(r,t) = e^{i\omega t} \sum_{m=-\infty}^{\infty} \phi_m(z)\, e^{i(m\omega^* t - \vec{k}_m \cdot \vec{r})} \tag{2-13}$$

where $\vec{k}_m = n_0 \vec{k} + m\vec{k}^*$

$\vec{r} = (x\hat{x} + y\hat{y} + z\hat{z})$

In the spatial coordinates, the phase term can be expanded as

$$\vec{k}_r \cdot \vec{r} = n_0 k x \sin\theta + n_0 k z \cos\theta + mk^* x \ . \tag{2-14}$$

The vectorial relationship between the propagation vectors is shown in Fig. 2.2. From Fig. 2.2, we have

$$\frac{n_0 k \sin\theta - mk^*}{n_0 k \cos\theta} = \tan(\theta - \beta_m) \ . \tag{2-15}$$

Since both θ and β_m are very small quantities Eq. (2-15) can be approximated as

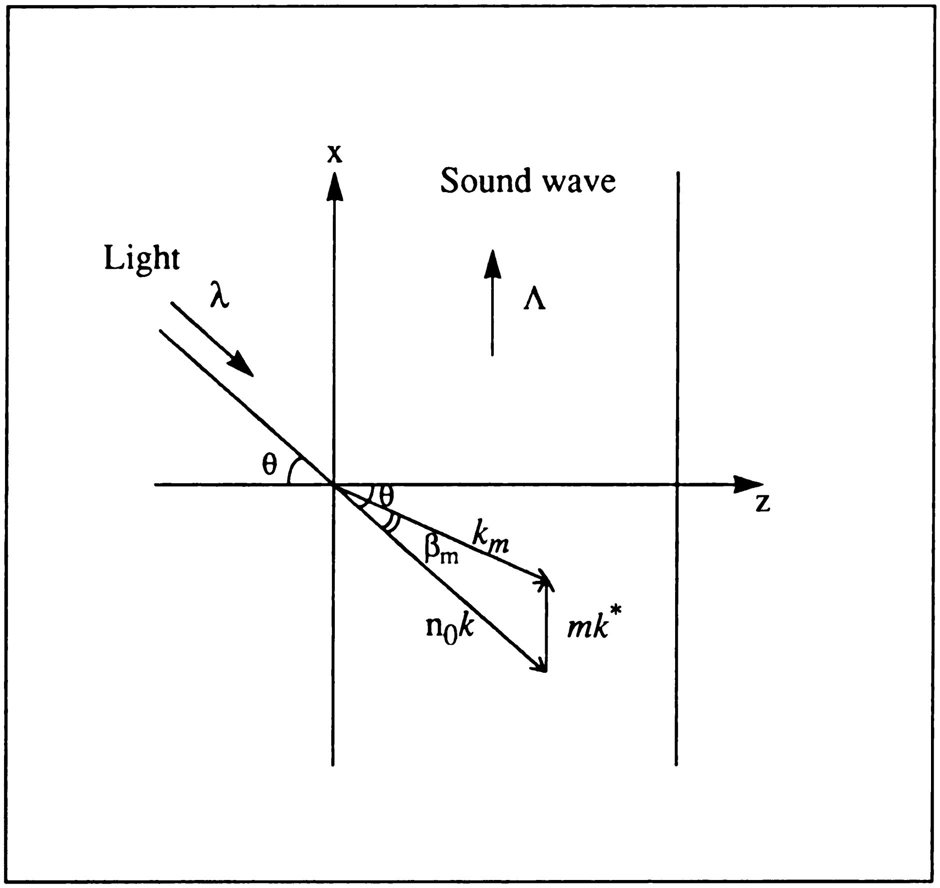

Figure 2.2 Orientation of the partial wave vector.

$$\theta - \frac{mk^*}{n_0 k} \approx \theta - \beta_m \ .$$

This implies that

$$\beta_m \approx \frac{mk^*}{n_0 k} \qquad (2\text{-}16)$$

where β_m relate to the directions of the wave vectors. These directions are measured with respect to the direction of the incident light beam. Notice that Eq. (2-16) resembles the usual grating equation. As a matter of fact, one can consider the acoustic wave function constitutes a sinusoidal amplitude grating[20] where the grating spacing is replaced by the wavelength of the acoustic wave. Eq. (2-13) is thus equivalent to assuming that within the acoustic field the light distribution can be expanded into a series of partial waves labeled by *m* which propagate in directions described by the usual grating, Eq. (2-16), and which have amplitudes labeled by ϕ_m. Our problem is to determine the values of the ϕ_m for various values of the experimental parameters. Since the electric field intensity *E* is a function of *x*, *z*, and *t*, Eq. (2-10) can then be reduced to

$$\frac{\partial^2 E}{\partial x^2} + \frac{\partial^2 E}{\partial z^2} = \left[\frac{n}{C}\right]^2 \frac{\partial^2 E}{\partial t^2} \qquad (2\text{-}17)$$

Substituting Eq. (2-13) into Eq. (2-17), we have

$$\frac{\partial^2 E}{\partial x^2} = e^{i\omega t} \sum_{m=-\infty}^{\infty} -\phi_m(z)\left(n_0 k \sin\theta + mk^*\right)^2 e^{i(m\omega^* t - \vec{k}_m \cdot \vec{r})}$$

$$\frac{\partial^2 E}{\partial z^2} = e^{i\omega t} \sum_{m=-\infty}^{\infty} \left[e^{i(m\omega^* t - \vec{k}_m \cdot \vec{r})} \frac{\partial^2}{\partial z^2}\phi_m(z) + 2(-in_0 k\cos\theta)\, e^{i(m\omega^* t - \vec{k}_m \cdot \vec{r})} \frac{\partial}{\partial z}\phi_m(z) - (n_0 k \cos\theta)^2 e^{i(m\omega^* t - \vec{k}_m \cdot \vec{r})} \phi_m(z) \right] . \qquad (2\text{-}18)$$

The LHS of Eq. (2-17) is then

$$\frac{\partial^2 E}{\partial x^2}+\frac{\partial^2 E}{\partial z^2} = e^{i\omega t}\sum_{m=-\infty}^{\infty} e^{i(m\omega^* t - \vec{k}_m\cdot\vec{r})}\left[\frac{\partial^2\phi_m}{\partial z^2} - (2in_0k\cos\theta)\frac{\partial\phi_m}{\partial z} - \left(\left(n_0k\sin\theta + mk^*\right)^2 + (n_0k\cos\theta)^2\right)\phi_m\right] \qquad (2\text{-}19)$$

In order to simplify the expression in the following development, let us define the function $f(x, z, t)$ as follows,

$$E(x,z,t) = e^{i\omega t}\sum_{m=-\infty}^{\infty}\phi_m e^{i(m\omega^* t - \vec{k}_m\cdot\vec{r})} = e^{i\omega t} f(x,z,t) \ .$$

The RHS of Eq. (2-17) becomes

$$\begin{aligned}\frac{n^2}{C^2}\frac{\partial^2 E}{\partial t^2} &= \left(\frac{n}{C}\right)^2\frac{\partial}{\partial t}\left(i\omega e^{i\omega t} f + e^{i\omega t}\frac{\partial f}{\partial t}\right) \\ &= n^2\left(-k^2 f + 2i\frac{k}{C}\frac{\partial f}{\partial t} + \frac{1}{C^2}\frac{\partial^2 f}{\partial t^2}\right)e^{i\omega t}\end{aligned} \qquad (2\text{-}20)$$

where $k = \frac{\omega}{C}$.

The last two terms in Eq. (2-20) can be neglected, since the time variation of f is of the order of magnitude of ω^*(variation in the refraction index), that is

$$\left|\frac{2k}{C}\frac{\partial f}{\partial t}\right| \ll \left|k^2 f\right|$$

and

$$\left|\frac{1}{C^2}\frac{\partial^2 f}{\partial t^2}\right| \ll \left|k^2 f\right| \ .$$

The RHS of Eq. (2-17) becomes

$$\frac{n^2}{C^2}\frac{\partial^2 E}{\partial t^2} = -n^2 k^2 e^{i\omega t} \sum_{m=-\infty}^{\infty} \phi_m e^{i(m\omega^* t - \vec{k}_m \cdot \vec{r})} \quad . \tag{2-21}$$

Substituting the expressions of n^2 and $\vec{k}_m \cdot \vec{r}$ given by Eq. (2-11) and Eq. (2-14) respectively into Eq. (2-21) and then comparing with Eq. (2-19), we obtain

$$\begin{aligned} &\frac{\partial^2 \phi_m}{\partial z^2} - (2in_0 k\cos\theta)\frac{\partial \phi_m}{\partial z} + \left[\left(n_0 k\sin\theta + mk^*\right)^2 + (n_0 k\cos\theta)^2\right]\phi_m \\ &\quad = -n_0^2 k^2 \phi_m + in_0 k^2 \sum_{j=1}^{\infty} n_j\left(\phi_{m-j} e^{i\delta_j} - \phi_{m+j} e^{-i\delta_j}\right) \quad . \end{aligned} \tag{2-22}$$

Since $\phi_m(z)$ is a slow varying function of z, then

$$\left| n_0 k \frac{\partial \phi_m}{\partial z} \right| \gg \left| \frac{\partial^2 \phi_m}{\partial z^2} \right| \quad .$$

We have then

$$\begin{aligned} &2n_0 k\cos\theta \frac{\partial \phi_m}{\partial z} + i\left[\left(n_0 k\sin\theta + mk^*\right)^2 + (n_0 k\cos\theta)^2\right]\phi_m \\ &\quad = (-i)\, n_0^2 k^2 \phi_m - n_0 k^2 \sum_{j=1}^{\infty} n_j\left(\phi_{m-j} e^{i\delta_j} - \phi_{m+j} e^{-i\delta_j}\right) \quad . \end{aligned}$$

Rearranging, we have

$$\begin{aligned} &\frac{\partial \phi_m}{\partial z} + \sum_{j=1}^{\infty} \frac{kn_j}{2\cos\theta}\left[\phi_{m-j} e^{i\delta_j} - \phi_{m+j} e^{-i\delta_j}\right] \\ &\quad = \frac{i\phi_m}{2n_0 k\cos\theta}\left[\left(n_0 k\sin\theta + mk^*\right)^2 + (n_0 k\cos\theta)^2 - n_0^2 k^2\right] \end{aligned} \tag{2-23}$$

RHS of Eq.(23)

$$= \frac{i\phi_m}{2n_0 k\cos\theta}\left[(mk^*)^2 + 2n_0 mkk^*\sin\theta + n_0^2k^2\left(\sin^2\theta + \cos^2\theta\right) - n_0^2k^2\right]$$

$$= \frac{ik^{*2}}{2n_0 k\cos\theta}\left[m^2 + 2mn_0\frac{k}{k^*}\sin\theta\right]\phi_m$$

$$= \frac{ik^{*2}Lm}{2Ln_0 k\cos\theta}\left[m + 2n_0\frac{k}{k^*}\sin\theta\right]\phi_m$$

Conforming with the parameters used by Klein and Cook, let's define the following quantities,

$$Q = \frac{k^{*2}L}{n_0 k\cos\theta}$$

$$\alpha = -n_0\frac{k}{k^*}\sin\theta$$

$$V_i = \frac{kn_jL}{\cos\theta}$$

where L is the width of the sound beam.

Since the incident angle θ is less than one degree, we can rewrite Q, V, and α in the following simplified forms

$$Q = \frac{k^{*2}L}{n_0 k} \tag{2-24}$$

$$\alpha = -n_0\frac{k}{k^*}\sin\theta \tag{2-25}$$

$$V_i = kn_jL\ . \tag{2-26}$$

In terms of these parameters, Eq. (2-23) becomes

$$\frac{\partial\phi_m}{\partial z} + \frac{1}{2L}\sum_{j=1}^{\infty} V_j\left[\phi_{m-j}e^{i\delta_j} - \phi_{m+j}e^{-i\delta_j}\right] = \frac{imQ}{2L}(m-2\alpha)\phi_m\ . \tag{2-27}$$

For a pure sinusoidal sound field, $n(x, t) = n_0 + n_1(\omega^* t - k^* x)$. In other words, under such excitation we have $j = 1$. In order to notation the subscript of V will be dropped in the subsequent development. Finally we have

$$\frac{d\phi_m}{dz} + \frac{V}{2L}(\phi_{m-1} - \phi_{m+1}) = \frac{imQ}{2L}(m - 2\alpha)\phi_m \tag{2-28}$$

Equation (2-28) is similar to the equation developed by Roman and Nath[4], and by Klein and Cook who developed a unified theory which is valid over a wide range of experimental conditions[11]. The parameters in Eq. (2-28) such as the acoustical pressure, the angle of incidence of the light on the sound field, and the sound wavelengths can easily be varied in a given experimental system. From an analytical viewpoint, we would like to use two dimensionless variables which are simply related to the two easily varied quantities. A third parameters is needed to complete the description of the interaction. For convenience, this third parameter should be independent of the acoustic pressure and angle of incidence. The parameters Q, V, and α used here satisfy the above conditions while other common choices of dimensionless parameters do not. It should be emphasized that experimental systems characterized by the same set of values of Q, V, and α are equivalent though k, k^*, n_1, n_0, and L may differ. Choices of parameters which are combinations of Q, V, and α have sometimes been taken for mathematical convenience. Also before experimental setups are designed to verify the theory developed, numerical simulation can easy be performed by using parameters (Q,V,α) to see the mode amplitude variations.

2.3.2 Characterizations of Acousto-Optics System

Equation (2-27) shows that the quantity Q is a measure of the differences in phase of the various partial wave due to their different directions of propagation. When the phase difference in these waves becomes large (say $Q > 1$), the diffracted light tends to remain in the lower orders. In fact, for large Q the diffraction is not found to occur at normal incidence. This phenomenon can be explained using elementary results of coupled mode theory[21]. A coupled mode interpretation of difference-differential equations in the Eq. (2-27) identifies the variable V_j as coupling coefficient between the light waves. The coupling coefficient V_j couples waves which differ in order number by j. The coefficient V_1 couples adjacent waves, V_2 couples alternate waves, etc. The amount of energy transfer between the waves depends upon the coupling coefficient and the degree of synchronization of the waves. In Eq. (2-27), the term $mQ(m\text{-}2\alpha)$ indicates the degree of synchronous, i.e. the phase difference between the waves is nearly constant, energy transfer between the various orders readily occurs. On the other hand, if the waves are highly nonsynchronous, the energy transfer is extremely weak.

For analysis of oblique incidence, using $\alpha = -n_0 \frac{k}{k^*} \sin\theta$ and $Q = \frac{k^{*2} L}{n_0 k \cos\theta}$, Eq. (2-28) can be rewritten as

$$\frac{d\phi_m}{dz} + \frac{V}{2L}(\phi_{m-1} - \phi_{m+1}) = i\left(\frac{m^2 Q}{2L} + mk^* \tan\theta\right)\phi_m \qquad (2\text{-}29)$$

For $Q \ll 1$ Eq. (2-29) becomes

$$\frac{d\phi_m}{dz} + \frac{V}{2L}(\phi_{m-1} - \phi_{m+1}) = imk^* \tan\theta\phi_m \ . \qquad (2\text{-}30)$$

Let $\phi_m = \psi_m e^{imk^* z\tan\theta}$, we have the difference-differential equation as follows

$$\frac{d\psi_m}{dz} + \frac{V}{2L}\left(\psi_{m-1} e^{-ik^* z\tan\theta} - \psi_{m+1} e^{ik^* z\tan\theta}\right) = 0 \qquad (2\text{-}31)$$

When the light beam is at oblique incidence, the phase term, $k^* z\tan\theta$, arises due to the fact that the light progresses through the acoustical field it encounters a continuous change of phase of the acoustical waves. If the light travels in such a manner that it enters and leaves the sound field at points having a phase change of $2n\pi$ (n being an integer). Consequently, the diffraction effects are completely cancelled. Therefore, if the phase term $k^*L\tan\theta$ equal to $2n\pi$ the diffraction effects will disappear at the angle of

$$\tan\theta = \frac{2n\pi}{k^*L} = \frac{n\Lambda}{L}.$$

With $Q << 1$ the solution of Eq.(29) at $z = L$ is

$$\phi_m = J_m\left[\frac{2V}{k^*L\tan\theta}\left(\sin\frac{k^*L\tan\theta}{2}\right)\right]e^{i\frac{mk^*L}{2}\tan\theta} \quad . \tag{2-32}$$

The intensity of the mth order can be written as

$$I_m = J_m^2\left[V\frac{\sin\frac{Q\alpha}{2}}{\frac{Q\alpha}{2}}\right] \quad . \tag{2-33}$$

Equation (2-33) shows that when Q is very small the intensity distribution follows the manner of a sinc function. The diffraction pattern is symmetric for all angles.

For $Q >> 1$ the diffraction effects are found to be symmetric for oblique incidence. As a matter of fact, the diffraction occurs predominantly around the angles associated with Bragg diffraction given by[1][4]

$$\sin\theta = \frac{m\lambda}{2\Lambda n_0} \quad . \tag{2-34}$$

This phenomenon can be explained by the use of coupled mode theory. From Eq.(29) the phase term is found to be $\frac{m^2Q}{2L} + mk^*\tan\theta$. The phase term will be vanished when $\frac{m^2Q}{2L} + mk^*\tan\theta = 0$. Hence we have

$$\tan\theta = \frac{-mQ}{2k^*L} . \tag{2-35}$$

Equation (2-35) can be reduced to the form of Eq.(34). The energy transfer between the coupled modes is most effective between orders which have the same phase term. Therefore, most diffracted light will lie into the order which satisfies the condition given by Eq.(35). From the manner in which the parameter α is defined Bragg diffraction occurs when $\alpha = \frac{n}{2}$, and the light is diffracted predominantly into the nth order. The sharpness of the light intensity distribution in the vicinity of the Bragg angles as a function of angle depends on the Q value. This will be shown by numerical analysis in next chapter.

2.4 Diffraction in the Bragg's Region

Although the Q is related to k^*, L, n_0, and k, however, in a typical experimental setup, the n_0 and k are fixed. The width and the frequency of the sound beam are the major factors to vary the Q value. Experiments for the low frequency and the shorter width of sound beam are said to be in the Debye-Sears[2] or Raman-Nath[4] region ($Q << 1$). The solution for the Roman-Nath interaction has well been studied[2][4][10][11][16]. In this dissertation, we will concentrate on the solution of the second order Bragg Diffraction. When the acoustic beam is wide enough and acoustic wavelength is short, the interaction can be observed in the Bragg region. The diffracted light reaches a maximum when the incident acoustic wave is at a particular angle. Figure 2.3 depicts the geometrical relationship between the light and acoustic beams. Equation (2-36) states the constructive interference condition for the interaction.

$$m\lambda_n = 2l - l' \tag{2-36}$$

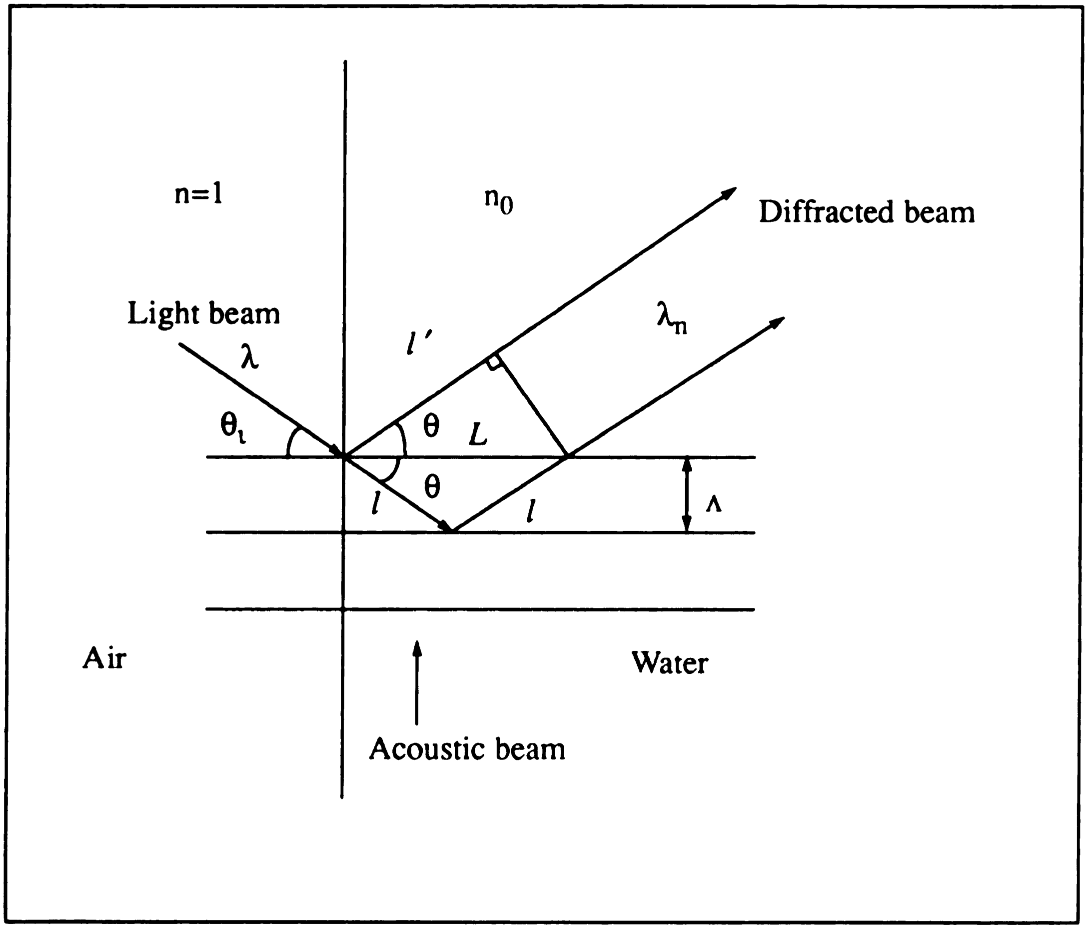

Figure 2.3 Diagram for diffraction path.

where $\lambda_n = \lambda / n_0$ is the wavelength of the light beam inside the interaction region. The λ is the wavelength of the incident light. Under constructive interference, the acoustic wavelength Λ, length of interaction L and optical path l' are related to the optical path l and incident angle θ in the following way,

$$\begin{cases} \Lambda = l\sin\theta \\ L = 2l\cos\theta \\ l' = L\cos\theta = 2l\cos^2\theta \end{cases} \tag{2-37}$$

Substituting these relations into Eq. (2-36), we have

$$m\lambda_n = 2\Lambda\sin\theta \tag{2-38}$$

or

$$m\lambda = 2\Lambda n_0 \sin\theta \tag{2-39}$$

Using Snell's law, $n\sin\theta_i = n_0\sin\theta$, we have $\sin\theta_i = n_0\sin\theta$ for n =1 in air, and Eq. (2-39) becomes

$$\sin\theta_i = \frac{m\lambda}{2\Lambda} \tag{2-40}$$

Equation (2-40) describes the Bragg relation for constructive interference at some specific incident angles.

2.4.1 First order Bragg Diffraction

For the first order mode m=1, Eq. (2-40) becomes

$$\sin\theta_i = \frac{\lambda}{2\Lambda} \tag{2-41}$$

Since θ_i has a value of less then one degree, one can approximate $\sin\theta_i \cong \theta_i$. The angle becomes,

$$\theta_B = \frac{\lambda}{2\Lambda} \tag{2-42}$$

where θ_B is the well-known Bragg angle[1]. When the incident angle is at the Bragg angle, the diffraction mode intensity is at its maximum.

In the case of m = 1, Eq. (2-28) becomes

$$\frac{d\phi_0}{dz} + \frac{V}{2L}(\phi_{-1} - \phi_1) = 0 \tag{2-43}$$

$$\frac{d\phi_1}{dz} + \frac{V}{2L}(\phi_0 - \phi_2) = i\frac{Q}{2L}(1 - 2\alpha)\phi_1 \tag{2-44}$$

These equations describe the possible coupling between various modes. In Eq. (2-43) the zeroth mode is coupled to the ± 1 modes. The quantity $\frac{V}{2L}$ relates to the coupling coefficient. Equation (2-44) describes the coupling between the first order mode and its adjacent mode. In order for modes to be coupled, the imaginary term in Eq. (2-44) should be vanished. The condition for the first order mode to be coupled is when $\alpha = 0.5$. Under this condition, Eq. (2-25) becomes

$$n_0 \sin\theta = \frac{1}{2}\frac{k^*}{k} = \frac{\lambda}{2\Lambda}$$

Since $\sin\theta_i = n_0 \sin\theta$, the incident angle before the light passes through the sound beam will be $\sin\theta_i \cong \theta_i = \frac{\lambda}{2\Lambda}$. Therefore, for $\alpha = 0.5$, the incident angle is equal to the Bragg angle, and this result confirms the geometrical relation in Fig. 2.3.

To evaluate the intensity of the first order mode, let us consider the coupling between ϕ_0 and ϕ_1 modes. Let's take a simple case of $\alpha = 0.5$, Eq. (2-43) and Eq. (2-44) reduce to

$$\begin{cases} \dfrac{d\phi_0}{dz} - \dfrac{V}{2L}\phi_1 = 0 \\ \dfrac{d\phi_1}{dz} + \dfrac{V}{2L}\phi_0 = i\dfrac{Q}{2L}(1-2\alpha)\phi_1 \end{cases} \tag{2-45}$$

From an analytical viewpoint, we ignore ϕ_{-1} and ϕ_2 because in this case, ϕ_{-1} and ϕ_2 are very small compared with ϕ_0 and ϕ_1. Equation (2-45) can be solved by using Laplace transformation. Putting this set of equations in matrix form, Eq. (2-45) becomes

$$\begin{bmatrix} \dot{\phi}_0 \\ \dot{\phi}_1 \end{bmatrix} = \begin{bmatrix} 0 & C_1 \\ -C_1 & C_2 \end{bmatrix} \begin{bmatrix} \phi_0 \\ \phi_1 \end{bmatrix} \tag{2-46}$$

where $C_1 = \dfrac{V}{2L}$

$C_2 = i\dfrac{Q}{2L}(1-2\alpha)$.

For a Linear system,[20] one can solve a set of difference-differential equation by using the Laplace transformation technique. For a system $[\dot{X}] = [A][X]$, the solution is $X(z) = e^{Az}X_0$, where X_0 is a initial condition, and the e^{Az} can be presented as

$$e^{Az} = \mathcal{L}^{-1}\left[(sI-A)^{-1}\right]$$

Applying this approach to Eq. (2-46) we have

$$\begin{bmatrix} \phi_0(z) \\ \phi_1(z) \end{bmatrix} = \begin{bmatrix} e_{11} & e_{12} \\ e_{21} & e_{22} \end{bmatrix} \begin{bmatrix} \phi_{inc} \\ 0 \end{bmatrix} = \begin{bmatrix} e_{11}\phi_{inc} \\ e_{21}\phi_{inc} \end{bmatrix} \tag{2-47}$$

where ϕ_{inc} is the mode amplitude of incident light at $z = 0$, and

$$e_{11} = \mathcal{L}^{-1}\left[\frac{s - C_2}{s^2 - sC_2 + C_1^2}\right]$$

$$e_{21} = \mathcal{L}^{-1}\left[\frac{-C_1}{s^2 - sC_2 + C_1^2}\right]$$

Then from Eq. (2-47), $\phi_1(z)$ can be put in the following form (The detailed steps are shown in Appendix A.1)

$$\phi_1(z) = \frac{-2V}{\sigma} e^{i\frac{Q}{4L}(1-2\alpha)z} \sin\left(\frac{\sigma}{4L}z\right) \tag{2-48}$$

where $\sigma = (4V^2 + [Q(1-2\alpha)]^2)^{1/2}$.

Finally, the first order mode intensity I_1 at $z = L$ becomes

$$I_1 = \phi_1 \cdot \phi_1{}^* = \frac{4V^2}{\sigma^2} \sin^2\left(\frac{\sigma}{4}\right) . \tag{2-49}$$

Similarly, one can obtain $\phi_0(z)$, and the zeroth mode intensity I_0 at $z = L$ is

$$I_0 = 1 - \frac{4V^2}{\sigma^2} \sin^2\left(\frac{\sigma}{4}\right) = 1 - I_1 . \tag{2-50}$$

The solutions given in Eq. (2-49) and Eq. (2-50) are consistent with those given by Pharisean[12][13]. From these equations, we can see that the distributions of the first order mode not only depend on the acoustical pressure and frequency of the acoustical wave but also the incident angle.

For the case of $\alpha = 0.5$ (the incident angle equal the Bragg angle) the first order mode intensity is expected to have maximum intensity. The mode intensities are

$$\begin{cases} I_0 = \cos^2\left(\frac{V}{2}\right) \\ I_1 = \sin^2\left(\frac{V}{2}\right) \end{cases} \tag{2-51}$$

The numerical solution of mode intensity variation will be given in the following chapter. It is noticed that the intensities predicted by Eq. (2-49) and (2-50) are quite accurate under the condition $Q >> 1$. In Eq. (2-51) the V value was chosen to be $(2n-1)\pi$, n being integer number. Under this condition, all light shall lie in the first order favored by Bragg diffraction.

2.4.2 The Second order Bragg Diffraction

For the second order mode m = 2, Eq. (2-38) becomes

$$\sin\theta_i = \frac{\lambda}{\Lambda} \tag{2-52}$$

Since θ_i also has a value of less then one degree, we can assume $\sin\theta_i \cong \theta_i$. Comparing with Eq. (2-42), we have

$$\theta_{2B} = 2\theta_B = \frac{\lambda}{\Lambda}$$

where θ_{2B} is equal to twice of the Bragg angle. When the incident angle of the light approaches to the double Bragg angle, the light is in phase and interferes constructively. As a result, the second order mode intensity reaches a maximum.

For $m = 2$, Eq. (2-37) becomes

$$\frac{d\phi_2}{dz} + \frac{V}{2L}(\phi_1 - \phi_3) = i\frac{2Q}{L}(1-\alpha)\phi_2 \tag{2-53}$$

This indicates that ϕ_2 couples to ϕ_1 and ϕ_3. Consider the coupling between ϕ_0, ϕ_1 and ϕ_2 (ignore ϕ_{-1} and ϕ_3 for the same reason as in the first order case.) We have a set of difference differential equation given below,

$$\begin{cases} \dfrac{d\phi_0}{dz} - \dfrac{V}{2L}\phi_1 = 0 \\ \dfrac{d\phi_1}{dz} + \dfrac{V}{2L}(\phi_0 - \phi_2) = i\dfrac{Q}{2L}(1-2\alpha)\phi_1 \\ \dfrac{d\phi_2}{dz} + \dfrac{V}{2L}\phi_1 = i\dfrac{2Q}{L}(1-\alpha)\phi_2 \end{cases} \quad \textbf{(2-54)}$$

This set of equations can be solved by using Laplace transformation. In matrix form, the set of equations can be expressed as

$$\begin{bmatrix} \dot{\phi}_0 \\ \dot{\phi}_1 \\ \dot{\phi}_2 \end{bmatrix} = \begin{bmatrix} 0 & C_1 & 0 \\ -C_1 & C_2 & C_1 \\ 0 & -C_1 & C_3 \end{bmatrix} \begin{bmatrix} \phi_0 \\ \phi_1 \\ \phi_2 \end{bmatrix} \quad \textbf{(2-55)}$$

where $C_1 = \dfrac{V}{2L}$

$$C_2 = i\frac{Q}{2L}(1-2\alpha)$$

$$C_3 = i\frac{2Q}{L}(1-\alpha) \ .$$

Since this is a 3x3 matrix, and the coefficients in the matrix could be complex quantities, finding the mode solutions becomes rather involved. A brief procedure is shown below, the detail steps will be given in appendix A.2. The coefficient matrix of the system equation is

$$A = \begin{bmatrix} 0 & C_1 & 0 \\ -C_1 & C_2 & C_1 \\ 0 & -C_1 & C_3 \end{bmatrix} \ . \quad (2\text{-}56)$$

Following the similar procedure in solving the first order mode, we have

$$e^{Az} = \mathcal{L}^{-1}\left[(sI-A)^{-1}\right] = \begin{bmatrix} e_{11} & e_{12} & e_{13} \\ e_{21} & e_{22} & e_{23} \\ e_{31} & e_{32} & e_{33} \end{bmatrix}$$

$$\phi(z) = e^{Az}\phi(0) \tag{2-57}$$

where $\phi(0) = \begin{bmatrix} \phi_0(0) \\ \phi_1(0) \\ \phi_2(0) \end{bmatrix} = \begin{bmatrix} \phi_{inc} \\ 0 \\ 0 \end{bmatrix}$

and

$$\left[SI-A\right]^{-1} = \frac{1}{\Delta}\begin{bmatrix} (s-C_2)(S-C_3)+C_1^2 & C_1(s-C_3) & C_1^2 \\ -C_1(s-C_3) & s(s-C_3) & sC_1 \\ C_1^2 & -sC_1 & s\left(s-C_2+C_1^2\right) \end{bmatrix}$$

where $\Delta = s^3-(C_2+C_3)s^2+\left(C_2C_3+2C_1^2\right)s-C_3C_1^2$

The set of equations is then in the following form.

$$\begin{bmatrix} \phi_0(z) \\ \phi_1(z) \\ \phi_2(z) \end{bmatrix} = \begin{bmatrix} e_{11} & e_{12} & e_{13} \\ e_{21} & e_{22} & e_{23} \\ e_{31} & e_{32} & e_{33} \end{bmatrix}\begin{bmatrix} \phi_{inc} \\ 0 \\ 0 \end{bmatrix} = \begin{bmatrix} e_{11} \\ e_{21} \\ e_{31} \end{bmatrix}\phi_{inc} \ . \tag{2-58}$$

Next, we can find e_{11}, e_{21} and e_{31} by the use of Laplace transform. The results are as follows

$$e_{11} = \mathcal{L}^{-1}\left[\frac{s^2-s(C_2+C_3)+C_2C_3+C_1^2}{s^3-s^2(C_2+C_3)+s\left(C_2C_3+2C_1^2\right)+C_3C_1^2}\right] \tag{2-59}$$

$$e_{21} = \mathcal{L}^{-1}\left[\frac{-C_1(s-C_3)}{s^3 - s^2(C_2+C_3) + s\left(C_2C_3 + 2C_1^2\right) + C_3C_1^2}\right] \tag{2-60}$$

$$e_{31} = \mathcal{L}^{-1}\left[\frac{C_1^2}{s^3 - s^2(C_2+C_3) + s\left(C_2C_3 + 2C_1^2\right) + C_3C_1^2}\right] \tag{2-61}$$

Since we are interested in second order Bragg diffraction for maximum excitation of the second order mode, the incident angle is $\theta_{2B} = \frac{\lambda}{\Lambda}$, and this means α equals to one [see Eq. (2-25)]. Therefore, with $\alpha = 1$ the C's become

$$C_1 = \frac{V}{2L}$$

$$C_2 = (-i)\frac{Q}{2L}$$

$$C_3 = 0 \quad .$$

For solving the mode intensities with $\alpha = 1$, one substitutes above C's to Eq. (2-59) ~ Eq. (2-61), and the results are given as follows

(a). The intensity of the first order mode with $\alpha = 1$.

Using $\alpha = 1$ in Eq. (2-60), it yields

$$e_{21} = \mathcal{L}^{-1}\left[\frac{-C_1}{s^2 - C_2 s + 2C_1^2}\right] \tag{2-62}$$

The detailed derivation of e_{21} will be shown in Appendix A.2, then we have

$$e_{21} = (-2)\frac{V}{\sigma}e^{i\frac{Q}{4}}\sin\left(\frac{\sigma}{4}\right), \quad \text{at } z = L \tag{2-63}$$

where $\sigma = (8V^2 + Q^2)^{1/2}$.

From Eq. (2-58) we have

$\phi_1 = e_{21} \cdot \phi_{inc}$, so the intensity of the first order mode is

$$I_1 = \phi_1 \cdot \phi_1{}^* = 4\frac{V^2}{\sigma^2}\sin^2\left(\frac{\sigma}{4}\right) I_{inc} \tag{2-64}$$

where $I_{inc} = \phi_{inc} \cdot \phi_{inc}{}^*$.

The value of the parameter σ in Eq. (2-64) for the first order mode is different than the one used in Eq. (2-49). The reason is that when $\alpha = 0.5$, the light is in phase and interferes constructively at the first order diffraction, thus ϕ_2 is small and can be ignored. However, in Eq. (2-64), $\alpha = 1$, the light is in phase and interferes constructively at the second order diffraction. As a result, ϕ_2 becomes large, and can no longer be neglected. In the case of $\alpha = 1$, the first order mode is strongly depend upon the parameter V and much more so than the case of $\alpha = 0.5$. Later, more specify information will be provided in the numerical analysis.

(b). The intensity of the second order mode with $\alpha = 1$.

From Eq. (2-61), e_{31} becomes

$$e_{31} = \frac{1}{2}\mathcal{L}^{-1}\left[\frac{2C_1^2}{s\left(s^2 - C_2 s + 2C_1\right)}\right] \quad . \tag{2-65}$$

From Appendix A.2 we can derive e_{31} sa follows

$$e_{31} = \frac{1}{2}\left[1 - e^{-i\frac{Q}{4}}\left(i\frac{Q}{\sigma}\sin\left(\frac{\sigma}{4}\right) + \cos\left(\frac{\sigma}{4}\right)\right)\right] \quad \text{at } z = L \tag{2-66}$$

where $\sigma = (8V^2 + Q^2)^{1/2}$.

Then the amplitude of the second order mode ϕ_2 becomes

$$\phi_2 = e_{31} \cdot \phi_{inc} \tag{2-67}$$

And the intensity of the second order I_2 is

$$I_2 = \phi_2 \cdot \phi_2^* = \frac{1}{4}\left[\left(\cos\frac{\sigma}{4} - \cos\frac{Q}{4}\right)^2 + \left(\frac{Q}{\sigma}\sin\frac{\sigma}{4} - \sin\frac{Q}{4}\right)^2\right] I_{inc} \tag{2-68}$$

It is interesting to note that for proper Q and σ values, I_2 can ideally be excited to 100% from I_{inc}. This indicates that if the incident angle of the light is twice of the Bragg angle, the I_{inc} can transfer most of its energy to I_2.

(c). The intensity of the zero order mode with $\alpha = 1$.

For the ϕ_0 part when $\alpha = 1$, we have

$$e_{11} = \mathcal{L}^{-1}\left[\frac{s^2 - 2C_2 + C_1^2}{s^3 - C_2 s^2 + 2C_1^2 s}\right] = \mathcal{L}^{-1}\left[\frac{1}{s}\right] - e_{31} = 1 - e_{31} \tag{2-69}$$

and

$$\phi_0 = e_{11}\phi_{inc} \tag{2-70}$$

Therefore, the intensity of the second order mode at $z = L$ becomes

$$I_0 = \phi_0 \cdot \phi_0^* = \frac{1}{4}\left[\left(\cos\left(\frac{\sigma}{4}\right) + \cos\left(\frac{Q}{4}\right)\right)^2 + \left(\frac{Q}{\sigma}\sin\left(\frac{\sigma}{4}\right) + \sin\left(\frac{Q}{4}\right)\right)^2\right] I_{inc} . \tag{2-71}$$

Finally, we have

$$\begin{aligned} I_0 &= \frac{1}{4}\left[\left(\cos\frac{\sigma}{4} + \cos\frac{Q}{4}\right)^2 + \left(\frac{Q}{\sigma}\sin\frac{\sigma}{4} + \sin\frac{Q}{4}\right)^2\right] I_{inc} \\ I_1 &= \left[\frac{2V}{\sigma}\sin\frac{\sigma}{4}\right]^2 I_{inc} \\ I_2 &= \frac{1}{4}\left[\left(\cos\frac{\sigma}{4} - \cos\frac{Q}{4}\right)^2 + \left(\frac{Q}{\sigma}\sin\frac{\sigma}{4} - \sin\frac{Q}{4}\right)^2\right] I_{inc} \end{aligned} \tag{2-72}$$

where

$$\sigma = \left(8V^2 + Q^2\right)^{\frac{1}{2}}$$

$$\alpha = (-n_0)\,\frac{k}{k^*}\sin\theta = 1$$

$$Q = \frac{{k^*}^2 L}{n_0 k \cos\theta}$$

$$V = \frac{k n_1 L}{\cos\theta}$$

The equations of ϕ_0, ϕ_1 and ϕ_2 derived above satisfy the solution of the difference differential equation given by Eq. (2-54) with α equals to one, and these confirms that the result derived in Eq. (2-72) are consistent. Also, the equation set, Eq. (2-72), is completely general for a pure sinusoidal excitation case. An interesting property of the second order mode results from pure sinusoidal grating is that its maximum value is periodic with $Q/4$ and $\sigma/4$. With proper Q and σ values, the diffraction efficiency of the second order will ideally be 100%. In chapter 4 we will discuss the conditions for high efficient diffraction in second order mode diffraction. From Eq. (2-72), it is easy to show that $I_0 + I_1 + I_2 \cong I_{inc}$. This implies that only a small diffraction appears in the high order modes and that the total energy of the system is practically conserved.

In the case when $\alpha = 1$, the conditions for maximum intensity for the second order mode are quite different from those for maximizing the first order mode intensity when $\alpha = 0.5$. For $\alpha = 0.5$ when the Q values are large, the first order mode is heavily dependent on the value of V. However, when $\alpha = 1$ the second order mode intensity becomes function of both Q and V. For maximizing the second order Bragg diffraction, we need to adjust Q and V to certain values which match the criterion for maximum second order diffraction. This means that only proper choices of acoustic frequency, amplitude, and width of acoustic beam can provide a high efficiency second order Bragg diffraction.

Chapter 3

Numerical Analysis of the Acousto-optics System

3.1 Introduction

In the previous chapter, we derived the conditions under which the second order Bragg diffraction occurs. Before the experimental setup is designed to verify the theory, numerical simulation can be readily performed to see the mode amplitude variations for a given set of system parameters (Q, V, α). Also, from the results of the numerical analysis, it is helpful to verify the criterion for determining an optimal set of parameter values for the acoustic optical interaction. In this chapter, the simulation for the first order and second order Bragg diffraction will be carried out in detail.

3.2 Numerical Analysis of the First order Diffraction

Klein and Cook[11] used numerical simulation to show the Roman and Nath condition and the first order Bragg diffraction. In the Bragg diffraction case, they only simulated certain Q and V values. However, a through analysis of the interaction was not given. For the sake of comparison, a detail mode variation under all parameter changes will be very useful in understanding the interaction as well as comparing with the second order mode variations.

First, we use the difference-differential equation set in Eq. (2-54) to perform the numerical simulation. Since Eq. (2-54) involves ϕ_0, ϕ_1 and ϕ_2, the numerical result for the first order mode will be more accurate than the result obtained from the difference-differential equation set Eq. (2-45), which was used by Klein and Cook considering only the ϕ_0 and ϕ_1 modes. Since the magnitudes of the higher order modes drop out rapidly, accurate result can be obtained by using the first three order modes. As incident angle of the light beam approaches the Bragg angle (say $\alpha = 0.5$), the second order diffraction will be very weak when a large Q value and a small V value is used. Then, the first order mode intensity can either be obtained by Eq. (2-54) or Eq. (2-45). However, for small Q, the diffractions analyzed by Eq. (2-45) did not work precisely, and we need Eq. (2-54) to analyze the diffractions in this region.

In the previous chapter, it has been shown that the first order mode can be synchronous with zeroth order mode and gives maximum mode intensity if the incident angle of light field is exactly equal to the Bragg angle $\theta_B = \frac{\lambda}{2\Lambda}$. The differential equations given in Eq. (2-54) are used to simulate the acousto-optic system. Figure 3.1(a) shows the distribution of I_1 with Q values from 1 to 40 and V values from 1 to 20 when the incident angle of the light field is equal to the Bragg angle ($\alpha = 0.5$). Figure3.1(b) shows the result solved by Eq. (2-45) with $\alpha = 0.5$. It can be readily seen that Fig. 3.1(a) gives more detailed information in the mode distribution of the first order than Fig.3.1(b), especially when $Q < 15$ and the value of V is large. This will be useful fact for experimental verification and practical applications. The first order diffraction has a rapid change in the small

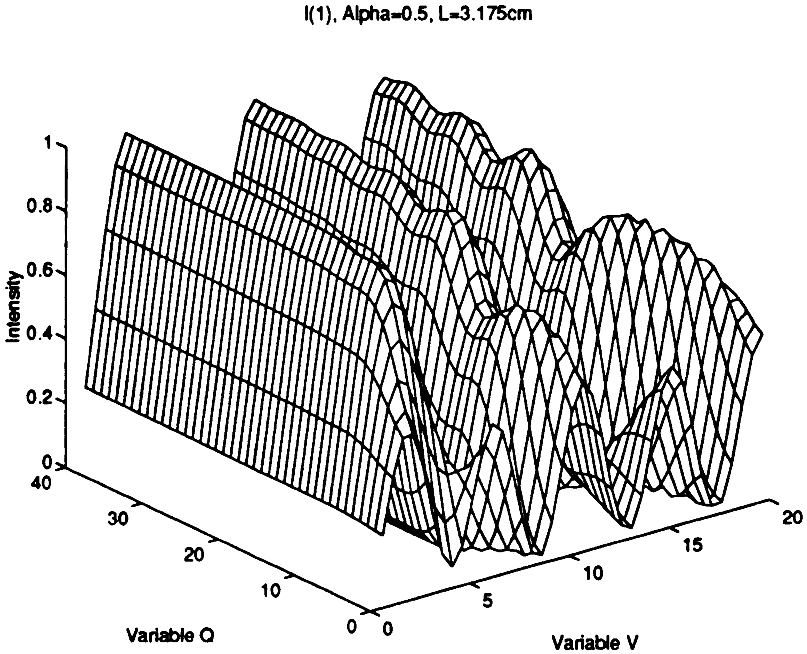

(a)

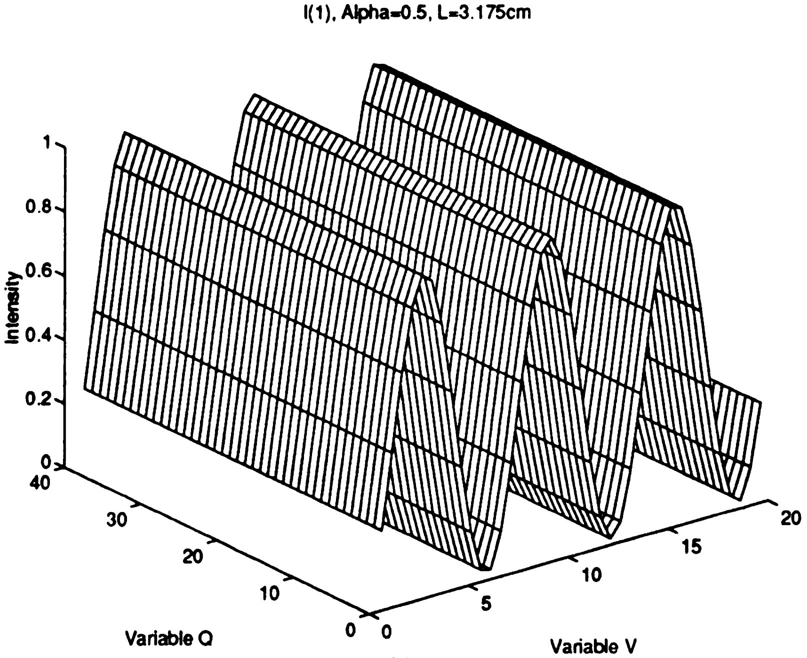

(b)

Figure 3.1 First order light intensities versus Q and V variations with α=0.5.
(a) The numerical result with Considering ϕ_0, ϕ_1 and ϕ_2.
(b) Consider only ϕ_0, ϕ_1.

Q region, and Q depends quadratically on the acoustic frequency. Consequently, one can use acoustic frequency to vary the diffraction intensities in this region. For large Q and small V, figures 3.1 (a) and (b) show the same character of diffracted light. Though we use Eq. (2-54) to analyze the interaction, comparing Fig.3.1(a) with (b), we see that for maximum I_1 $V = (2n-1)\pi$ (n being integer) can be applied for the case of $\alpha = 0.5$ as well. The result shown in Fig.3.1(a) is appeared to be correct, therefore, in future analysis we will refer to those numerical data.

3.2.1 Diffraction in the Raman-Nath Region

In order to compare the characteristics of the Bragg region with the Raman-Nath Region, a brief review of the properties of the Raman and Nath diffraction is given below. With Q <<1, the intensity of the nth diffraction order is given by

$$I_n = J_n^2 \left[V \frac{\sin \frac{Q\alpha}{2}}{\frac{Q\alpha}{2}} \right] . \tag{3-1}$$

For normal incident of the light beam, the intensity can be reduced

$$I_n = J_n^2 [V] . \tag{3-2}$$

Raman and Nath first obtained this result and indeed suggested the correct angular dependence from geometric arguments[5]. Occasionally, one finds in the literature the designation of Raman and Nath diffraction as all diffraction at normal incidence. However, in the interests of historical accuracy and a consistent description of the problem, Klein and Cook suggested the designation of Raman and Nath diffraction for all diffraction under condition Q << 1.

The acoustic fields described by the condition $Q \ll 1$ are equivalent to optical gratings which produce only a modulation of the phase of light passing through them. The light is modulated in phase but not in amplitude. This agrees with the early speculation of Raman and Nath that a sound beam of narrow width and low frequencies could be considered as an optical phase grating[4]. The parameter V, known as the Raman and Nath parameter, describes completely the diffraction in this limiting case. It measures the degree of phase modulation of the light produced by the acoustic wave. Examining the intensity, the following properties in the Raman and Nath region are observed.

- The diffraction pattern is symmetric at all angles of incidence since $I_n = I_{-n}$. Many diffraction orders can be observed. When the angle is normal incidence, the intensities of the first few diffraction orders is a function of V.

- The angular dependence of the arguments of the Bessel functions is such that the effect of oblique incidence is to alter the effective value of V by a factor of $\left(\sin\frac{Q\alpha}{2}\right)/\frac{Q\alpha}{2}$. Maximum diffraction will occur at normal as well as on both sides with respect to the normal. When $Q\alpha = 2m\pi$ (m being a nonzero integer), all diffraction effects will disappear.

- The light intensities in I_n and I_{-n} will vanish together when the argument of Eq. (2-33) is equal to any root of the nth order Bessel function. This can be made to occur by changing either V or α. The intensity of a particular order as a function of the incidence angle will be symmetrical with respect to the normal.

The above observations are restricted for $Q \ll 1$. When the magnitude of Q approaches to unity the observed light intensity distribution begins to deviate from those predicted by Eq. (2-33). The excess amount of light is found in the lower orders. Also, the maxima and minima of the light intensities as functions of V are shifted, and the total diffraction effect does not vanish at $Q\alpha = 2m\pi$. These effects become more pronounce for larger Q value.

3.2.2 Diffraction in Bragg Region

For $Q << 1$ the diffraction is described by Eq. (2-33) while for $Q >> 1$ Eq. (2-51) should be used. However, when the Q value is in the range from 1 to 10, there is no close form solution for the difference-differential equation Eq. (2-54). Numerical methods have to be used to analyze the interaction.

The mode intensity variation of the zeroth and first diffraction orders for normal incidence was given by Klein and Cook[11]. They mentioned that for $Q < 2$, the dependence on acoustical pressure is similar in nature to Raman-Nath diffraction but differs in essential detail. It is seen that more light appears in the lower diffraction order than is predicted by Raman and Nath. By summing the intensities of the zeroth and the first orders, it is found that essentially no light appears in the second or higher orders with $Q = 4$. For $Q = 7$, only a small fraction appears in the first order. When $Q = 10$, diffraction effects essentially vanished at normal incidence for small acoustic pressures. However, in the case of oblique incidence the diffractions have quite different characteristics than these from normal incidence when Q is large. From previous development, we have established that $V = (2n-1)\pi$ is the condition for providing a high efficiency diffraction in the first order. In order to investigate the mode intensity variation as a function of the incident angle of the light field and the frequency of the acoustic wave in the first order diffraction, various α and Q values are used while keeping $V = 3$. The mode distribution of I_1 is shown in Fig. 3.2. Figure 3.2 depicts the rapid change in the angular dependence with Q for the first order diffraction. The first order mode is excited to its maximum when the

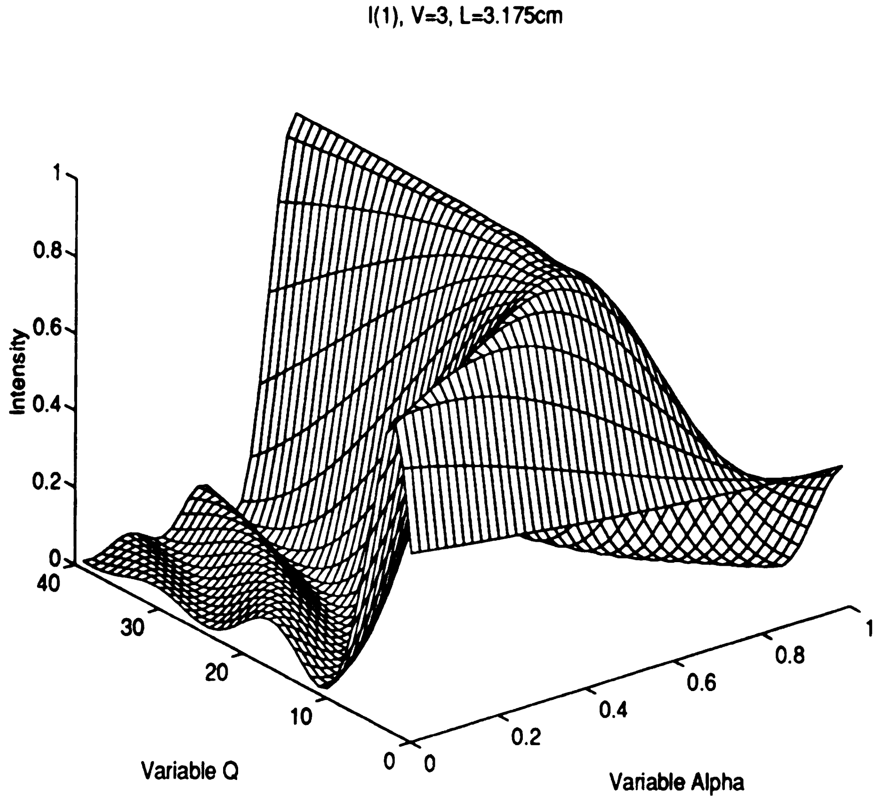

Figure 3.2 First order light intensities versus Q and α variations with V=3.

incident angle approaches the Bragg angle ($\alpha = 0.5$) with large Q. This is referred to as the First Bragg Diffraction. It is observed that for small Q, even though the incident angle is the Bragg angle and $V = (2n-1)\pi$, the magnitude of I_1 remains small.

Figure 3.3 shows the mode intensities versus various Q values with $V = 3$ and $\alpha = 0.5$. When $Q = 1$, a considerable amount of light is found to be appeared in the orders other than the zeroth and first. Most of this light will be in the negative first order or positive second order. For $Q < 3$, the diffracted light is very similar in nature to Raman and Nath diffraction but differs in detail. As Q is increased, less light appears in those orders. It is found that essentially no light appears in the second or higher order while $Q > 12$, and most light is found to appear in first order with only a small fraction in zeroth order. When $Q >> 12$, all light lies in the first order, and this phenomenon was considered as Bragg diffraction. It is seen that for $Q = 6$, about 92 percent of light lies in the first order, and when $Q = 18$, it contains almost 99 percent. These results are seen to be in agreement with the results given by Phariseau.

With $V = 3$, Fig. 3.4 shows the angular variation with Q for the zeroth and first orders. It is interesting to note that when $Q < 2$, the dependence on the incident angle is similar to those of the Raman and Nath diffraction. A slight difference is that the zeroth order is symmetrical with respect to normal incidence, whereas the first order are symmetric about their respective Bragg angle ($\alpha = \pm 1/2$). This is not very apparent with small Q values, however, at larger Q values it becomes noticeable since the range of α decreases. Figure 3.4 also illustrates that when Q is increased further, Bragg diffraction predominates over other effects. Then, in order to observe the Bragg diffraction phenomenon, high acoustic frequencies are required. Comparing Figs. 3.4 (b), (c) and (d), the sharpness of the intensity distribution is seen to increase with Q.

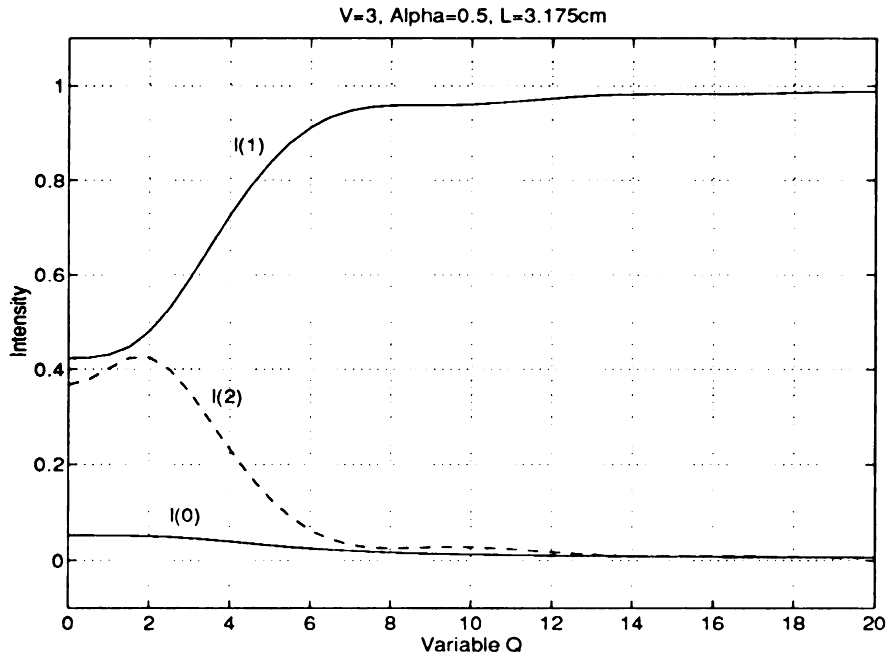

Figure 3.3 First order light intensities versus Q with V=3 and α=0.5.

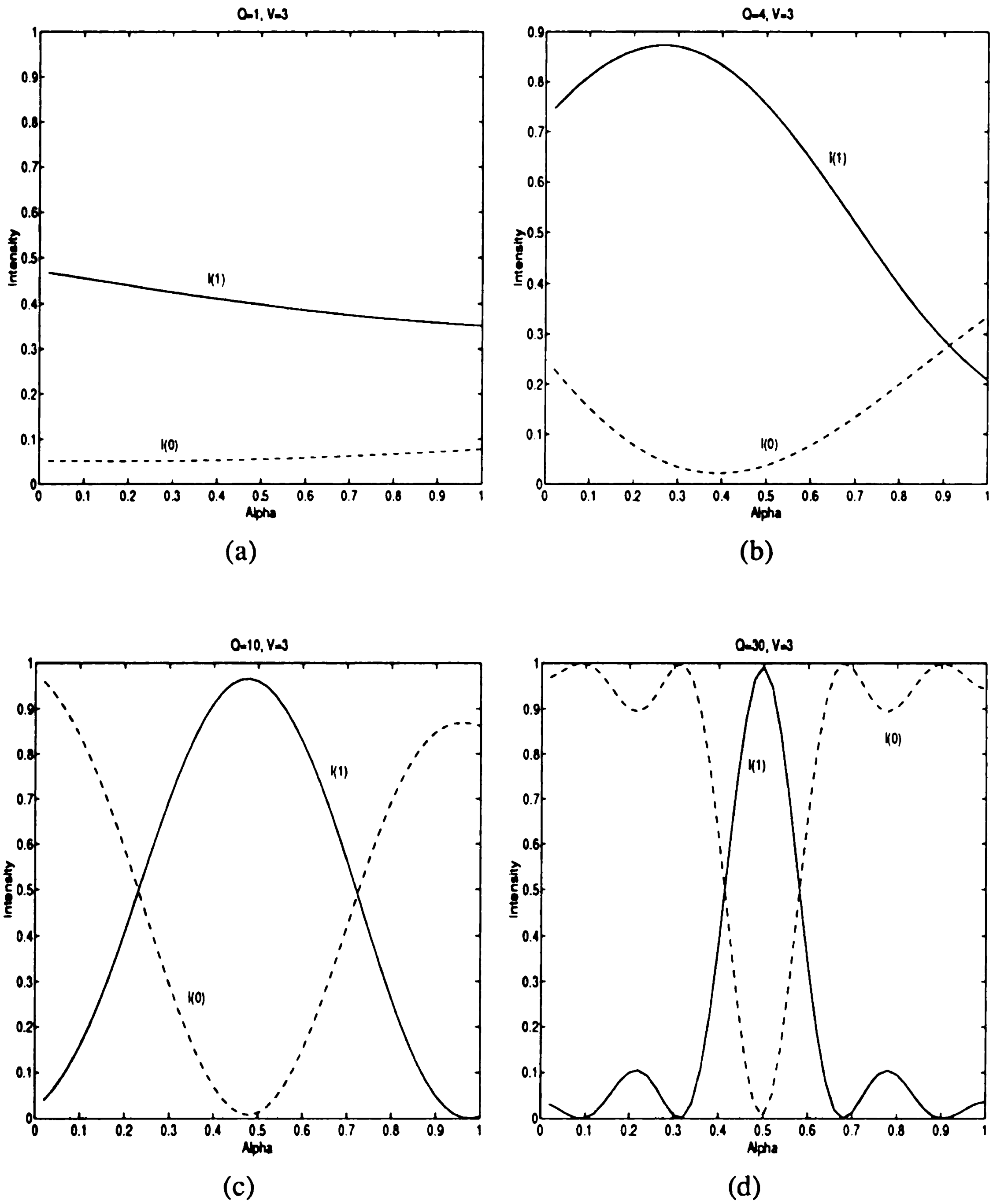

Figure 3.4 Zeroth and first order light intensities versus incidence angle with Q as a parameter.

3.3 Numerical Analysis of the Second Order Bragg Diffraction

In this section we will concentrate on the analysis of the second order Bragg diffraction. When the incident angle equals twice of the Bragg angle $\theta_{2B} = \frac{\lambda}{\Lambda}$ (say $\alpha = 1$), the second order mode can be synchronous and give maximum intensity. With $\alpha = 1$, Eq. (2-72) describes the diffractions with pure sinusoidal grating, and this interaction can be referred to as a double diffraction or the Second order Bragg Diffraction. The expression given by Eq. (2-72) is rather complex, in order to obtain more insight of the interaction, a numerical simulation has been performed. Since Eq. (2-72) only provides the special case $\alpha = 1$, if we want to observe the mode distribution with different incident angle, we still need to simulate the whole system by using difference-differential equation Eq. (2-54).

3.3.1 Optimum set for the second order Bragg Diffraction

With $\alpha = 1$ and $L = 3.175cm$, the numerical simulation is shown in Fig. 3.5. Figure 3.5 shows the distribution of the diffracted intensities with Q values (0 to 40) and V values (0 to 15). As can be seen from Fig. 3.5, when the incident light make a double Bragg angle with respect to the acoustic beam, most energies are coupled between the zeroth, Fig. 3.5(a), and the second order, Fig. 3.5(c), and only a small fraction appears in the first order diffractions, Fig. 3.5(b). In the first Bragg diffraction case ($\alpha = 0.5$ see Fig. 3.1(a)) when Q values are large, all energies are coupled to the zeroth and the first order diffractions and both maximum diffractions are only a function of V. However, in the second Bragg diffraction ($\alpha = 1$), all diffracted light are not only a function of V but also a function of Q. Figure 3.5(c) indicates that the maximum second order diffraction is periodic with Q and V. When an optimum set of Q and V values is used, the intensity I_2 reaches a

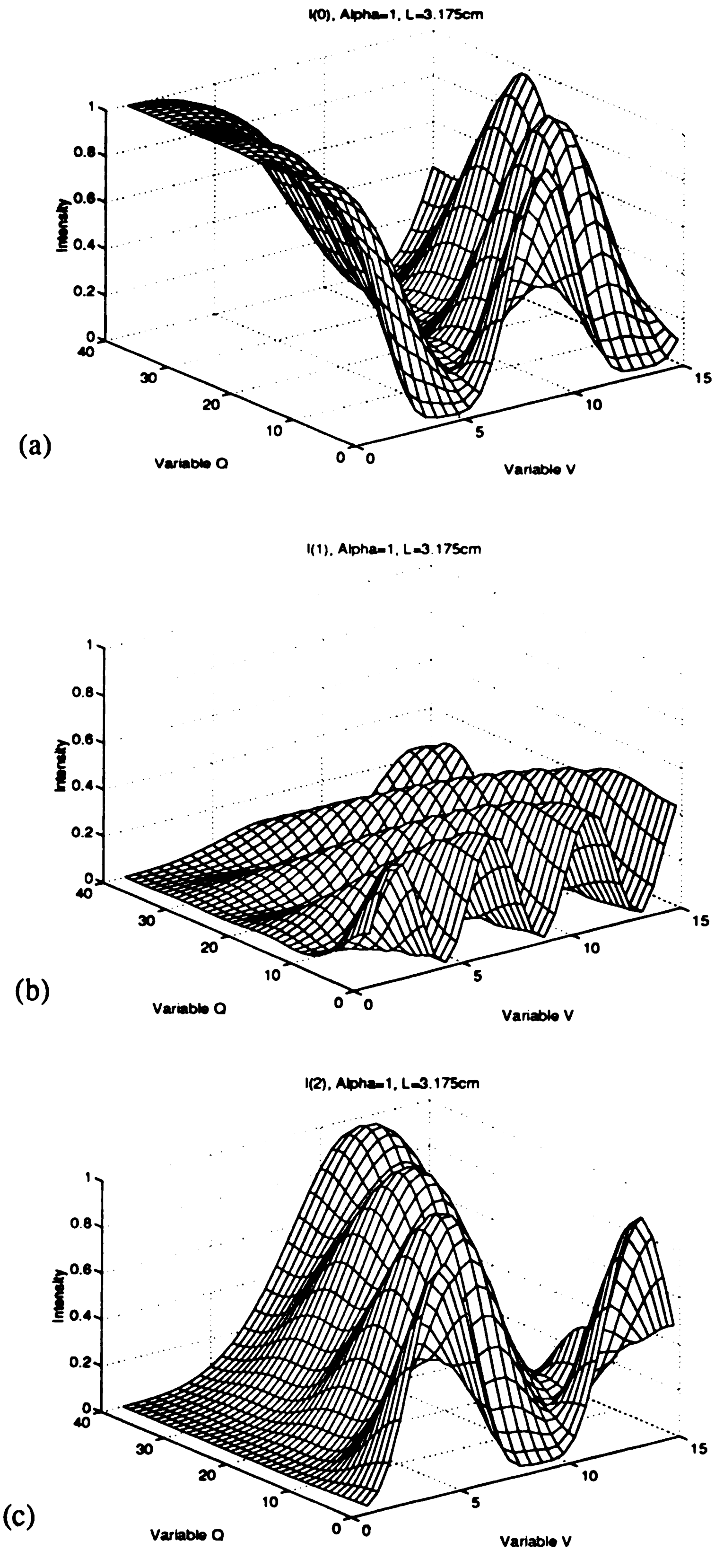

Figure 3.5 Diffracted light intensities versus Q and V variations with α=1

maximum, and almost 99% energy couples from I_{inc} to I_2. In the first order Bragg diffraction, there is a wide range of system parameters to be used to obtain the maximum first order diffraction. In the second order Bragg diffraction, the maximum intensity can only be achieved if a certain set of parameter is selected. In Fig. 3.5(c), there are three sets of Q and V values for obtaining the maximum I_2, they are: (Q=13, V=7.5), (Q=25, V=10), and (Q=38, V=11.5). These parameter sets show that for small Q value (say Q = 13) the minimum required V value to excite the maximum I_2 is smaller than the V value for large Q value (say Q = 38). The physical interpretation of this is as follows. For a given width of an acoustic beam with low Q values, the required acoustic frequency as well as acoustic power could be lower. This property is also same to the first order Bragg diffraction.

From the results of the above simulation, we learn how the second order Bragg diffraction can be excited to its maximum intensity with certain α, V and Q parameters. Next chapter, experimental setup will be described.

3.3.2 Second order mode Intensity Variation with Parameter α and V

To analyze the distribution of the second order Bragg diffraction with V and α as parameters, we choose the optimum set (Q=13) for detail analysis. Figure 3.6 shows the distribution of diffracted light intensities with Q = 13, while V and α are variables. For a system setup with the incident light, medium and the width of acoustic beam are fixed, the Q value can be directly related to the acoustic frequency. Furthermore, V can be related to the acoustic pressure and α in term of the angle between the light and the acoustic beam.

For a given acoustic frequency such as to give Q = 13, Fig. 3.6 shows the distribution of the diffracted light with various intensities of the acoustic beam and angles of incidence. It is observed that from Figs. 3.6 (a) and (b) when the incident angle approaches

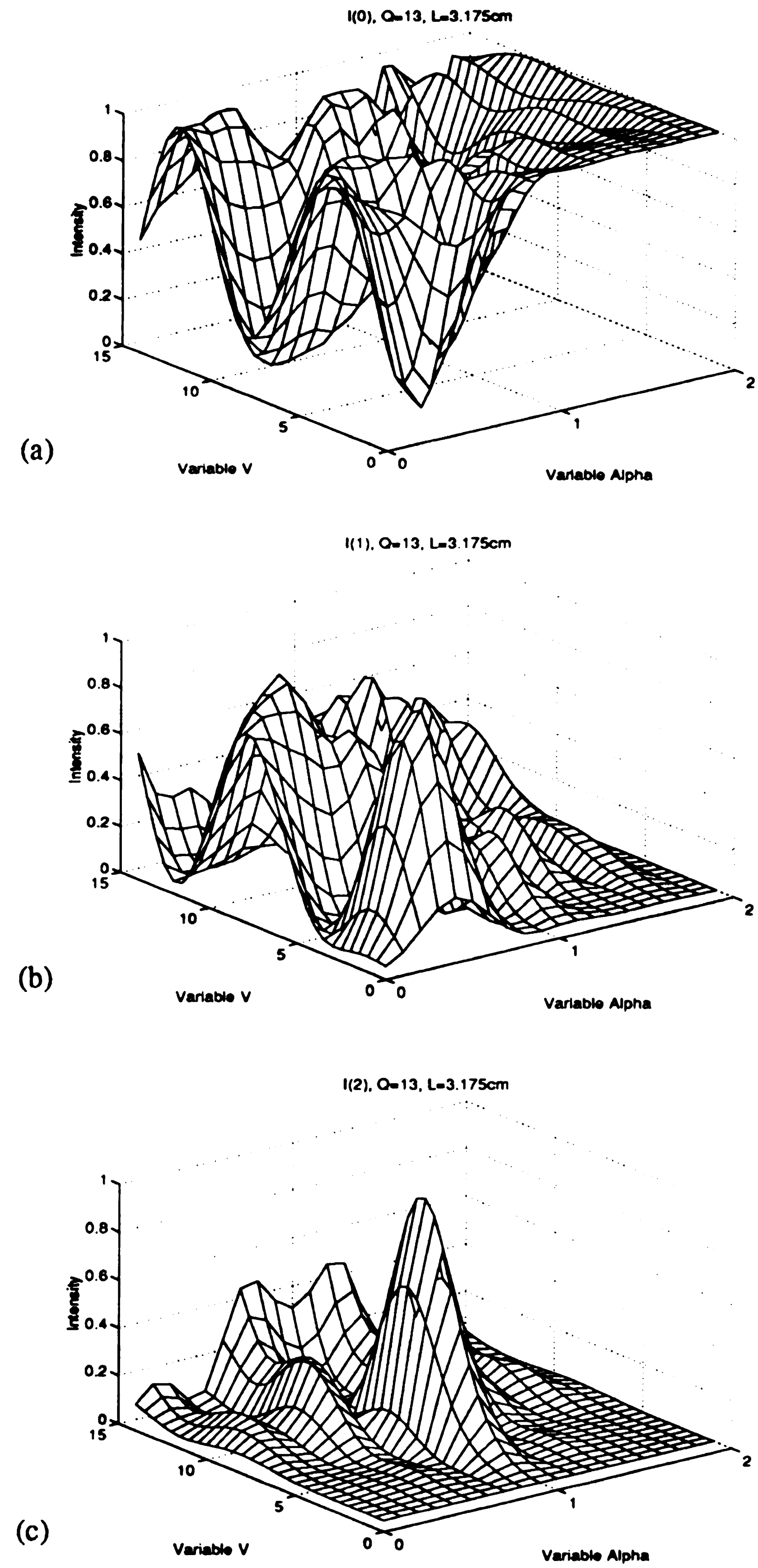

Figure 3.6 Diffracted light intensities versus V and α variations with Q=13.

the Bragg angle ($\alpha = 0.5$), most of the energies are coupled from the zeroth to the first order modes. With $\alpha = 0.5$ since the intensity of the first order diffraction can be maximized by adjusting the acoustic beam intensity, under such excitation the second order diffraction is too weak to be observed experimentally. However, when the incident angle equals to twice of the Bragg angle ($\alpha = 1$, see Fig. 3.6(c)) it is noted that the most energy is transferred from the first order to the second order mode. In addition, the second order mode intensity can be maximized by adjusting the acoustic beam intensity. This indicates that the second order diffraction can be strongly excited with a pure sinusoidal grating when the incidence angle of the light beam approaches to twice of the Bragg angle with an optimum set of Q and V values. Under such excitation, the first order mode intensity I_1 can only reach about 45% of I_{tol} (see Fig. 3.5(b)). When the incident angle greater than the double Bragg angle (say $\alpha > 1$), only a small fraction of the incident light appears in the first or higher order. Practically all diffraction effects vanish for $\alpha >> 1$ under small acoustic pressures.

With $Q = 13$, Fig. 3.7 displays more detail variation of the angular distribution when the V value changes. With $V = 1$, some diffractions appear on the first order at $\alpha = 0.5$, but most of the energies are still contained in the zeroth order. When V increases to 3, the first order reaches its maximum at $\alpha = 0.5$, and a noticeable second order diffraction was observed at $\alpha = 1$. When $V = 5$ (see Fig. 3.7(c)), the first order dips down to 40% of I_{tol}. A stronger second order mode intensity is visible when V increases from 3 to 5. It is rather surprising that the first order mode reappears at $\alpha = 1$. This explains why in an experimental setup the first order mode can easily be observed since there exists a wide range of system parameters to excite the first order mode. When V is further increased to 7.5, Fig. 3.7 (d), the diffracted light energy is almost completely transferred into the second order mode at $\alpha = 1$. It is important that a strong second order mode excitation can provide attractive features in engineering applications. The second order diffraction provides not

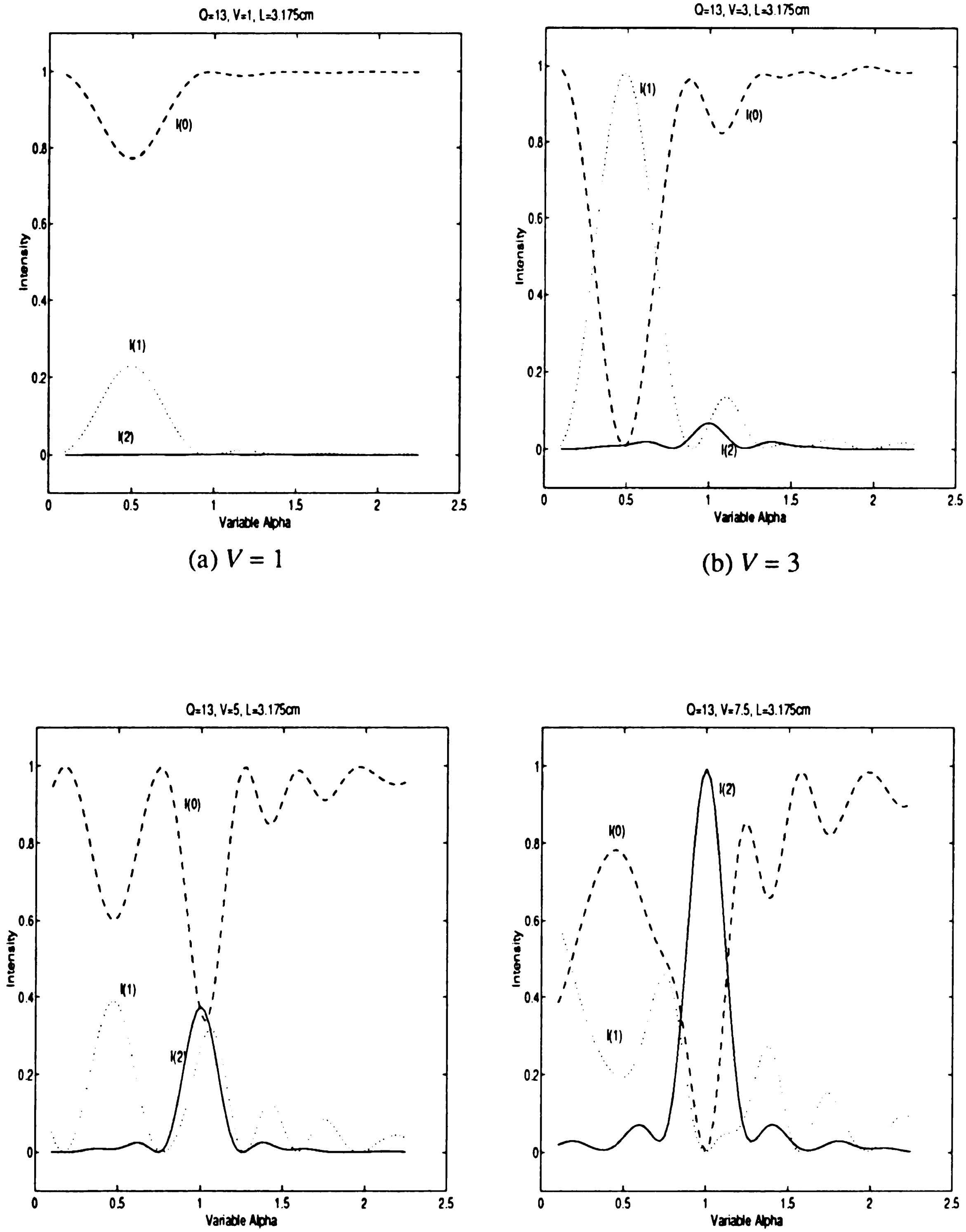

(a) $V = 1$

(b) $V = 3$

(c) $V = 5$

(d) $V = 7.5$

Figure 3.7 Diffracted light intensities versus V and α variations with Q=13.

only a larger deflection angle and frequency shift in the light beam, but also gives a better resolution in beam deflector and optical imaging. Another interesting result has also been noted as shown in Fig. 3.7(d) that when Q = 13 and V = 7.5 the maximum diffraction appeared at $\alpha = 0.5$ is not the first but the zeroth order, and the maximum of the first order is shifted to $\alpha = 0.75$ instead.

In previous section, we mentioned that using the optimum parameter sets, for small Q values the minimum required V values to excite maximum I_2 is smaller than the V values for large Q values. On the other hand, the large Q provides a wider range of V values which drives I_2 to greater than 70% of the maximum I_2. Comparing Fig. 3.8 (a) and Fig. 3.9 (c), when Q equal to 38, the magnitude of I_2 is in excess of 70% of the maximum I_2 with various V values from 9.5 to 13.8. However, when Q equal to 13, the ranges of the V which have I_2 greater than 70% of the maximum I_2 are only from 6.2 to 9. This indicates that if high Q is used for optimum set, there exists a broader range of V values for exciting the second order Bragg order.

Physically, the V value is proportional to the amplitude of the Fourier component of the acoustic wave and is directly related to the intensity of the acoustic grating. Then, the V value is a function of the acoustical pressure.[23][24] In acousto-optical application, the transfer function of amplitude modulation can be related to the result in Fig. 3.8.

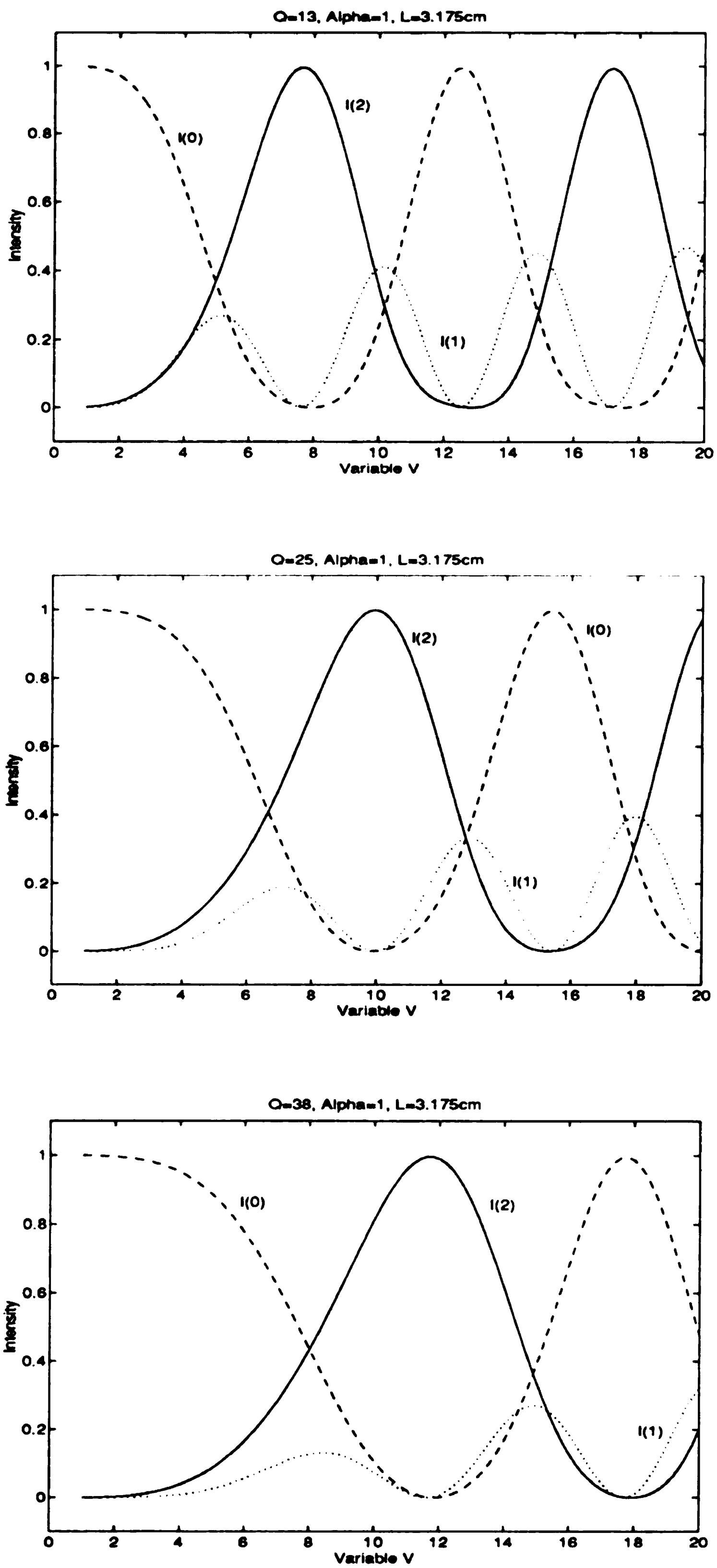

Figure 3.8 Light intensities versus V with α=1.

3.3.3 Second order mode Intensity Variation with Parameters Q and α:

For observing the distribution of the second order diffraction with Q and α as variables, we choose optimum sets (V=7.5, V=10 and V=11.5) for in-depth analysis. Figure 3.9 shows the distributions of the second order mode with Q and α as parameters while using the three optimum V values. From the mode distributions, one can see that with optimum V values, the second order mode is very sensitive to Q and α. Only a narrow range of α values can efficiently drive the second order mode. With α =1, the maximum second order diffractions are located in Q = 13 for V = 7.5, Q = 25, for V = 10 and Q =38 for V = 11.5. Figure 3.9 indicates that the mode distributions with varying Q values are quite different for each optimum V value. For small V value, say V = 7.5 in Fig. 3.9(a), the Q value required to achieve the maximum second mode is small (Q =13), and the range of α which can efficiently drive the second order mode is large. Under such excitation, when Q is increasing, the intensity of the second order mode is decreasingly and the range of α which can efficiently drive the second order mode becomes narrower. However, for case V = 11.5 in Fig. 3.9(c), the Q value required to achieve the maximum second order is change to large (Q =38), and the mode distribution with Q various is wholly different to the case V = 7.5.

From Fig. 3.1(a) and Fig. 3.2, we see that when the conditions $V = (2n-1)\pi$ and α = 0.5 are met, the first order Bragg diffraction is strongly excited at large Q values. In addition, when Q is large, the first order mode intensity is saturated and does not change too much with increasing Q. Quite different from the first Bragg diffraction, the maximum second Bragg diffraction shown in Fig. 3.9 is heavily dependent on the Q value, and for different optimum V value, the mode distributions with various Q become versatile. For a fixed acoustic beam, light wavelength and medium n_0, the Q value is only function of the acoustic frequency. Then, an acousto-optical frequency modulation can be applied by using the Bragg diffraction, and the second order Bragg diffraction provides a versatile

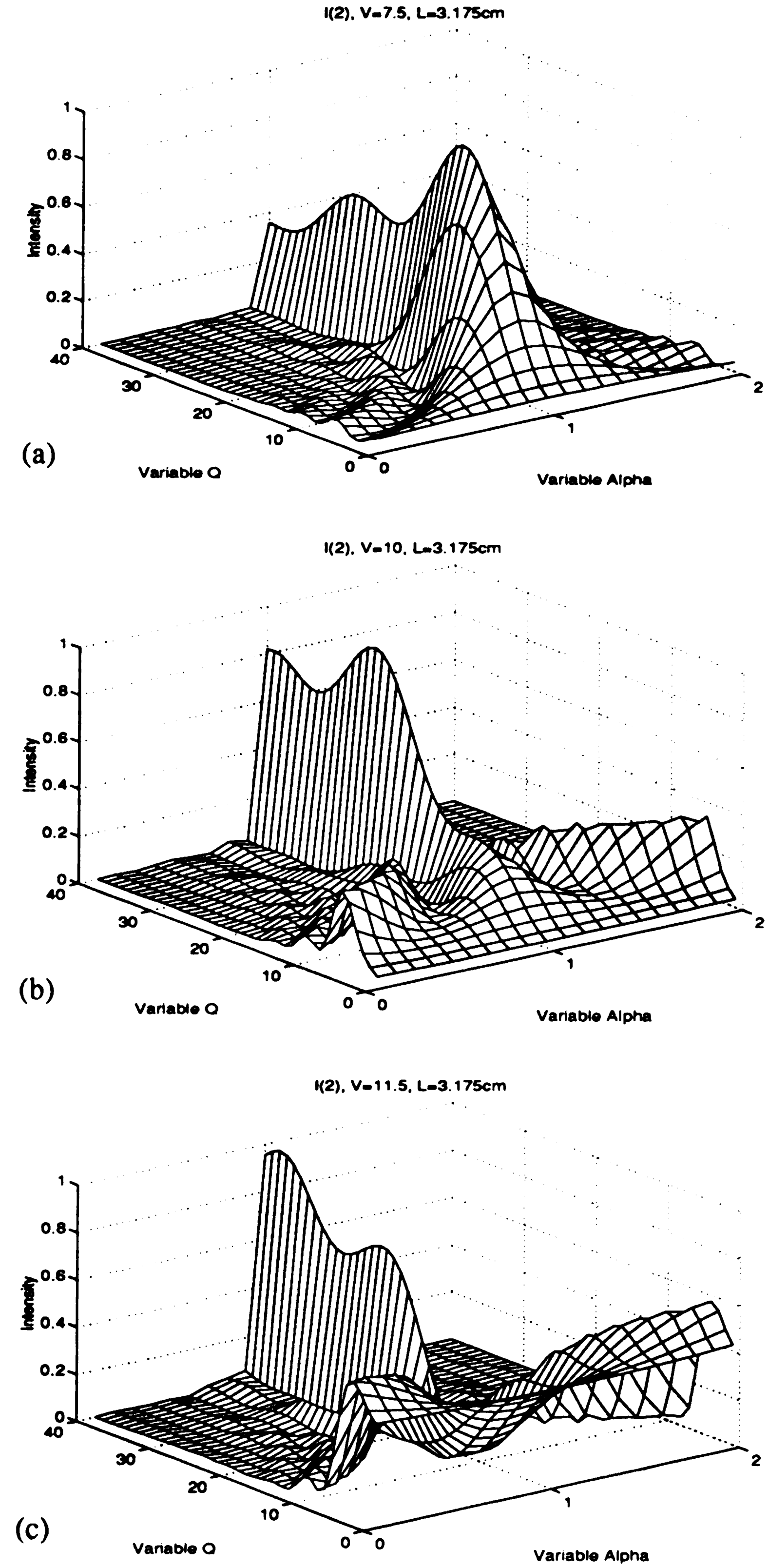

Figure 3.9 Second order light intensities versus Q and α variation.

transfer function than the first order one. Since only a short range of frequency can provide the maximum diffraction in the second order mode, it is useful that using the second Bragg diffraction to implement a frequency filter to acousto-optical signal processing.

Equation (2-25) indicates that the variable α is a measure of the incidence angle of the light on the sound field (see Fig. 2.3). In the Bragg diffraction, the diffraction angle is $\theta = \dfrac{m\lambda}{2\Lambda}$, where m is the diffraction order. The diffraction angle θ is thus proportional to the acoustic frequency. Therefore, for a higher Q value the diffraction angle θ is large. Using this result, we can apply the Bragg diffraction to an acousto-optic(AO) deflector, and using acoustic frequency controls the deflected light beam. Since the second Bragg diffraction has a double Bragg angle, the AO deflector using the second Bragg diffraction would have a larger deflected light effect than that using the first Bragg diffraction. In the next section we will also show that using the second Bragg diffraction would have a double resolution on the acousto-optic deflectors. In addition, the second Bragg diffraction provides a double frequency shifting to the diffracted light. Since the frequency shifting is extremely important for heterodyning application[25]-[27], the frequency modulation by using the second Bragg diffraction is a good study topic for future application. Another useful application is that since the second order intensity is also a function of the Q value, using this result we can apply to acousto-optic devices and optical signal processing which prefer using acoustic frequency to control the amplitude of the diffraction not by using acoustic pressure.

For the purpose of demonstrating how the diffraction intensity be affected by the acoustic frequency, let's consider the incident light be a Helium-Neon Laser beam $\lambda_0 = 6.328 \times 10^{-5}\ cm$, and the acoustic system has an acoustic beam width of $L = 3.175\ cm$. Figure 3.10 shows the mode distribution as a function of the acoustic frequency with $V = 7.5$. As can be seen, when the acoustic frequency approaches 17 MHz, the second order

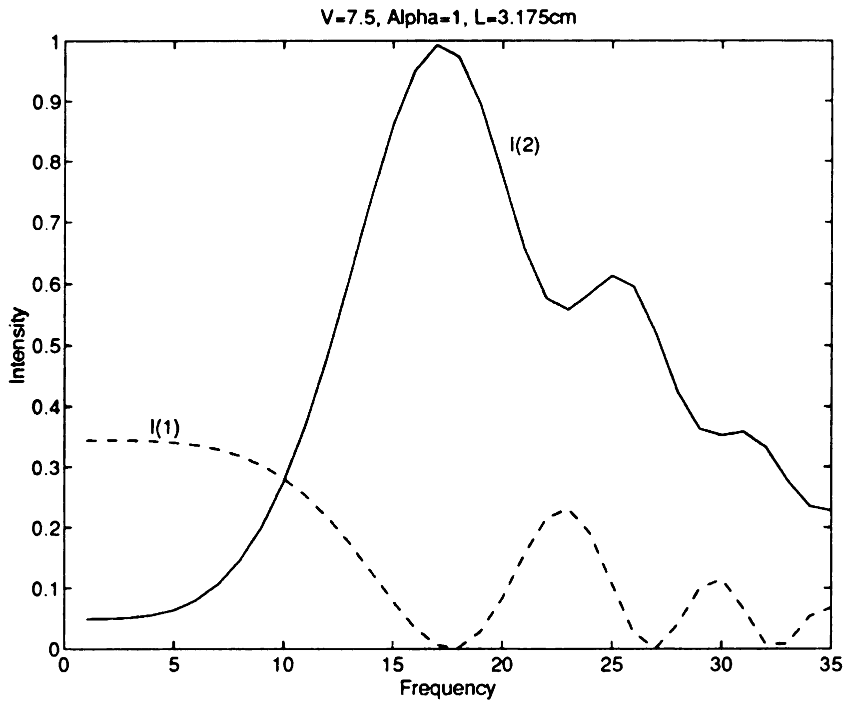

Figure 3.10 Light intensities versus frequency f (MHz) with V=7.5 and α=1.

diffraction reaches a maximum intensity. As a result, one can control the mode intensities by varying the acoustic frequency.

3.3.4 Deflection Resolution and Angular Resolution:

One of the advantages of using the second Bragg diffraction in acousto-optical system is due to the fact that it provides a better deflection resolution. Light deflection[28]~[30] by ultrasound is based on the relationship between the acoustic frequency and the Bragg angle. This relationship can be obtained by substituting the quotient of sound velocity v and acoustic frequency f for the acoustic wavelength Λ into the Bragg diffraction condition. For the first Bragg diffraction, the condition is $2\sin\theta_B = \frac{\lambda}{\Lambda}$. With $\Lambda = \frac{v}{f}$, the condition becomes

$$2\sin\theta_B = f\frac{\lambda}{v}. \qquad (3\text{-}3)$$

Typically, the Bragg angles are rather small, $2\sin\theta_B$ can be approximated by $2\theta_B$. Hence, $2\theta_B$ represents the angle by which the diffracted light departs from the path of the incident light. As indicated in Eq. (3-3), the direction of the diffracted light ca be changed by varying the acoustic frequency f.

$$\Delta(2\theta_B) = \Delta f\frac{\lambda}{v}. \qquad (3\text{-}4)$$

Light deflection is potentially useful for television projection[31] and for memory or switching devices. The major factor in a light deflection devices is the number of angular positions that can be clearly distinguished from each other, usually called the number of resolvable spots. A light beam, no matter how well collimated, eventually spreads through diffraction: far away from a source with uniform phase and amplitude across an aperture D, radiation of wavelength λ spread out over an angle $\pm\lambda/D$. Figure 3.11 shows that to determine the number of resolvable spots, we divide the angular displacement $\Delta(2\theta_B)$ by the unavoidable diffraction spread $\beta_{min} = \lambda/D$ of a light beam projection from an aperture D. This spread determines how small a spot one can make. Now for the first Bragg diffraction the number of resolvable spots can be defined as follows:

$$N_1 = \frac{\Delta(2\theta_B)}{\beta_{min}} = \frac{\Delta f(\lambda/v)}{\lambda/D} = \Delta f\frac{D}{v} = \Delta f\,\tau \qquad (3\text{-}5)$$

where D is the width of light beam that the acoustic wave traverse at its velocity v. Hence, the transit time τ of the sound across the optical aperture is D/v. The number of resolvable spots equals this transit time multiplied by the total acoustic frequency shift Δf.

For the second Bragg diffraction, the condition is

$$2\sin\theta_{2B} = 2\frac{\lambda}{\Lambda} = 2f\frac{\lambda}{v}\ . \qquad (3\text{-}6)$$

To vary the direction of the diffracted light, an incremental change of acoustical frequency Δf is required,

$$\Delta(2\theta_{2B}) = 2\Delta f\frac{\lambda}{v}\ . \qquad (3\text{-}7)$$

Hence, the number of resolvable spots for the second Bragg diffraction can be written as

$$N_2 = \Delta\left(\frac{2\theta_{2B}}{\beta_{min}}\right) = 2\Delta f\frac{D}{v} = 2\Delta f\,\tau \qquad (3\text{-}8)$$

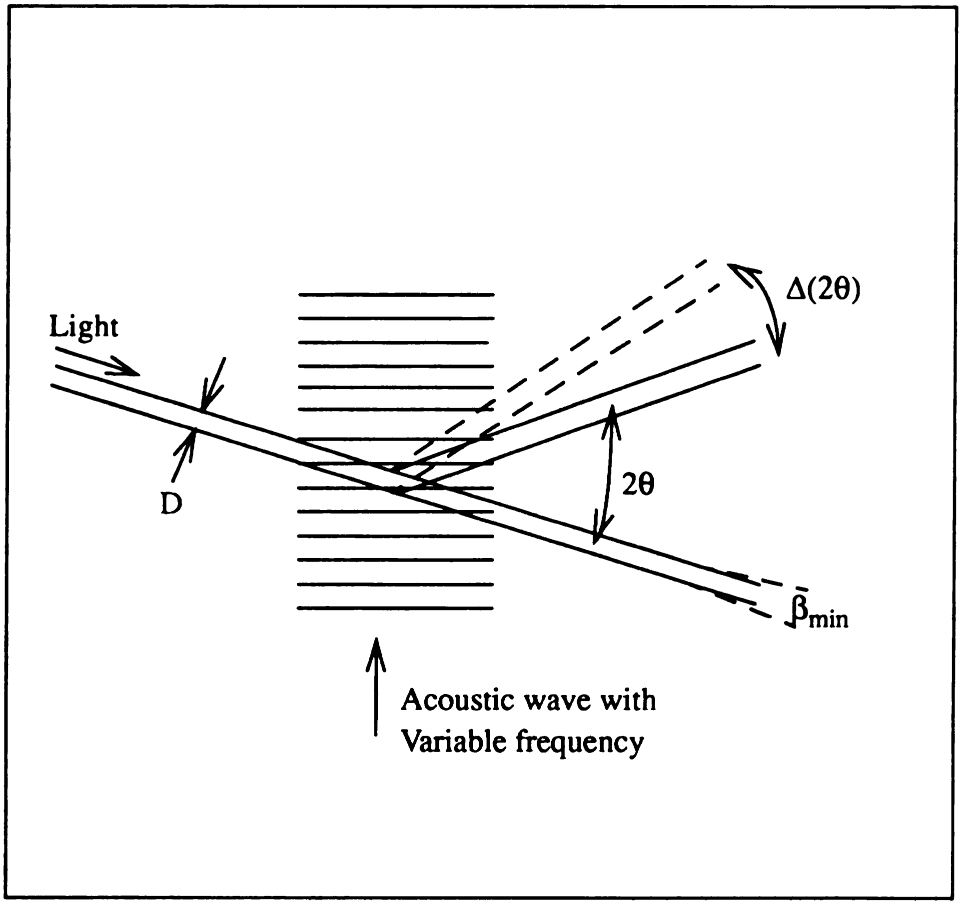

Figure 3.11 Deflected light by varying acoustic frequency.

This clearly shows that the second order Bragg diffraction provides twice as many resolvable spots when comparing with the first order diffraction. Even though, the second order gives a better deflected resolution, it is however that there exists a limitation on the number of resolvable spots. Since the diffraction efficiency of the second order diffraction is a function of the acoustic frequency and the optimal mode intensity which can only occur over a range of the acoustic frequencies, as a result the number of the resolvable spots is limited. For example, Fig. 3.10 shows that the range of acoustic frequencies which drive I_2 above 70% of $I_{2\max}$ are $f_{min} = 13.8\ MHz\ and\ f_{max} = 21\ MH,$ the band limit is then $\Delta f = 7.2\ MHz$. With one inch diameter light beam. the transit time is $\tau = 17.1us,$ thus the maximum number of resolvable spots is limited to $N_2 = 246$.

Angular resolution of the diffracted beam is another important feature of the interaction. Cohen and Gorden[32] probed the column of sound by varying the entrance angle of the incident light, and recorded the intensity of the diffracted light as a function of angular position. The result shows that the angular distribution of the diffracted light intensity is very similar to the distribution of power density in far-field diffraction pattern of the sound beam. Consequently, one can explore acoustic radiation patterns by the use of the Bragg diffraction. Our analysis shows that the second Bragg diffraction provides a better angular resolution than the first Bragg diffraction.

In the case of $Q = 13$, for example, Fig. 3.12(a) shows the mode distribution of I_1 and I_2 as a function of α. When comparing I_1 with I_2, both intensities are being optimized. The result shows that the 3 dB bandwidth of I_2 is much narrower than that of the I_1. In other words, the response of the second order mode is more sensitive to the angular variation of the incident light. When the interaction is used for imaging purpose, the second order mode should give a superior angular resolution.

In Figures 3.12(b), it is also observed that the narrowness of the I_2 response is proportional to the Q value. This can be explained as follows. Since the Q quantity is proportional to the frequency of the sound wave, when the frequency of the sound wave is raised, the wavelength becomes shorter, which in term will give a shorter equivalent slit spacing. Shorter slit spacing in light diffraction always give narrower interference pattern.

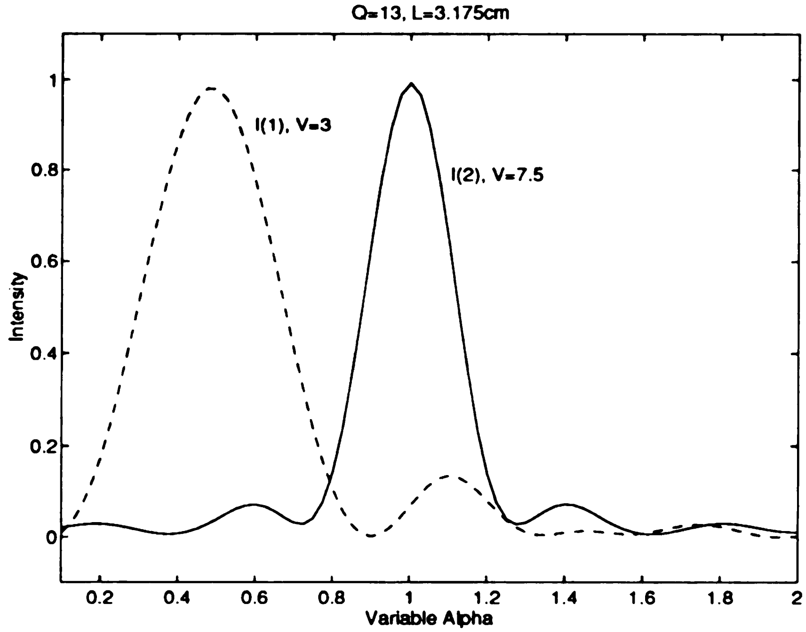

Figure 3.12(a) Light intensities versus α with Q=13.

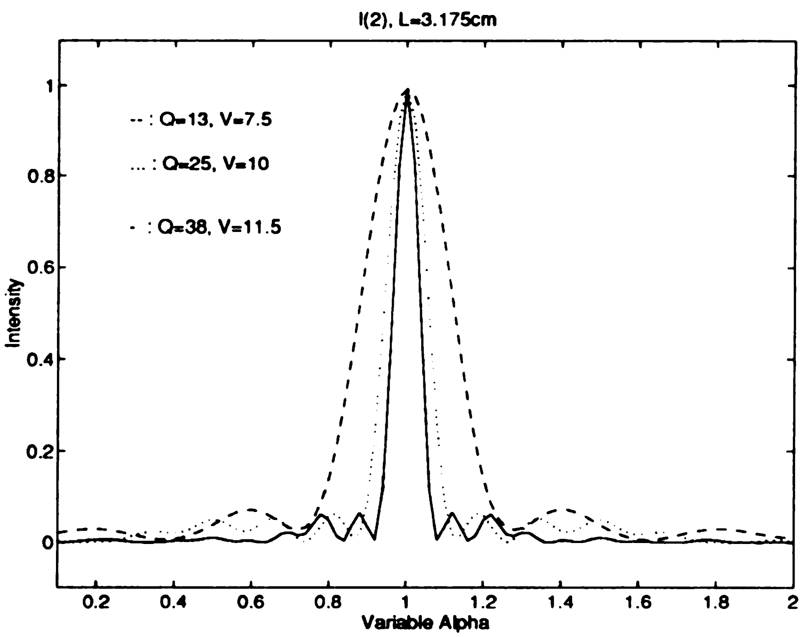

Figure 3.12(b) Second order light intensities versus Q, V and α.

Chapter 4

Criteria for Bragg Diffraction Effects in Acousto-Optic System

4.1 Introduction

Acoustic-light diffraction occurs when the acoustic waves diffract the light beam in a manner satisfying the Bragg diffraction law.[31]-[35] Such phenomenon has been utilized in the study of crystal structures by using X-rays. Strong intensity in a given portion of the diffraction is obtained only when the glancing angles of incidence ϕ and reflection θ are equal, as in mirror reflection, and when λ, Λ, and θ satisfy the Bragg law $m\lambda = 2\Lambda\sin\theta$ (λ and Λ are light and acoustic wave length, respectively, and m is the order of diffraction). In this chapter two types criteria for acousto-optic system will be discussed. One criterion analyzes the minimum requirement in acoustic frequency and acoustic beam size for satisfying the Bragg diffraction condition. Another criterion anatomizes the conditions for maximum second order Bragg diffraction.

4.2 Basic Formulation of Bragg Diffraction

Let us consider the destructive and constructive interferences of light rays passing through a plane acoustic beam in the same manner as has long been used in establishing the angular relations for Bragg diffraction of X-rays in crystals. In Fig. 2.3, it shows that Eq. (2-38) describes the condition for Bragg diffraction in the case of constructive interference, which can be expressed as follows:

$$m\lambda = 2\Lambda \sin\theta \tag{4-1}$$

In order to understand the phenomenon of constructive interference, we will go through the theoretical analysis. In Fig. 4.1, let the horizontal lines represent the acoustic wave fronts, space Λ apart, the solid line indicates the wave crest. The width of the acoustic field is L. Let the distance from A_1 to C_1 represents the wave front of the incident light beam, whose perpendicular rays $A_1\ A_2$, $B_1\ B_2$, etc., make the glance angle ϕ with the acoustic wave fronts. As the light rays pass through the acoustic beam, a small portion of the ray is assumed to be scattered at each acoustic wave front and the remainder pass undeviated to the next wave front. Next, let us consider only the light rays scattered in the specific direction $A_2\ A_3$, which makes the glancing angle θ with the acoustic wave fronts, and arrive later at a plane $B_3\ B_3''$ which is normal to all the rays. By considering light path lengths from the plane $A_1\ C_1$ to the plane $B_3\ B_3''$ we can find the conditions under which two or more rays will arrive in phase and thus give constructive interference of the light intensity in the θ direction. These conditions will be examined below.

First, let us consider any two scattering points A_2 and B_2 in the first wave front. The path length $A_1\ A_2\ A_3$ will be equal to the path length $B_1\ B_2\ B_3$ if $\theta = \phi$. For this condition, then, there will be constructive interference of all scattered rays. Next, consider the single incident light ray $B_1\ B_2$ which may be scattered from one or more acoustic wave fronts besides the first, at B_2, B_2', and B_2''. Thus, the scattered rays $B_2\ B_3$, $B_2'\ B_3'$, etc., will arrive in phase at the $B_3\ B_3''$ plane if the path length $B_1\ B_2\ B_3$ equals the path length B_1 $B_2'\ B_3'$, or if the difference in path length is $m\lambda$. When $\theta = \phi$, it satisfies the condition.

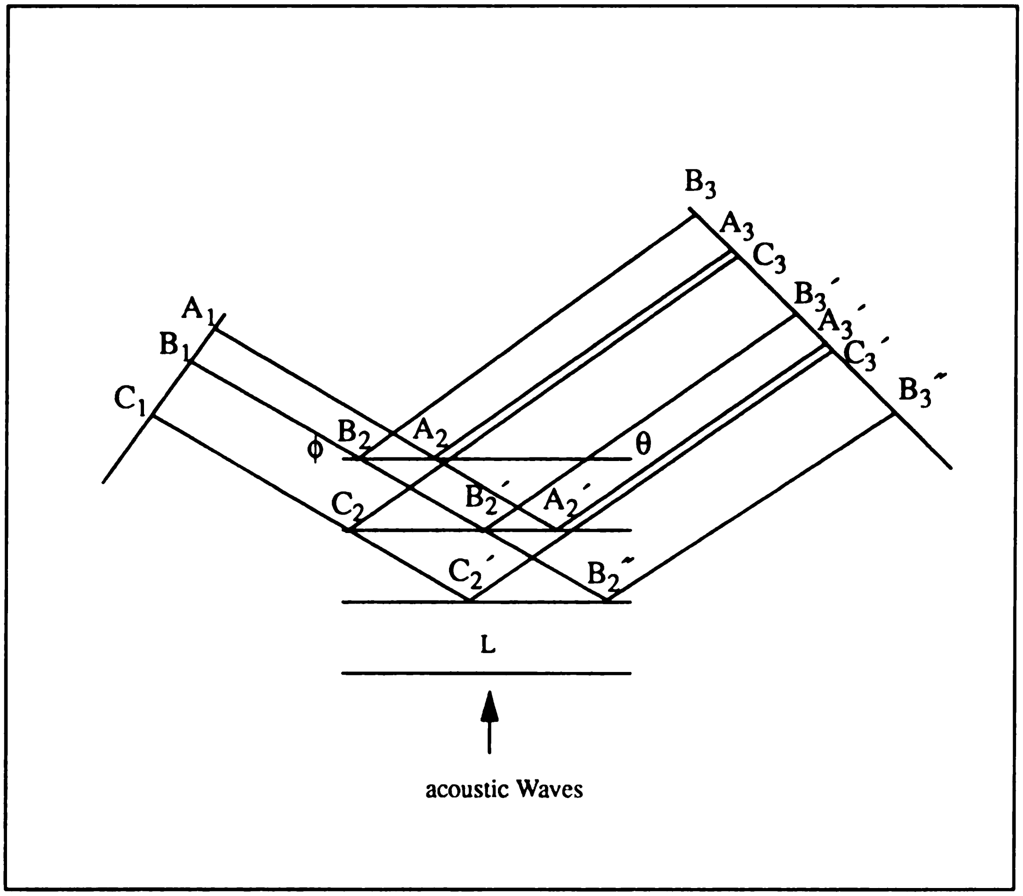

Figure 4.1 Bragg diffraction developed from path length consideration.

Reinforcement will occur in the direction θ defined by the relation. The more acoustic waves that a single light ray passes through, the more will be the reinforcement. As a result, the diffraction spectra will be more intense and sharper. Further, if a single light ray passes through fewer than two acoustic wave fronts, no reinforcement will occur, and hence no Bragg diffraction can exist.

4.2.1 Criteria for Bragg Diffraction

The Bragg diffraction occurs when incident the angle $\phi = \theta$ and $\sin\theta = (m\lambda_n)/(2\Lambda)$. It requires that the acoustic beam should be wide enough such that a single incident light ray may cross one wave length of the acoustic beam. Figure 4.2 shows that

$$\tan\phi = \frac{N\Lambda}{L} \tag{4-2}$$

where N is the number of acoustic wave fronts crossed by a light ray in traversing the acoustic beam. In order to obtain Bragg diffraction in a liquid medium, the incident angle should satisfy the following relationship,

$$\sin\phi = \frac{m\lambda_n}{2\Lambda} \tag{4-3}$$

where λ_n is light wave length within the liquid medium, $\lambda_n = \lambda/n_0$, and n_0 is the refractive index in the medium.

Since the angle ϕ is very small, both $\tan\phi$ and $\sin\phi$ can be approximated by ϕ. Then, we have

$$\frac{N\Lambda}{L} \cong \frac{m\lambda}{2\Lambda n_0} \quad . \tag{4-4}$$

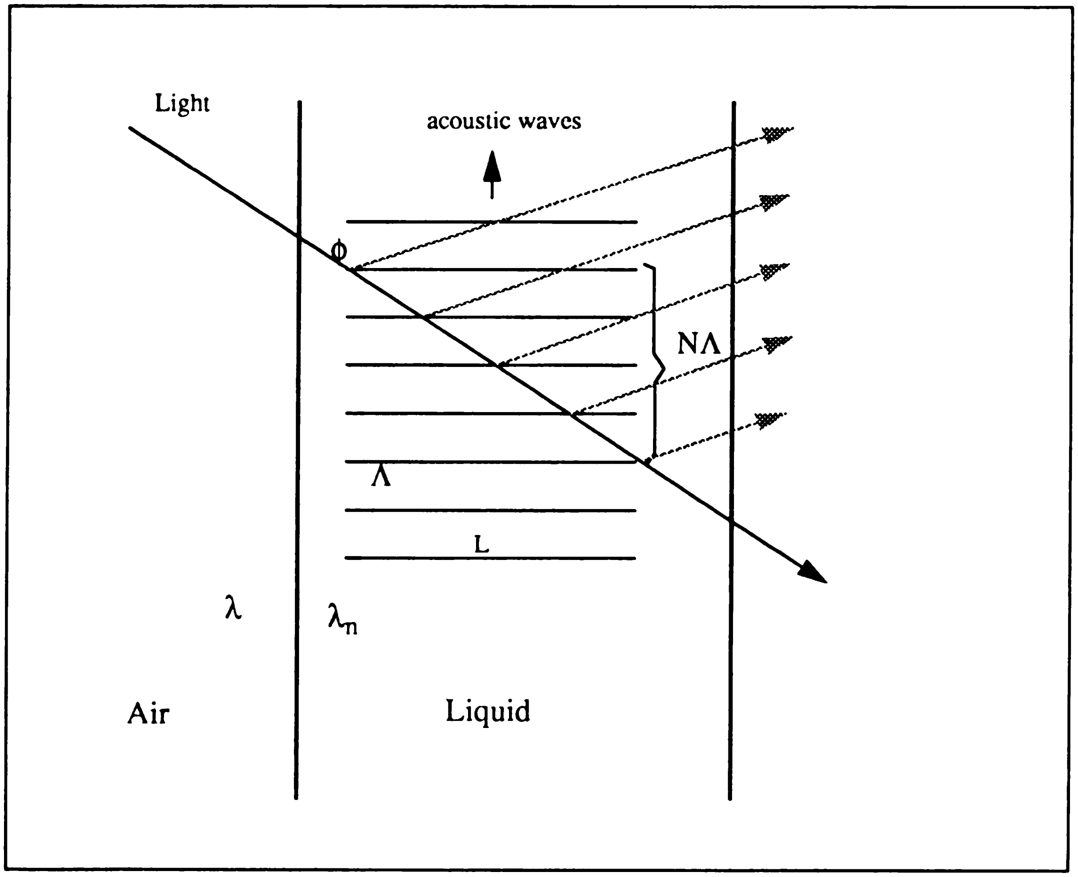

Figure 4.2 Schematic drawing of Bragg diffraction.

The acoustic wave length Λ is equal to υ / f, where υ is the velocity of acoustic beam within the liquid, and f is the acoustic frequency. Substitute υ / f into Eq. (4-4), we have

$$Lf^2 = \frac{2N\upsilon^2}{m\lambda} n_0 . \tag{4-5}$$

In Eq. (4-5), N must ≥ 1 in order to give Bragg diffraction. For acoustic beam in water, the refractive index $n_0 = 1.33$, and the velocity $\upsilon = 1.483 \times 10^5$ *cm / sec* (velocity in water at 20 °C). By using Helium-Neom light, $\lambda = 6.328 \times 10^{-5}$ *cm* and the acoustic beam width L in *cm*, Eq. (4-5) becomes

$$Lf^2 = 9.2447 \frac{N}{m} \times 10^{14}$$

The condition can be simplified by putting frequency in *MHz*. We have then

$$LF^2 = 924 \frac{N}{m} \tag{4-6}$$

where F is *MHz*.

Equation (4-6) is the criterion for Bragg diffraction in water, when the light source is a Helium-Neom laser. The integer m describes different order of diffractions.

For $m = 1$, the criterion for the first order Bragg diffraction becomes

$$LF^2 = 924N . \tag{4-7}$$

For $m = 2$ the criterion for the second order Bragg diffraction becomes

$$LF^2 = 462N . \tag{4-8}$$

It is clear that LF^2 must have the largest value for the first order Bragg diffraction and progressively lower value for the higher order modes. The first appearance of Bragg diffraction occurs when $N = 1$. The intensity of higher order mode can be normalized with respect to the first order mode (N=1) for comparison purpose. Geometrically, the factor N describes the number of acoustic wavelengths passed through by an undiffracted light ray in traversing the acoustic beam. Therefore, a greater sharpness is expected in all orders for larger N value. For various N values, Fig. 4.3 shows the distribution of the second order mode intensities by varying the incident angle. It can be seen that the 3dB bandwidth resolution with $N = 4$ is twice better than that with $N = 2$, while the resolution with $N = 6$ is thrice as good as that with $N = 2$. This result could be very useful to the acousto-optic Bragg imaging applications. It is estimated that the imaging resolution can be enhanced to twice as good when the acoustic frequency is raised from 17 MHz to 24 MHz. Judging from the results, the N value acts pretty much like a figure of merit. However, when N becomes too large, the further increase in N will not give marked improvement in sharpness of diffraction. This is because that there is little intensity left in the traversing light ray as it reaches the far side of the acoustic beam.

Another important factor for the interaction is m. From Eq. (4-6), different m value indicates different order of diffraction for a given LF^2 value. For given LF^2 value, for example f= 17 MHz and L = 3.175 cm, the second order has $N = 2$ while the first order has $N = 1$. Using the system setup mentioned above, Fig. 4.4 shows that the second order Bragg diffraction provides a sharper resolution than the first order. This implies that if we produce the same sharpness of diffraction in both the first and second orders, the acoustic frequency for exciting the first order diffraction is twice that for the second order. In experimental setup, lower acoustic operating frequency is preferred, since low frequency transducers are easier to be fabricated as well as low cost. However, good resolution still can be achieved by operating at low frequency, provided that second order diffraction is used.

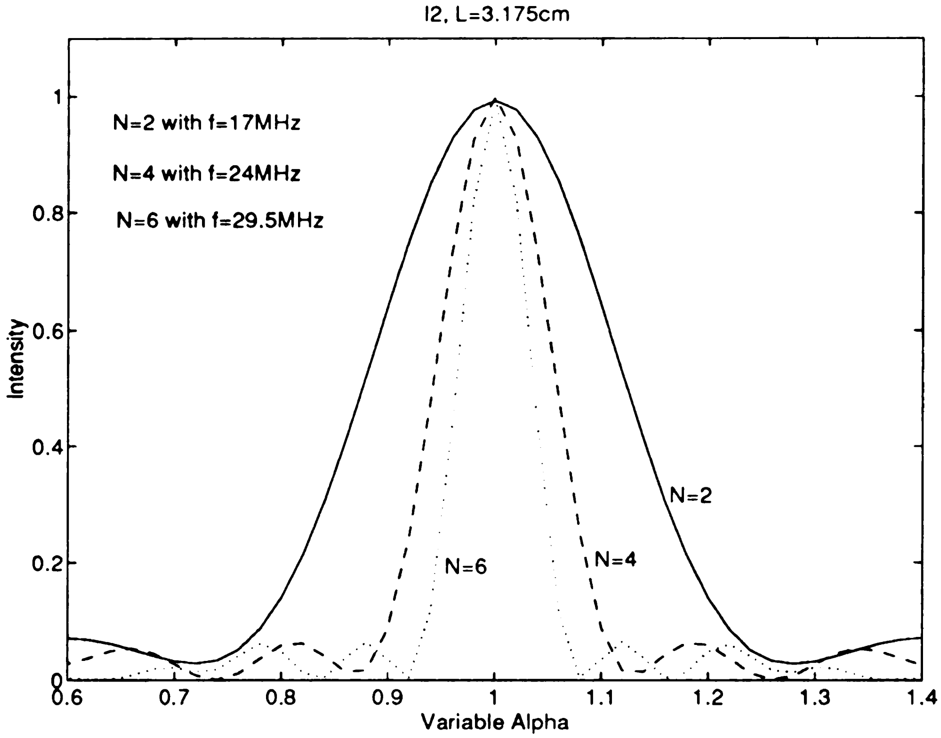

Figure 4.3 Second order light intensities versus with N as a parameter.

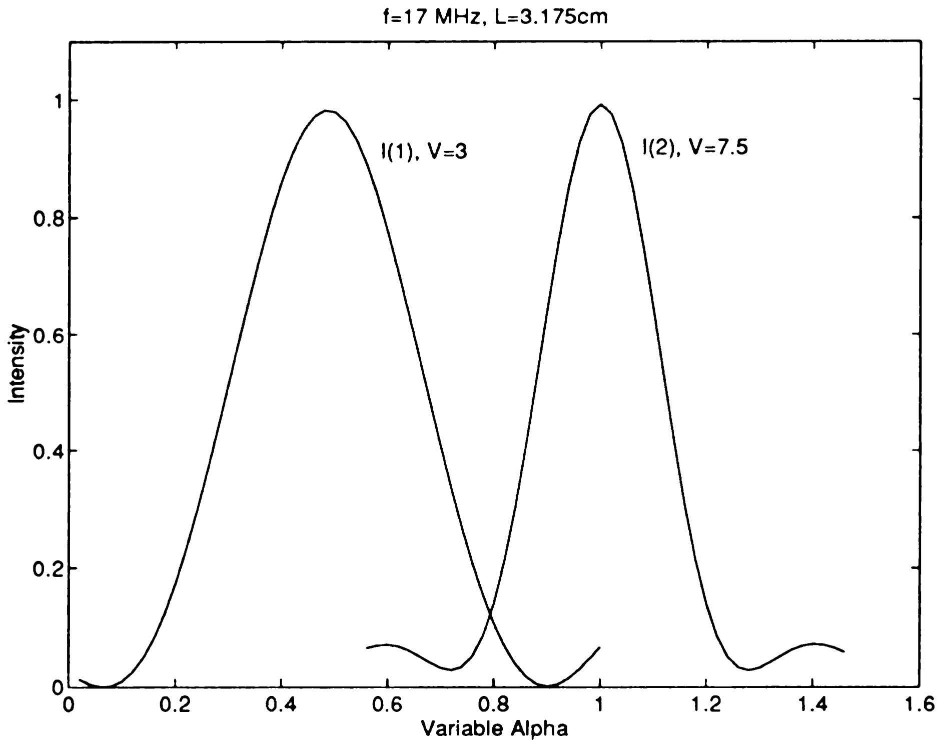

Figure 4.4 Light intensities versus α with $f = 17\ MHz$.

4.3 Criteria For The Second Order Bragg Diffraction

Although the incident angle of the light beam satisfies the double Bragg angle $\theta_{2B} = \lambda/\Lambda$, the intensity of the second order is usually rather weak. The second order diffraction intensity can be maximized by choosing an optimal set of system parameters. In this section, we will analyze the condition for optimum second order Bragg diffraction. With incident angle $\theta = \theta_{2B} = \lambda/\Lambda$, the diffraction intensities are

$$
\begin{aligned}
I_1 &= \left[\frac{2V}{\sigma}\sin\frac{\sigma}{4}\right]^2 I_{inc} \\
I_2 &= \frac{1}{4}\left[\left(\cos\frac{\sigma}{4} - \cos\frac{Q}{4}\right)^2 + \left(\frac{Q}{\sigma}\sin\frac{\sigma}{4} - \sin\frac{Q}{4}\right)^2\right] I_{inc}
\end{aligned}
\tag{4-9}
$$

where
$$
\sigma = \left(8V^2 + Q^2\right)^{\frac{1}{2}}
$$
$$
Q = \frac{k^{*2} L}{n_0 k \cos\theta}
$$
$$
V = \frac{k n_1 L}{\cos\theta} \quad .
$$

For maximum I_2, $\dfrac{dI_2}{dQ} = 0$.

The detailed derivation of $\dfrac{dI_2}{dQ}$ will be given in Appendix A.3. Taking the derivative of I_2 with respect to Q, we have

$$
\frac{dI_2}{dQ} = \left[\frac{Q}{\sigma}\sin\frac{\sigma}{4} - \sin\frac{Q}{4}\right]\left[\left(-\frac{1}{4}\right)\cos\frac{\sigma}{4} + \frac{1}{\sigma}\sin\frac{\sigma}{4} + \left(\frac{Q}{\sigma}\right)^2\left(\frac{1}{4}\cos\frac{\sigma}{4} - \frac{1}{\sigma}\sin\frac{\sigma}{4}\right)\right] \tag{4-10}
$$

For I_2 to be maximum, I_1 must be minimum. Ideally, for complete mode energy conversion, the first order mode should be vanished. In Eq. (4-9) if $I_1 = 0$ we need $\frac{\sigma}{4} = n\pi$.

Substitute $\frac{\sigma}{4} = n\pi$ into Eq. (4-10), it becomes

$$\frac{dI_2}{dQ} = \frac{1}{4}\sin\frac{Q}{4}\left[\cos\frac{\sigma}{4} - \left(\frac{Q}{\sigma}\right)^2\cos\frac{\sigma}{4}\right] \tag{4-11}$$

For $\frac{dI_2}{dQ} = 0$, $\sin\frac{Q}{4}$ must equal to zero, which requires that $\frac{Q}{4} = m\pi$. As a result, the conditions for I_2 maximum are $\frac{\sigma}{4} = n\pi$ and $\frac{Q}{4} = m\pi$. Since σ is related to Q and V we need to consider the following cases.

Case 1. $\frac{\sigma}{4} = n\pi$, $\frac{Q}{4} = m\pi$, and m = even.

With m = even and $\frac{\sigma}{4} = n\pi$, Eq. (4-9) becomes

$$I_2 = \frac{1}{4}(\cos n\pi - 1)^2 \tag{4-12}$$

For I_2 maximum, $\cos n\pi$ must be (-1), therefore, we need n to be odd, or let

$$\frac{\sigma}{4} = (2n-1)\pi \tag{4-13}$$

where n = 1, 2, 3,....

Since $\sigma = \left(8V^2 + Q^2\right)^{1/2}$ and $\frac{\sigma}{4} = (2n-1)\pi$, we can obtain the corresponding V value as follows:

$$4(2n-1)\pi = \left(8V^2 + Q^2\right)^{1/2}$$

With $Q = 4m\pi$, we have

$$V = \sqrt{2}\pi\left[(2n-1)^2 - m^2\right]^{1/2} \qquad (4\text{-}14)$$

For $V > 0$, we need $n \geq \frac{m+1}{2}$.

For example, When $m = 2$ and $n = 2$

$$Q = 4m\pi = 25.13$$

$$V = \sqrt{2}\pi\left[(2n-1)^2 - m^2\right]^{1/2} \cong 10$$

This result confirms with the numerical solution of the optimum parameter set (Q=25, V=10) which excited the second order Bragg diffraction to maximum diffraction.

Case 2. $\frac{\sigma}{4} = n\pi$, $\frac{Q}{4} = m\pi$, and m = odd.

With m = odd and $\frac{\sigma}{4} = n\pi$, Eq. (4-9) becomes

$$I_2 = \frac{1}{4}(\cos n\pi + 1)^2$$

For I_2 to be maximum, $\cos n\pi$ must be 1, therefore, we need n to be even, or let

$$\frac{\sigma}{4} = 2n\pi$$

where n = 1, 2, 3,....

If we substitute $\frac{\sigma}{4} = 2n\pi$ into $\sigma = \left(8V^2 + Q^2\right)^{1/2}$, we can obtain V as follows:

With $Q = 4m\pi$, and $\sigma = 8n\pi$, we have

$$V = \sqrt{2}\pi\left[(2n)^2 - m^2\right]^{1/2} . \tag{4-15}$$

For $V > 0$, the requirement becomes $n \geq \frac{m}{2}$.

For example, when $m = 1$ and $n = 1$

$$Q = 4m\pi \cong 13$$

and

$$V = \sqrt{2}\pi\left[(2n)^2 - m^2\right]^{1/2} \cong 7.7$$

Also, for $m = 3$ and $n = 2$

$$Q = 4m\pi \cong 38$$

and

$$V = \sqrt{2}\pi\left[(2n)^2 - m^2\right]^{1/2} \cong 11.75$$

Again, these results confirm with the optimum parameter sets of (Q=13, V=7.5) and (Q=38, V=11.5).

Finally, we can conclude that for the second order Bragg diffraction to occur, the Q and V values must satisfy the following conditions:

$$Q = 4m\pi$$

$$V = \begin{cases} \sqrt{2}\pi\left[(2n-1)^2 - m^2\right]^{1/2} & \text{for m = even and } n \geq \frac{m+1}{2} \\ \sqrt{2}\pi\left[(2n)^2 - m^2\right]^{1/2} & \text{for m = odd and } n \geq \frac{m}{2} \end{cases} . \tag{4-16}$$

Both m and n are integers.

In terms of physical quantities the Q value can be expressed as

$$Q = \frac{k^{*2} L}{n_0 k \cos\theta_{2B}} = 4m\pi . \tag{4-17}$$

The wave numbers of acoustic wave and light beam are $k^* = (2\pi)/\Lambda$ and $k = (2\pi)/\lambda$ respectively. Substituting k^* and k into Eq. (4-17), we have

$$m = \frac{L\lambda}{2\Lambda^2 n_0 \cos\theta_{2B}} . \tag{4-18}$$

The wavelength of the acoustic wave is $\Lambda = \upsilon/f$, where f is the frequency of the acoustic wave and υ is the wave velocity in liquid. The condition in Eq. (4-17) can be alternately stated as

$$m = \frac{Lf^2\lambda}{2n_0\upsilon^2 \cos\theta_{2B}} . \tag{4-19}$$

In addition to the necessary second order Bragg condition, an auxiliary condition, Eq. (4-19) has to be satisfied for an effective excitation of the second order mode with a pure sinusoidal grating. Notice that this auxiliary condition is completely independent of index modulation. For a given L, λ, and n_0, the above condition implies that the second order mode can be effective excited only for discrete grating frequencies.

The auxiliary condition, Eq. (4-19), is by no mean contradictory to the Bragg diffraction condition given by Eq. (4-5). This can be shown as follows. Rewriting the Eq. (4-19), we have

$$Lf^2 = \frac{2n_0 v^2 m \cos\theta_{2B}}{\lambda} \quad . \tag{4-20}$$

In the experimental setup, the light source is a He-Ne laser and water is used as interacting medium. The wavelength of the laser beam is 632.8 nm, the velocity of the acoustic wave in water is 1.483×10^5 cm / sec, and the refractive index in water is 1.33. For $m = 1$, which gives $Q = 4\pi = 13$, Eq. (4-20) becomes

$$Lf^2 \cong 924.5 \times 10^{12} \ \ cm \times Hz^2 \tag{4-21}$$

The criterion for the second order Bragg diffraction in Eq. (4-8) is then $LF^2(cm \times M^2Hz) =$ 462 N. Therefore, for $Q = 13$ and the LF^2 product above, it has $N = 2$ which is larger than the minimum requirement of $N \geq 1$ in Eq. (4-8). This means that in an acoustic-optic system, if the criterion for optimizing the second order Bragg diffraction is satisfied, then the criterion for Bragg diffraction is automatically satisfied.

From the definition of $V = \dfrac{kn_1L}{\cos\theta_{2B}}$, for a given m value, one can choose n_1 to satisfy Eq. (4-16). Since n_1 relates to the pressure of the transducer, one can adjust the acoustic power output to furnish the required pressure.

Chapter 5

Experimental Measurements for Bragg Diffraction

5.1 Introduction

In this chapter, the experimental setup and the measurement procedures are described, and the experimental findings for verifying the Bragg diffraction are presented. The experimental verifications include the intensity distribution of the diffraction mode with various acoustic amplitudes, acoustic frequencies and incident angles of the light beam. The results show that when the incident angle equals to twice of the Bragg angle, the second order diffraction can be exited to its maximum intensity at several particular sets of system parameters. Comparing the angular sensitivity of the diffraction modes, the second order diffraction provides a sharper angular resolution than the first order mode. In general, the experimental results agreed with the theory qualitatively.

5.2 Experimental Measurement System

A proto-type system for observing the acousto-optical interaction has been designed and constructed at the MSU Ultrasonic Laboratory. The acoustic wave is generated in water which diffracts the incident laser beam. The full range of Bragg diffraction can easily be observed at a range of acoustical frequencies (6 to 30 MHz). The coherent light source provides a well collimated beam for the interaction. A block diagram of the measurement setup is depicted in Fig. 5.1(a). The acoustic cell shown in Fig. 5.1(b) is made of a plexiglass measuring $27 \times 10 \times 13$ cm. A quartz transducer is mounted on one side of the acoustic cell. Four different transducers are used in this experiment. The transducers have a fundamental frequency of 5.8 MHz, 8.8 MHz, 17 MHz and 20 MHz respectively, but they can also be excited at their odd harmonics.

The acoustic signal is generated from a R.F. generator (Model 191 constant amplitude signal generator TEKTRONIX, Inc.), and then amplified by a R.F. power amplifier (Model 310L ENI Inc.) to attain a maximum power of 15 watts before triggering the transducer. The diffraction output is detected by a photo detector (Model 115-9) and power meter (Model 40 optometer made by United Detector Technology). A rotator which supports the acoustic cell is used to vary the angle between the incident light and acoustic beam. The laser source is a 20 mW He-Ne laser. An acoustic absorber is placed at the end of the acoustic cell, therefore, all of the transmitted acoustic signal after the interaction region will be completely absorbed such that no standing wave exists in the interaction region. The transducer is placed on one end of the cell. Since the transducer is submerged in water, the heat generated by the transducer during high power operation will be diffused by the water without overheating the transducer.

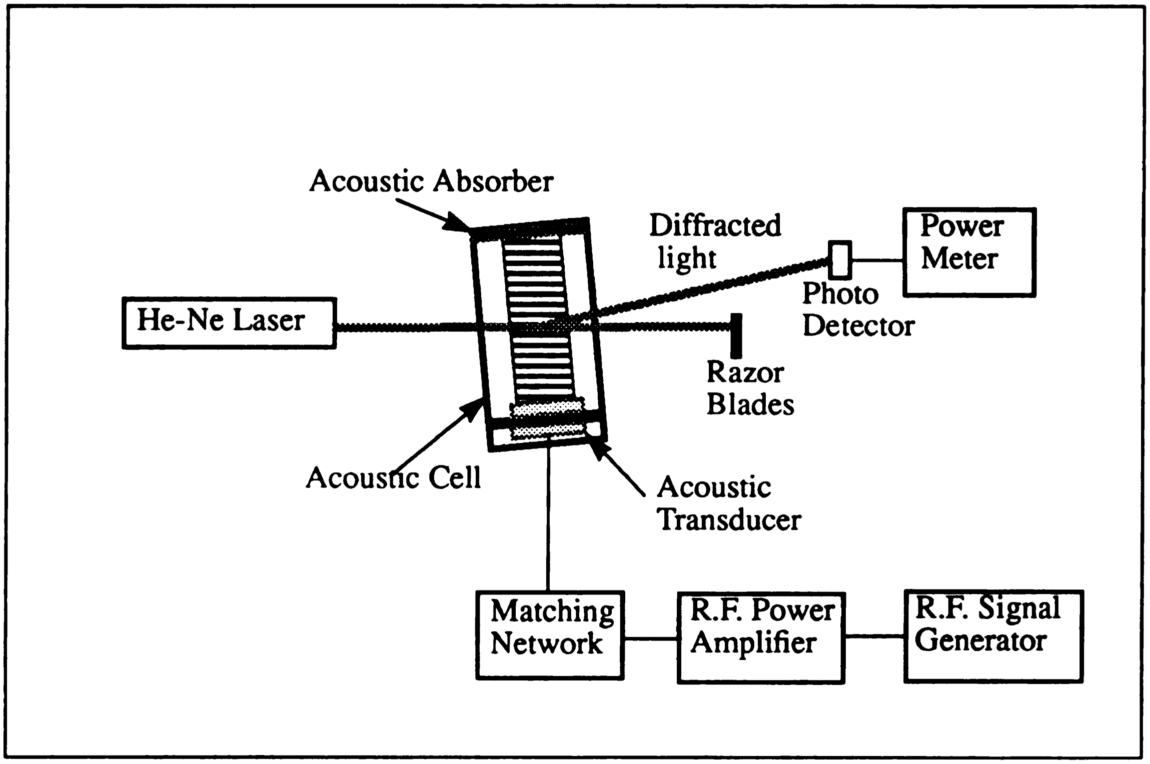

Figure 5.1(a) Block diagram of the measurement system.

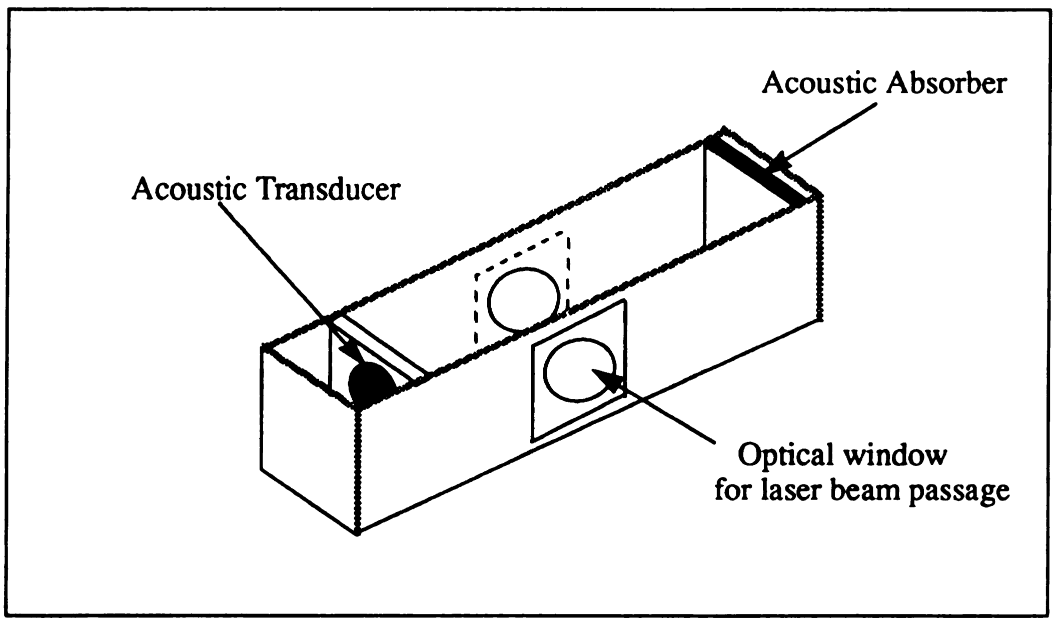

Figure 5.1(b) A plexiglass water tank for observing acousto-optical interaction.

5.2.1 Network for Acoustic Impedance Matching

Since the impedance of acoustic transducer and the output impedance of the r.f. power amplifier vary as function of operating frequency, to maximize the acoustic output of a acoustic beam it is necessary to match the impedance between the transducer and the r.f. power amplifier by using a matching network. Figure 5.2(a) shows an electrical representation of the acoustic transducer. The capacitance C_0 is the transducer capacitance and R_a is the real part of the impedance which represents acoustic power flow into the medium. The technique of impedance matching of acoustic transducer is well reported [37]~[39]. A T-matching network shown in Fig. 5.2(b) is chosen to put between the transducer and the power amplifier. There are many possible ways to match the acoustic system, however the reason for choosing the T-matching network is as follows. The theory of matching networks[40] states that only two reactive elements are required to match the input and output resistances of two interfacing system. But, one needs to add a third element. The reason is that one element of the T-matching network can be assigned a value arbitrarily, and the other two components can be determined accordingly. From such a T-matching network, it is rather easy to accomplish the matching at hand. Since we have several transducers that need to be matched to the r.f. power amplifier over a wide range of operating frequencies a simpler and more flexible matching network should be used. The T-matching network can provide the functions required for the acousto-optics system. A T-matching network (Made T-1000, Tucker Electronics Inc.) is used in our experiment. By using the T-1000 matching network, the power transferred to the acoustic transducer can reach 75% ~ 85% of the input power. On the other hand, only 25% ~ 35% of input power is transferred to the acoustic transducer, if the matching network is not used. For such a poor transmitting efficiency, the eventual interaction would be too weak to be observed.

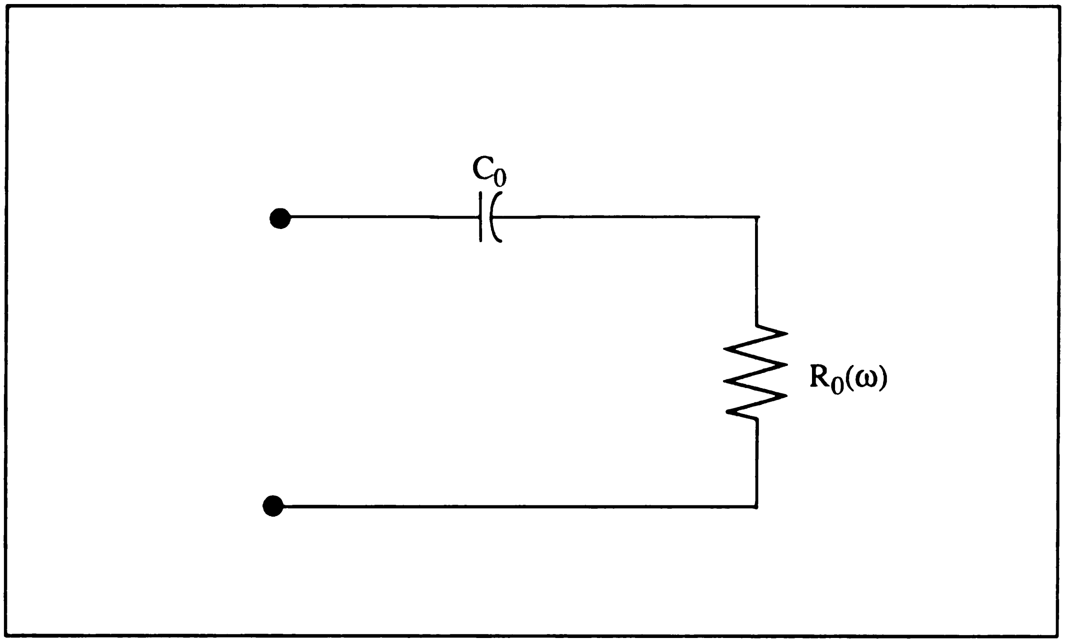

Figure 5.2(a) Electrical equivalent circuit of the acoustic transducer.

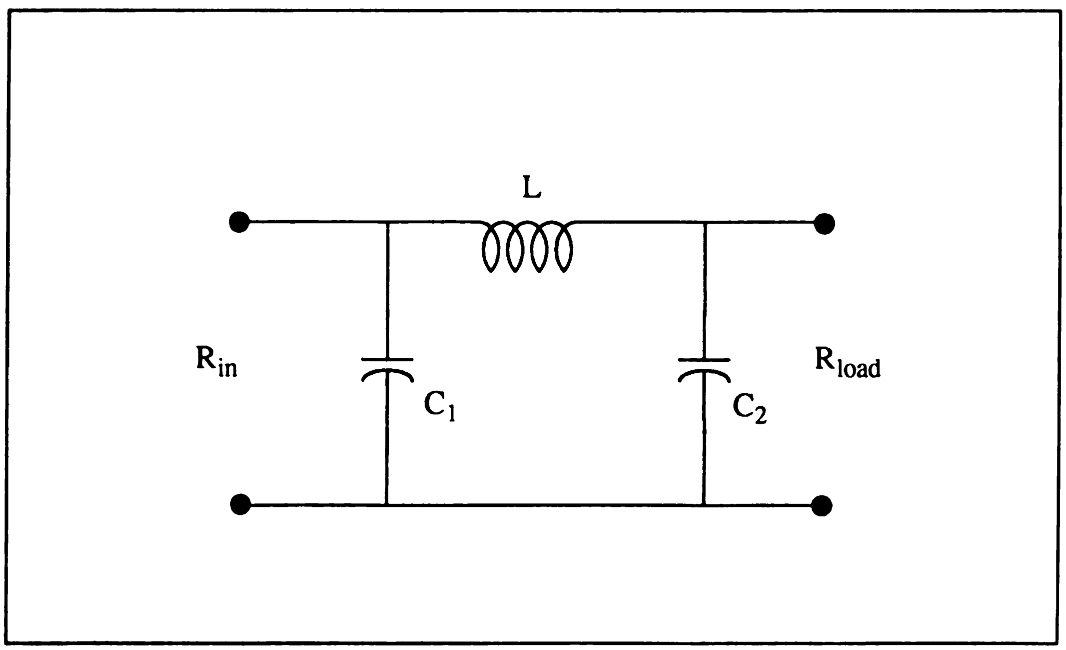

Figure 5.2(b) T matching network.

5.3 Experimental Results

Several experiments were performed to verify the simulation results obtained in chapter 3. The pure sinusoidal grating was established by an acoustic transducer, while the incident light source is from a He-Ne laser. For the sake of comparison of various mode intensities, the measured irradiance of each mode is normalized with respect to the total transmitted irradiance.

Experiments were performed in a way that the results can be compared with the theory developed. To make quantitative comparison, the gratings were established by different acoustic transducers. In the experimental setup, the wavelength of the laser beam is $\lambda = 6.328 \times 10^{-5}\ cm$, the acoustic velocity in water is $v = 1.483 \times 10^{5}\ cm / sec$ and the refractive index in water is $n = 1.33$. With these parameters, the Q value is found to be

$$Q = 1.359 \times 10^{-14} \cdot f^2 \cdot L \tag{5-1}$$

where f is the acoustic frequency and L is the width of the acoustic beam.

5.3.1 Bragg diffraction with various V and Q value

The first experiment was performed to observe the maximum diffraction as a function of V value. An acoustic transducer, which operates at a fundamental frequency of 5.8 MHz with 2.54 cm beam width, was driven at its third harmonic of 17.4 MHz. With f = 17.4 MHz and L = 2.54 cm, the Q value becomes 10.5. Using this setup with the double Bragg incident angle $\alpha = 1$, Fig. 5.3(a) shows the diffraction efficiency with various intensities of the acoustic beam. In Fig. 5.3 the solid curve represents the theoretical result, while the "o" curve indicates the experimental result. A separate experiment was performed by using an acoustic transducer having a fundamental frequency of 17 MHz and 3.175 cm beam width. With an acoustic frequency of 17 MHz and beam width of 3.175

cm, the Q value becomes 12.5. Included in Fig. 5.3(b) are the theoretical and experimental results for Q = 12.5. It can readily be seen that the experiment result of the second order mode is a function of V. For Q = 12.5 and V approaching to 6.5 the second order diffraction reaches a maximum.

It can generally be said that the experimental results agree with the theory well. The experimental result of the first order diffraction is very close to the theoretical prediction which shows that the intensity starts decreasing when the incident angle is approaching twice of the Bragg angle. The intensity of the second order is 30% lower than we expected. This could due to surface reflection on the imperfection of the experimental setup. However, it is strong enough for practical application.

The next experiment was performed to observe the maximum diffraction of the second order interaction as a function of Q. It is more difficult to observe the diffraction in various Q values, since this experiment needs a wide range of acoustic frequencies to provide different Q values and we have only a limit of transducers available. However, each transducer can still be driven over a narrow range frequencies around its central frequency, enough data were collected to show the diffraction effects. However for each frequency we need to compensate the diffraction intensity by power spectrum distribution of the individual transducer. Figure 5.4(a) shows the experiment result of the first order diffraction with various Q values. Since the Bragg angle is a function of the acoustic wavelength, for each acoustic frequency the Bragg angle will be different. Therefore, at each Q value, the incident angle was optimized to achieve maximum diffraction in the first order interaction. The result indicates that when Q is large, the first order diffraction becomes very efficiency. This means that higher acoustic frequency and wider acoustic beam provide higher diffraction efficiency in the first order Bragg diffraction.

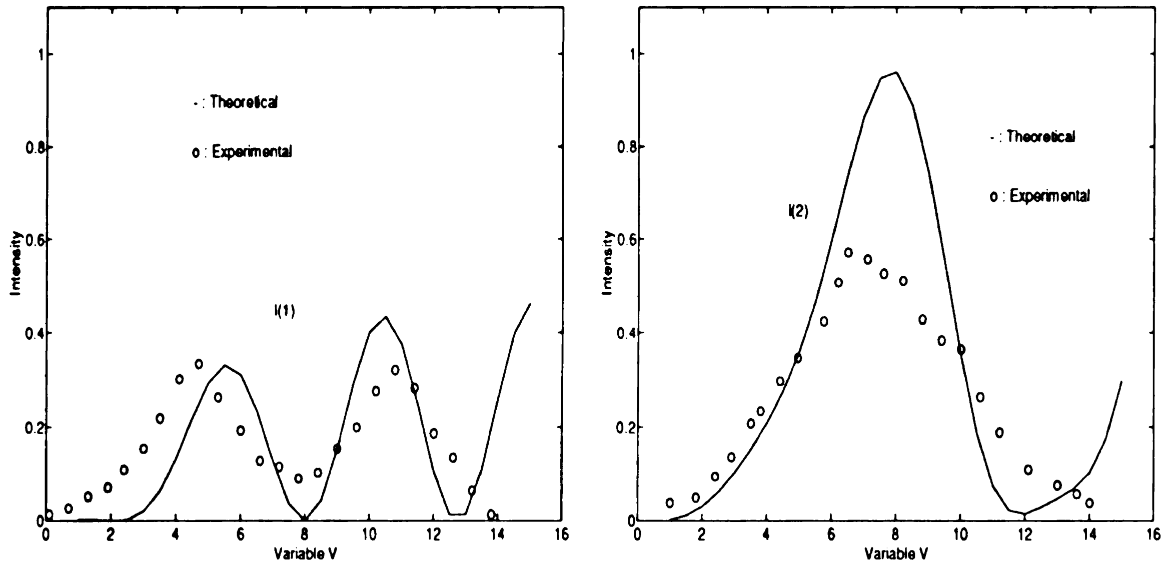

Figure 5.3(a) First and Second order diffraction intensities versus V at double Bragg angle with $Q = 10.5$.

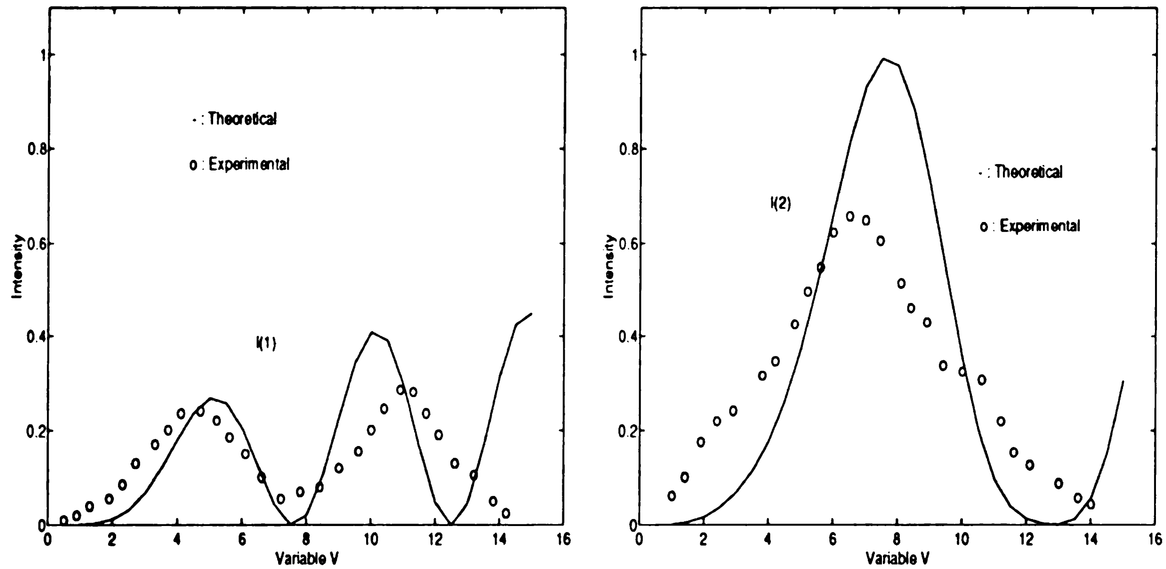

Figure 5.3(b) First and Second order diffraction intensities versus V at double Bragg angle with $Q = 12.5$.

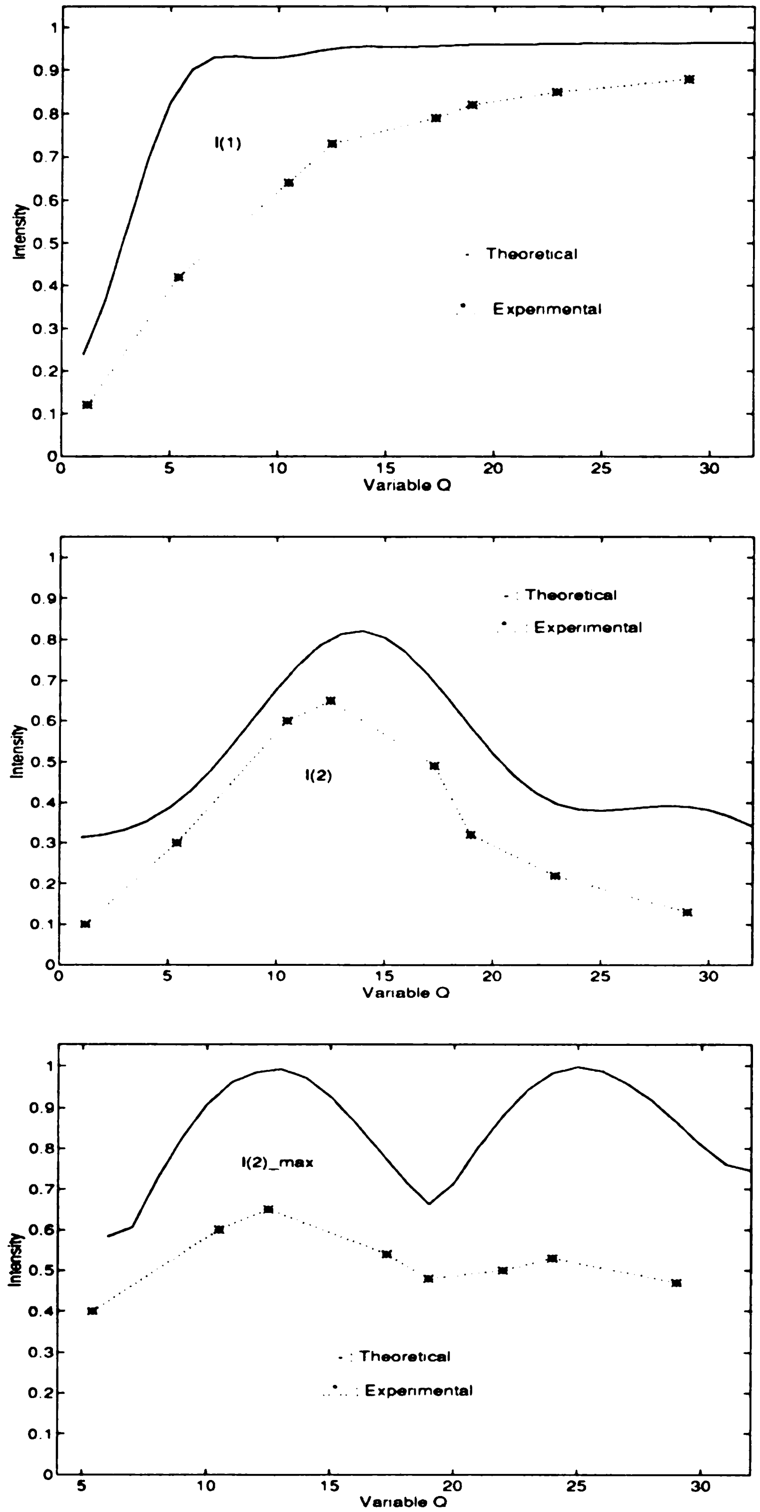

(a)

(b)

(c)

Figure 5.4 (a) The First order diffraction versus Q with $V = 3$ and $\alpha = 0.5$. (b) The second order diffraction versus Q with $V = 6.5$ and $\alpha = 1$. (c) At each Q the acoustic amplitude was optimized to achieve maximum power in the second order with $\alpha=1$.

For the second order diffraction, the experiment result shown in Fig 5.4(b) illustrates that the maximum diffraction efficiency is very sensitive to the Q values. In this experiment the V value is set to 6.5 and the incident angle is optimized to $\alpha = 1$. The diffraction I_2 is driven to maximum when Q approaches 12.5.

From the theoretical prediction in Fig. 3.5(c), the maximum diffraction I_2 is also related to the intensity of acoustic beam V. Therefore, we repeated the experiment with optimizing the acoustic amplitude to achieve maximum power in the second order at each Q, and the result is shown in Fig. 5.4(c). The experiment result indicates that when incident angles are at double of the Bragg angle, the second order diffraction becomes very strong. Unlike the first order, the maximum second order mode only appears in certain Q values which can be obtained by adjusting the acoustic frequency and beam width. A rough check confirmed that the criterion of the Q value for the maximum second order is very close to $Q = 4m\pi$ (m is integer).

5.3.2 The Bragg diffraction with various incident angle

In this section, the experiments describe the diffraction modes with different incident angles. An acoustic transducer with Q =12.5 (17 *MHz* acoustic frequency and 3.175 *cm* acoustic beam) was used in the experiments. The acoustic amplitude was optimized to obtain the maximum diffraction in the first and second order mode. With the frequency f = 17 *MHz* and the velocity of acoustic wave in the water $v = 1.483 \times 10^5$ *cm / sec*, the wavelength of the acoustic wave is 8.72×10^{-3} *cm*. With these physical parameters, the theoretical Bragg angle θ_B is predicted to be 0.208 °, and the double Bragg angle θ_{2B} equals to 0.416 °. From the definition $\alpha = \frac{k}{k^*} \cdot \sin\theta$, the α equals to 0.5 for $\theta_B = 0.208$ °, and equals to 1 for $\theta_{2B} = 0.416$ °. Figure 5.5(a) shows the intensity distribution of the first order with various α. From the experiment result, when the incident angle approaches 0.185° (equivalent to $\alpha = 0.44$), the first order diffraction is driven to maximum intensity. The Bragg angle θ_B used in the experiment is very close to the theoretical Bragg angle.

Figure 5.5(b) indicates that the incident angle which drives the second order diffraction to maximum power is 0.371° (equivalent to $\alpha = 0.88$). The value of the double Bragg angle found in the experiment also closely confirmed with the theoretical prediction. Observing the experiment result of the first and second order shown in Fig. 5.5(c), the response of the second order diffraction is more sensitive to the angular variation of the incident light. For imaging application purpose, the second order diffraction should provide a better angular resolution than the first order diffraction.

From the experimental results, we can conclude that when the incident angle equals to twice of the Bragg angle, with proper system setup, the second order diffraction can be strongly excited and a better angular resolution can be achieved. The limitation of the second Bragg diffraction is that only certain optimum parameter sets in the system setup can provide the maximum diffraction. But for the first Bragg diffraction when Q is large enough, the first order diffraction can always be excited to its maximum intensity.

Another interest property of diffraction observed is that the angular sensitivity of the diffraction is proportional to the Q values. Three Q values, 5.8, 12.5 and 19 were used to check this property. Figure 5.6 shows the intensity distribution of the first order mode with various α values. In order to compare the mode intensity distribution, the maximum diffraction of each data set is normalized to unity and the location of the peak value is shifted to $\alpha = 0.5$. The result shows that the 3 dB bandwidth of I_1 for $Q = 19$ is only one third of the bandwidth of I_1 for $Q = 5.8$. With this property, the Bragg diffraction can provide a higher angular resolution in large Q values. A rough check confirmed that the second order Bragg diffraction also have the same property.

(a)

(b)

(c)

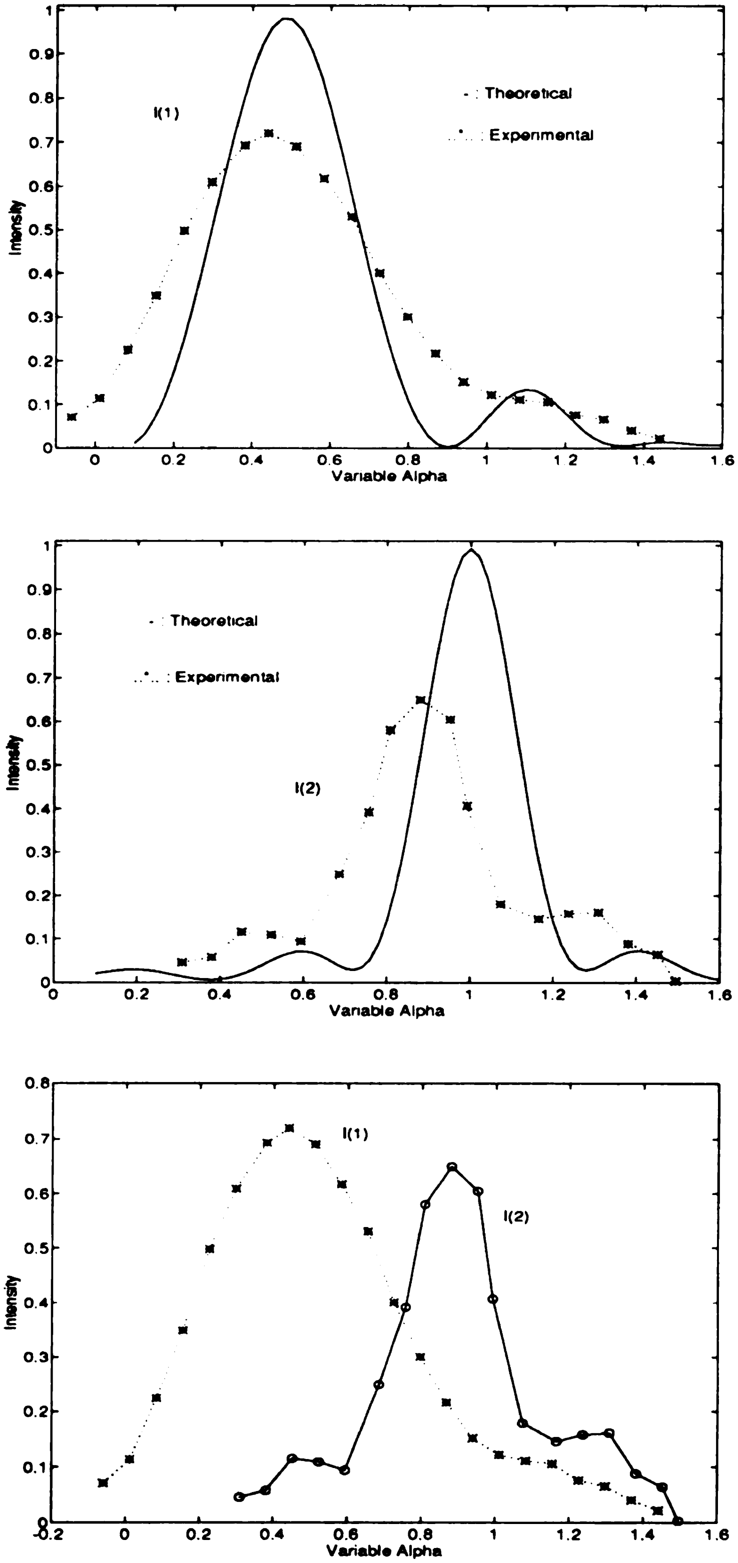

Figure 5.5 (a) The First order diffraction versus α with Q = 12.5.
(b) The second order defloration versus α with Q = 12.5.
(c) The comparison of the angular sensitivity to the diffractions with various α.

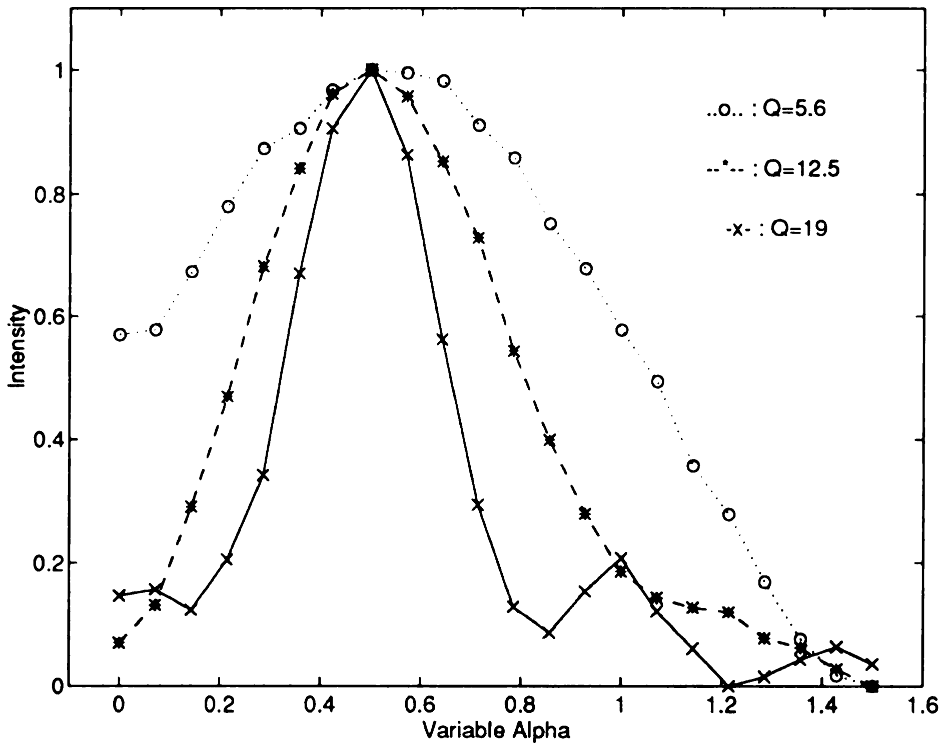

Figure 5.6 The first order light intensities versus α with Q = 5.6, 12.5 and 19.

All experiments we performed were up shifted interaction. This means that the incident angle between light beam and the normal of the acoustic beam has positive value, and the diffractions appear in plus order diffraction. For the incident angle is negative, the diffractions are down shifted interaction, and minus order diffraction will appear strong. All the down shifted interactions will be symmetrical to the up shifted interactions.

Chapter 6

Application of Acousto-optic Interaction

6.1 Introduction

From previous discussion it is clear that an acoustic cell may be used to modulate light by applying Bragg diffraction theory. In recent years, many Bragg diffraction applications have been investigated, including acousto-optic modulation, Bragg diffraction imaging, optical signal processing, television projection, light deflection, frequency shifting, the guided wave effect, acoustic velocity measurement, Q switching, and mode locking in lasers.[41]-[59] Some products are already on the market. Newport Electro-optics Systems Inc. offers acousto-optic (AO) modulators, AO beam deflectors, AO mode lockers, a Q-switching system, and a 2-D beam projector all based on Bragg diffraction theory. However, most of the applications utilize the first Bragg diffraction. By applying the second Bragg diffraction, greater resolution can be achieved.

In this chapter a Bragg diffraction imaging system was designed and performed. Imaging resolution for the first and second orders are observed. Imaging quality for different acoustic frequencies and beam widths are compared.

6.2 Acoustic Imaging base on the Bragg Diffraction

One useful application of Bragg diffraction is the acoustic imaging. The technique of acoustic visualization has potential applications in nondestructive testing of materials and medical diagnostics.[60] Korpel[61]-[64] was the first to show that acoustic Bragg diffraction possesses image-translation properties. The basic diffraction imaging method was also independently developed by Tsai[65]-[67], and Wade[68]-[69] for different applications. It is possible to use pulsed sound and pulsed light sources to improve the usefulness of Bragg diffraction imaging by providing range gating to achieve the depth discrimination.[70]

A brief description of Bragg imaging theory is given below. Figure 6.1 shows that the interaction between the waves emanating from a point source ***S*** of single frequency sound and a point source ***O*** of monochromatic light produces diffracted light that appears to come from a point ***O'***; a virtual image of the sound sources but one that is visible to the eye. For a number of sound sources S_1, S_2, S_3, etc., the virtual image points O_1', O_2', O_3', etc., form a corresponding pattern. In this translation process, amplitude ratios and phase angles are preserved and an acoustic field is transformed into an equivalent optical field.

For the first order Bragg diffraction imaging, the angle between incident light ray and acoustic beam equals the Bragg angle θ_B, and it may also be shown that *OSO'* is an isosceles triangle with apex angle equal to $2\theta_B$. This affords a convenient construction for locating virtual images which has been used in Fig. 6.1 in order to illustrate the image transformation properties. As θ_B is usually a small angle, we can see that the imaging involves a rotation of close to 90^o. This is the reason why with this technique it is very convenient to obtain an image of a cross section perpendicular to the propagation direction

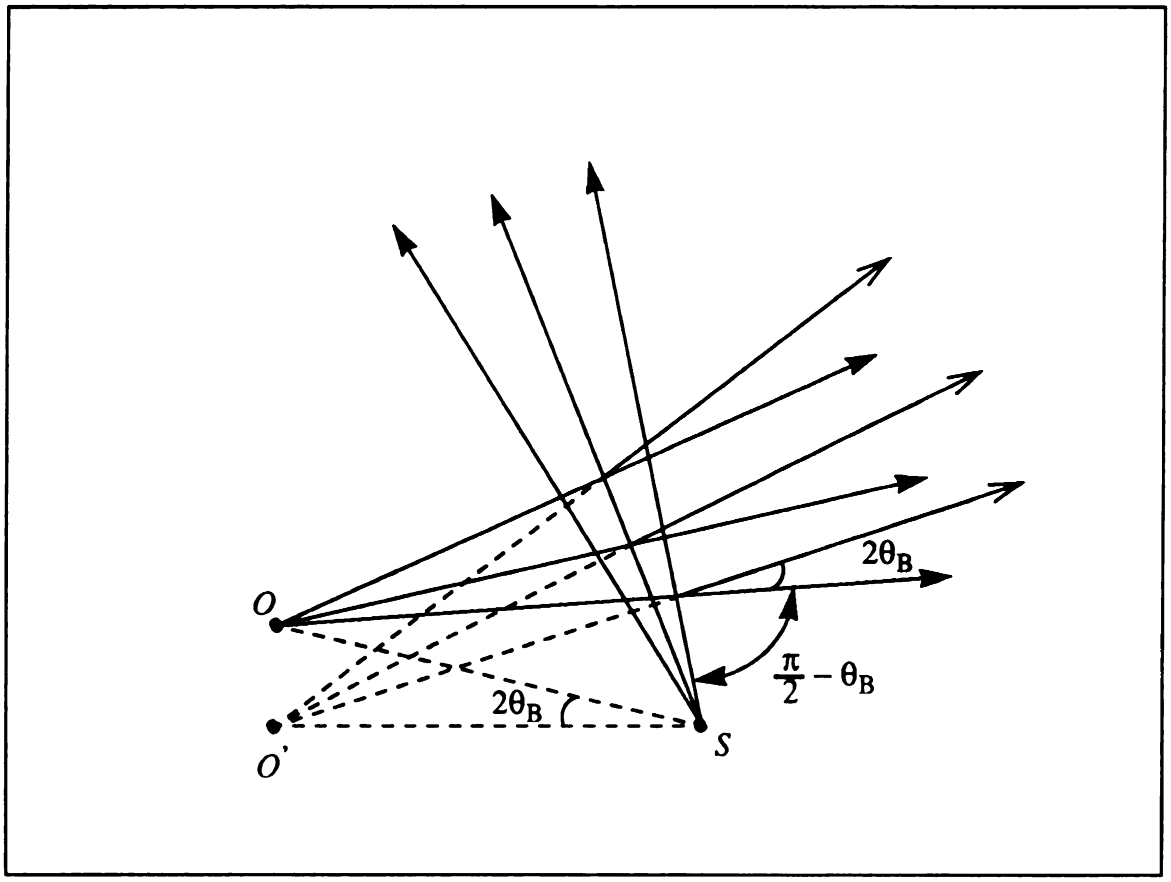

Figure 6.1 Acoustic rays from source S interact with optical rays from source O to form new light rays, which seem to come from O', a virtual image of S.

of the acoustic wave. The imaging process involves a demagnificated factor M which equals the ratio of light wavelength to sound wavelength, i.e. $M = 2\sin\theta_B = \frac{\lambda}{\Lambda}$.

In optical microscopy, resolution is limited by the numerical aperture (the sine of one half the angle formed by the most divergent rays that the optical system accepts from object) and the wavelength of the light. In acousto-optical imaging, the same rule applies. We must substitute the wavelength of the acoustic wave for that of the light and consider the angle formed by acoustic and optical rays. Therefore, the minimum resolvable detail is limited to $1/M$ times the size of the point source of light, and this cannot be smaller than half a wavelength of acoustic wave divided by the numerical aperture of the incident light beam. For higher acoustic frequency, the wavelength of the acoustic wave is shorter, and this provides a better diffraction imaging resolution.

For the second order Bragg diffraction imaging, the imaging process is the same as above except that the Bragg angle θ_B is changed to the double Bragg angle θ_{2B}. Therefore, the demagnificated factor M equals to $2\frac{\lambda}{\Lambda}$, and the minimum resolvable detail is one half of the first order. This means that the imaging resolution by the second order Bragg diffraction is twice that of the first order Bragg diffraction.

6.2.1 Experiment Facility and Measurement System

A diagram of the measurement system used in our experiment is shown in Fig. 6.2. Figure 6.2 shows that a He-Ne laser beam is expanded in diameter by the telescope formed by spherical lenses S_1 and S_2, then the beam size is controlled by the aperture. A cylindrical converging lens, C_1 forms a vertical wedge of light which passes through the acoustic field and comes to a line focus at P which is perpendicular to the plane of the

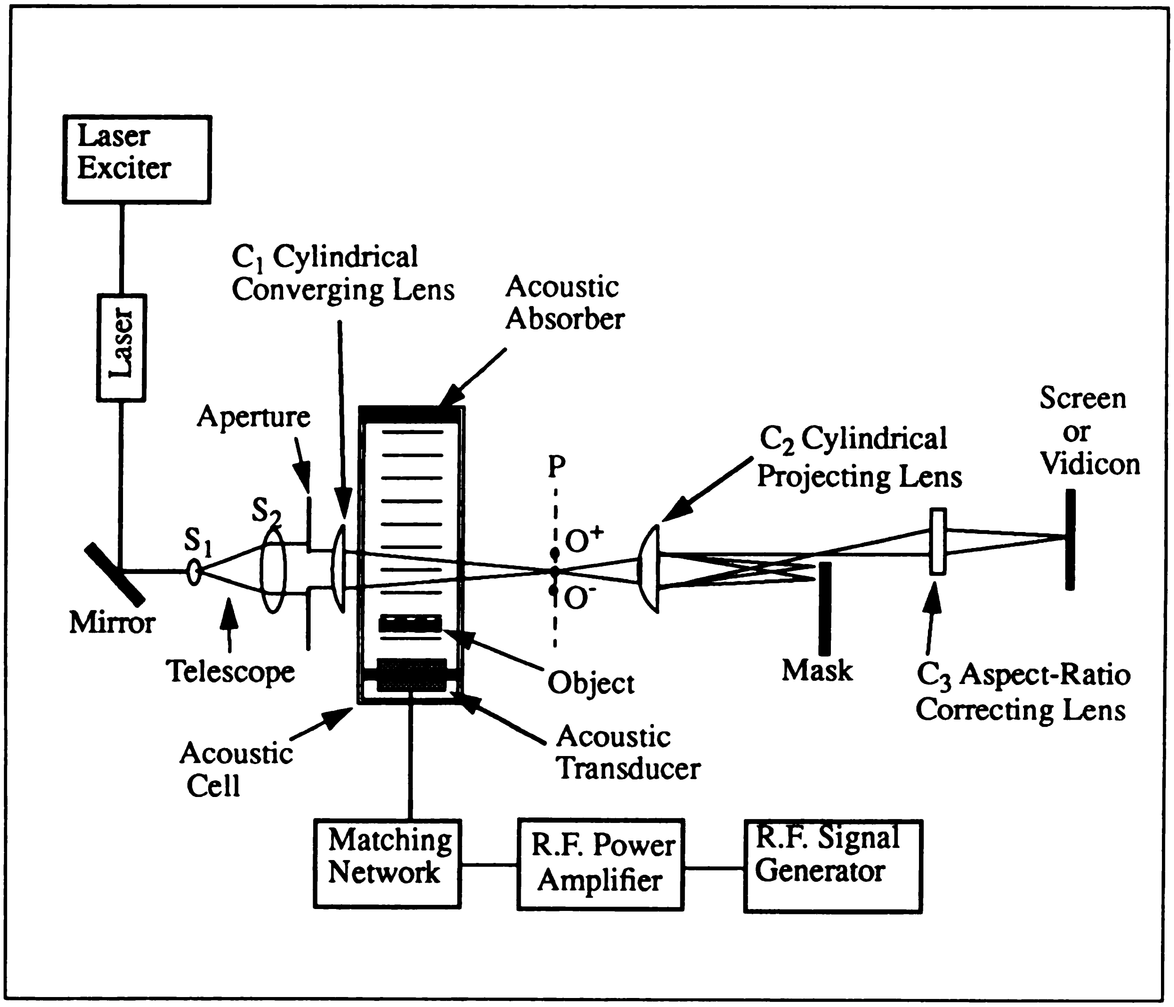

Figure 6.2 Experimental setup for Bragg diffraction imaging.

paper. When the light beam within the acoustic cell interacts with an acoustic wave, the Bragg diffracted images which include the information of the acoustic pattern appear at O^+ and O^- respectively, where the '+' corresponds to the Doppler up shifted light and the '-' corresponds to the Doppler downshifted light.

For imaging in the direction vertical to the paper there is no demagnificated involved. A cylindrical projecting lens C_2 and a cylindrical aspect-ratio correcting lens C_3 compensate for the horizontal demagnification inherent in this imaging process. While the imaging in the horizontal direction (and thus the resolution in that direction) depends on the angular selectivity of Bragg diffraction, the imaging in the vertical direction is essentially a shadow of the acoustic wave cross section in the region of the acousto-optic interaction. Therefore, the vertical resolution improves as object is moved away from the transducer and toward the light beam, while the horizontal resolution is unchanged.

Since we need the diffracted image to be focused on the screen, the projection lens C_2 may have a shorter focal length than lens C_1. Also the positions of C_2, C_3 and the screen distance must be properly chosen. By changing the position of C_2, different acoustic cross sections can be brought to a focus on the screen. The undiffracted beam and one of the images are removed by a masking stop. The other diffracted image is projected to the screen. A video camcorder, RCA pro 807, is used to line in the imaging signal, and the signal is captured by a video capture card added on the PC computer.

Two transducers with different beam size and acoustic frequencies are used to compare the imaging results. The first transducer has a fundamental frequency of 5.8 MHz with 2.54 cm diameter for beam size but is driven at its third harmonic at 17.5 MHz. The other one has a fundamental frequency of 20 MHz with 3.175 cm diameter for beam size. For each transducer, the incident angle and the acoustic amplitude were optimized to achieve maximum power in Bragg interaction.

6.2.2 Experimental Result of Bragg Diffraction Imaging

In this section, six experimental samples shown in Fig. 6.3 were used as imaging objects for Bragg imaging interaction. Four of the samples are round aluminum washers. The biggest one has a 18 *mm* outside diameter and an 8 *mm* inside diameter. The smallest one has a 5 *mm* outside diameter and 3 *mm* inside diameter. The width of the aluminum washer is 5 *mm* for the biggest one and 1mm for the smallest one. Another object made by steer material has a star shape and has a 1.2 *mm* width for each star side. The last object is cut from a thin copper sheet with the characters "*MSU*" and has a 2 *mm* width for its line shape.

Three acoustic imaging experiments are performed. One experiment compares the imaging resolution of the first order Bragg imaging with that of the second order mode. The others analyze the imaging resolution with various acoustic frequencies.

The first imaging experiment used a 17.5 *MHz* acoustic transducer with a diameter of 2.54 *cm*. Four washers were used for comparing the imaging resolution to the first and second Bragg diffraction imaging. The imaging results are shown in Fig. 6.4. Figures 6.4 (a) ~ (d) are the first order Bragg images of the four washers and figures 6.4 (e) ~ (h) are the second order Bragg images. For the biggest washer, there is a little difference between the first and second Bragg images. However, when the object (washer) size is reduced, the resolution difference between the first and second Bragg images becomes evident. For the smallest washer, the inside circle of the washer in the second order Bragg image, Fig. 6.4(h), can be distinguished while only a small spot shows up in the first order Bragg image, Fig. 6.4(d). It is clear that the second Bragg diffraction provides a better imaging resolution than the first Bragg diffraction.

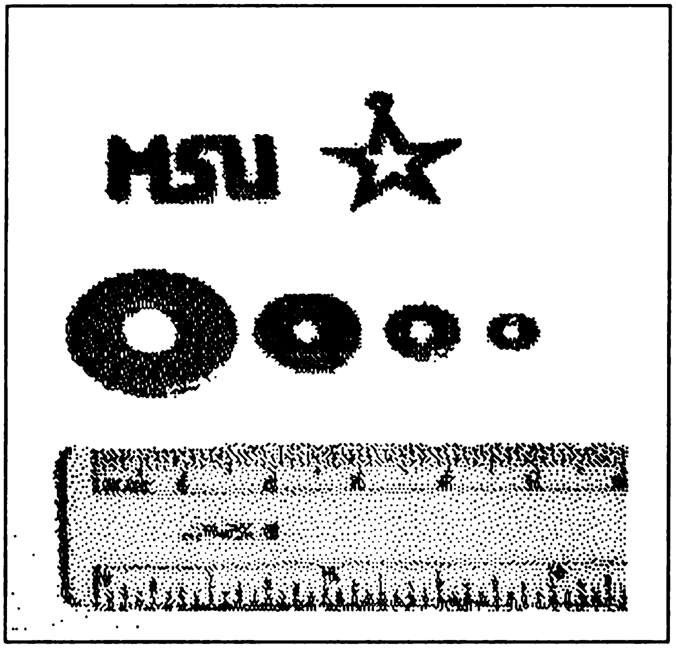

Figure 6.3 Experimental samples for imaging objects.

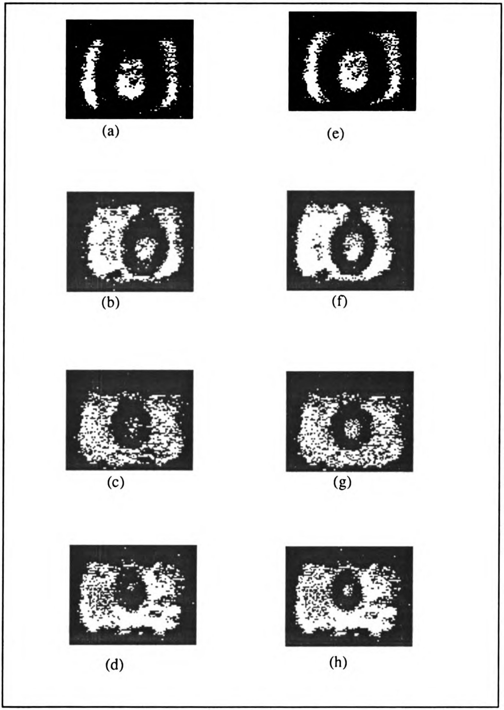

Figure 6.4 The first and second Bragg diffraction imaging for four round washers with acoustic frequency f = 17.5 MHz and beam size L = 2.54 cm. (a) ~ (d) show the imaging result by using the first Bragg diffraction, and (e) ~ (h) show the imaging result by using the second Bragg diffraction.

The next experiment shows that the imaging resolution is proportional to the acoustic frequency and the width of the acoustic beam. The "*MSU*" shaped object was used to demonstrate the first Bragg imaging interaction with two different acoustic frequencies. The imaging results in Fig. 6.5(a) were produced by using acoustic frequency $f = 17.5$ MHz and beam size $L = 2.54$ cm (which gives $Q = 10.5$). The images shown in Fig. 6.5(b) were produced by using $f = 20$ MHz and $L = 3.175$ cm ($Q = 19.2$). Comparing Fig. 6.5(a) and (b), it is obvious that the image in Fig. 6.5(b) has a better imaging resolution than Fig. 6.5(b). This means that higher acoustic frequency and wider acoustic interaction area provide better Bragg imaging quality.

Figure 6.6 shows the star object imaging results using the second order Bragg diffraction. In this experiment, the system setup is the same as the previous experiment but the acoustic amplitude and incident angle of light were optimized to produce a higher diffraction intensity of the second order mode. From Fig. 6.6(a) to 6.6(b), operating frequency and interaction region length are both raised. The outside of the star shapes from the Bragg images in Fig. 6.6 (a) and (b) are both clear and sharp. However, the inside of the star is less clear in Fig. 6.6(a) than in Fig. 6.6(b). This means that with a higher Q value, the second order Bragg diffraction imaging method also provides better imaging resolution.

From above results, one can conclude that the final Bragg image resolution is directly proportional to the acoustic frequency. Therefore, it is desirable to use the highest possible operating frequency. However, for medical diagnostic applications, biological materials generally have higher attenuation at higher frequencies, so it is not practical in medical applications with high acoustic frequency. Using the same acoustic frequency, second order Bragg imaging should provide a better imaging resolution than the first order Bragg imaging. Based on this result, the second Bragg diffraction has high potential in medical diagnostic applications than the first order mode. Another useful application of

(a)

(b)

Figure 6.5 The first Bragg imaging with *MSU* shape in different acoustic frequencies. (a) Bragg imaging by using f = 17.5 *MHz* and L = 2.54 *cm*. (b) Bragg imaging by using f = 20 *MHz* and L = 3.175 *cm*.

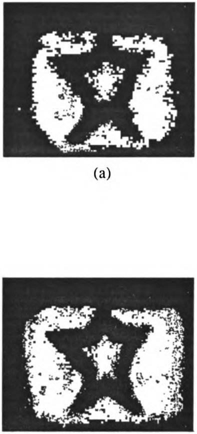

(a)

(b)

Figure 6.6 The second Bragg imaging with *STAR* shape in different acoustic frequencies. (a) Bragg imaging by using $f = 17.5\ MHz$ and $L = 2.54\ cm$. (b) Bragg imaging by using $f = 20\ MHz$ and $L = 3.175\ cm$.

Bragg imaging is in the area of nondestructive material testing. Since acousto-optic interaction can provide real-time capability and high resolution properties, it should be a powerful technique for nondestructive evaluation.

Chapter 7

Conclusion and Suggestion for Future Study

7.1 Conclusion

In this dissertation, the second order Bragg diffraction of an acousto-optic interaction has been investigated in detail by using the partial wave approach. The intensity of light diffraction waves passing through the acoustic field are governed by a set of difference-differential equation. The numerical simulations are obtained for various acoustic frequencies, acoustic pressures, and incident angles of the light beam. The criteria of the optimum system parameter sets (Q, V) which provide a maximum second order Bragg diffraction are established. These results indicated that when the incident angle equals to the Bragg angle, with $V = (2n-1)\pi$, n being integer number, the first order Bragg diffraction can be strongly excited at large Q values (high acoustic frequency and wide acoustic beam width). However, for optimal excitation of the second order Bragg diffraction, the incident angle must equal to twice of the Bragg angle, and only a discrete range of Q and V values can provide the maximum second order Bragg diffraction.

The experiments were designed and performed to verify the theory developed. These experiments include the intensity distribution of the diffraction mode with various acoustic amplitudes, acoustic frequencies, and incident angles of the light. The experimental results agreed well with the theory developed. Finally, acoustic Bragg imaging experiments are performed. The image resolution of the first and second order mode are compared, and the images with various acoustic frequencies are analyzed. The image results indicate that the second order Bragg image provides better image resolution than that of the first order mode. In addition, the Bragg image resolution is directly proportional to the acoustic frequency and acoustic beam width.

The advantage of the second Bragg diffraction is that the second order Bragg diffraction provides a double Bragg angle to deflect diffraction light, and a double frequency shifting to the diffraction light. In addition, the angular sensitivity of the second order diffraction light is better than the first order mode. Therefore the acoustic Bragg imaging of the second order mode can provide a superior imaging resolution than that of the first order mode. Also, in light deflection system, the number of resolvable spots of the second order Bragg diffraction are better than that of the first order mode. The drawback of the second Bragg diffraction is that the system parameters required to excite the second order mode are more critical than that of the first order mode, and this makes a little complicate requirement in application of the second Bragg diffraction.

7.2 Suggestion for Future Application

Acousto-optic interactions are useful in AO modulation, light deflection, frequency shifting, and Bragg diffraction imaging. Therefore, there are many topics to pursue in future applications. For example, in the imaging application, the acoustic Bragg image could be a powerful tool to the nondestructive evaluation of materials. For real-time imaging, a pulsed Bragg diffraction system by using the second order Bragg diffraction would be a good topic to purpose in evaluating the internal damage structure of composite material. In addition, high power solid-state laser sources have become available in recent years due to the advancement of laser technology. By using such diodes as laser beam sources, the proposed method of acousto-optical interaction could lead to a way of providing the possibility of low-cost, portable and real-time imaging systems.

APPENDIX

Appendix A

A.1 The Solution for The First Bragg Diffraction

To evaluate the intensity of the first order mode, let us consider the coupling between ϕ_0 and ϕ_1 modes. From difference-differential equation Eq.(2-45), we have

$$\begin{cases} \dfrac{d\phi_0}{dz} - \dfrac{V}{2L}\phi_1 = 0 \\ \dfrac{d\phi_1}{dz} + \dfrac{V}{2L}\phi_0 = i\dfrac{Q}{2L}(1-2\alpha)\phi_1 \ . \end{cases} \tag{A-1}$$

Equation (A.1-1) can be solved by using Laplace transformation. Putting this set of equations in matrix form, Eq. (A-1) becomes

$$\begin{bmatrix} \dot{\phi}_0 \\ \dot{\phi}_1 \end{bmatrix} = \begin{bmatrix} 0 & C_1 \\ -C_1 & C_2 \end{bmatrix} \begin{bmatrix} \phi_0 \\ \phi_1 \end{bmatrix} \tag{A-2}$$

where $C_1 = \dfrac{V}{2L}$

$C_2 = i\dfrac{Q}{2L}(1-2\alpha)$.

For a Linear system,[20] one can solve a set of difference-differential equation by using the Laplace transformation technique. For a system $\left[\dot{X}\right] = \left[A\right]\left[X\right]$, the solution is $X(z) = e^{Az}X_0$, where X_0 is a initial condition, and the e^{Az} can be presented as

$$e^{Az} = \mathcal{L}^{-1}\left[(sI - A)^{-1}\right] .$$

Applying this approach to Eq. (A-2) we have

$$\begin{bmatrix} \phi_0(z) \\ \phi_1(z) \end{bmatrix} = \begin{bmatrix} e_{11} & e_{12} \\ e_{21} & e_{22} \end{bmatrix} \begin{bmatrix} \phi_{inc} \\ 0 \end{bmatrix} = \begin{bmatrix} e_{11}\phi_{inc} \\ e_{21}\phi_{inc} \end{bmatrix} \tag{A-3}$$

where ϕ_{inc} is the mode amplitude of incident light at $z = 0$, and

$$e_{11} = \mathcal{L}^{-1}\left[\frac{s - C_2}{s^2 - sC_2 + C_1^2}\right] \tag{A-4}$$

$$e_{21} = \mathcal{L}^{-1}\left[\frac{-C_1}{s^2 - sC_2 + C_1^2}\right] . \tag{A-5}$$

From the table of the Laplace transformation[71], we have

$$\frac{w^2}{s^2 + 2\xi ws + w^2} \Leftrightarrow \frac{we^{-1\xi wt}}{\sqrt{1 - \xi^2}} \sin\left(wt\sqrt{1 - \xi^2}\right) . \tag{A-6}$$

Let $w = C_1$ and $\xi = -\frac{C_2}{2C_1}$, the Laplace transform pair becomes as follows

$$\frac{1}{C_1}\,\frac{C_1^2}{s^2 - C_2 s + C_1^2} \Leftrightarrow \frac{1}{C_1}\,\frac{C_1 e^{\frac{C_2}{2} z}}{\sqrt{1 - \frac{C_2^2}{4C_1^2}}} \sin\left(C_1 \sqrt{1 - \frac{C_2^2}{4C_1^2}}\; z \right)$$

$$\text{where } 1 - \frac{C_2^2}{4C_1^2} = 1 + \frac{\frac{Q^2}{4L^2}(1-2\alpha)^2}{4\frac{V^2}{4L^2}} = \frac{4V^2 + (1-2\alpha)^2 Q^2}{4V^2}$$

let $\sigma = \left(4V^2 + (1-2\alpha)^2 Q^2\right)^{\frac{1}{2}}$, then $\sqrt{1 - \frac{C_2^2}{4C_1^2}} = \frac{\sigma}{2V}$.

Finally, Eq. (A-5) becomes

$$e_{21} = -\frac{e^{i\frac{Q}{4L}(1-2\alpha) z}}{\frac{\sigma}{2V}} \sin\left(\frac{\sigma}{4L} z\right) . \tag{A-7}$$

Then,

$$\phi_1 = e_{21} \cdot \phi_{inc} = -2e^{i\frac{Q}{4L}(1-2\alpha) z} \frac{V}{\sigma} \sin\left(\frac{\sigma}{4}\right) \phi_{inc} \quad \text{at } z = L. \tag{A-8}$$

where $\sigma = (4V^2 + [Q(1-2\alpha)]^2)^{1/2}$.

Finally, the first order mode intensity I_1 at $z = L$ becomes

$$I_1 = \phi_1 \cdot \phi_1{}^* = \frac{4V^2}{\sigma^2} \sin^2\left(\frac{\sigma}{4}\right) I_{inc} . \tag{A-9}$$

where $I_{inc} = \phi_{inc} \cdot \phi_{inc}^*$.

Similarly, one can obtain $\phi_0(z)$, and the zeroth mode intensity I_0 at $z = L$ is

$$I_0 = 1 - \frac{4V^2}{\sigma^2} \sin^2\left(\frac{\sigma}{4}\right)\phi_{inc} = 1 - I_1 \quad . \tag{A-10}$$

A.2 The Solution for The Second Bragg Diffraction

To evaluate the intensity of the second order mode, let us consider the coupling between ϕ_0, ϕ_1 and ϕ_2 modes. From difference-differential equation Eq.(2-53), we have

$$\begin{cases} \dfrac{d\phi_0}{dz} - \dfrac{V}{2L}\phi_1 = 0 \\ \dfrac{d\phi_1}{dz} + \dfrac{V}{2L}(\phi_0 - \phi_2) = i\dfrac{Q}{2L}(1 - 2\alpha)\phi_1 \\ \dfrac{d\phi_2}{dz} + \dfrac{V}{2L}\phi_1 = i\dfrac{2Q}{L}(1 - \alpha)\phi_2 \end{cases} \tag{A-11}$$

Following the similar procedure in solving the first order mode, we have

$$e_{11} = \mathcal{L}^{-1}\left[\frac{s^2 - s(C_2 + C_3) + C_2C_3 + C_1^2}{s^3 - s^2(C_2 + C_3) + s\left(C_2C_3 + 2C_1^2\right) + C_3C_1^2}\right] \tag{A-12}$$

$$e_{21} = \mathcal{L}^{-1}\left[\frac{-C_1(s - C_3)}{s^3 - s^2(C_2 + C_3) + s\left(C_2C_3 + 2C_1^2\right) + C_3C_1^2}\right] \tag{A-13}$$

$$e_{31} = \mathcal{L}^{-1}\left[\frac{C_1^2}{s^3 - s^2(C_2 + C_3) + s\left(C_2C_3 + 2C_1^2\right) + C_3C_1^2}\right] \tag{A-14}$$

where $C_1 = \frac{V}{2L}$

$$C_2 = i\frac{Q}{2L}(1-2\alpha)$$

$$C_3 = i\frac{2Q}{L}(1-\alpha) \quad .$$

Since we are interested in second order Bragg diffraction for maximum excitation of the second order mode, the incident angle is $\theta_{2B} = \frac{\lambda}{\Lambda}$, and this means α equals to one [see Eq.(2-25)]. Therefore, with $\alpha = 1$ the C's become

$$C_1 = \frac{V}{2L}$$

$$C_2 = (-i)\frac{Q}{2L}$$

$$C_3 = 0 \quad .$$

For solving e_{21} for $\alpha = 1$, Eq. (A-13) can be reduced as follows

$$e_{21} = \mathcal{L}^{-1}\left[\frac{-C_1}{s^2 - C_2 s + 2C_1^2}\right] \quad . \tag{A-15}$$

From the Eq. (A-6), we have the transform pair

$$\frac{w^2}{s^2 + 2\xi ws + w^2} \Leftrightarrow \frac{we^{-1\xi wt}}{\sqrt{1-\xi^2}}\sin\left(wt\sqrt{1-\xi^2}\right) \quad . \tag{A-16}$$

Let $w^2 = 2C_1^2$ and $2\xi w = -C_2$,

then

$$w = \sqrt{2}C_1 = \sqrt{2}\frac{V}{2L}$$

$$\xi = -\frac{C_2}{2w} = i\frac{Q}{2\sqrt{2}V}$$

$$\sqrt{1-\xi^2} = \frac{1}{2V}\left(\frac{1}{2}\left(8V^2+Q^2\right)\right)^{\frac{1}{2}}$$

then, substituting w, ξ, and $\sqrt{1-\xi^2}$ to Eq. (A-15) and Eq. (A-16), we have

$$\begin{aligned} e_{21} &= -\frac{1}{2C_1}\mathcal{L}^{-1}\left[\frac{-2C_1^2}{s^2-C_2s+2C_1^2}\right] \\ &= -\frac{1}{2C_1}\frac{\sqrt{2}C_1e^{-i\frac{Q}{2\sqrt{2}V}\sqrt{2}\frac{V}{2L}z}}{\frac{1}{2V}\left(\frac{1}{2}\left(8V^2+Q^2\right)\right)^{1/2}}\sin\left(\sqrt{2}\frac{V}{2L}\frac{1}{V}\left(\frac{1}{2}\left(8V^2+Q^2\right)\right)^{\frac{1}{2}}z\right) \qquad \text{(A-17)} \\ &= -\frac{e^{-i\frac{Q}{4L}z}2V}{\sigma}\sin\left(\frac{\sigma}{4L}z\right) \end{aligned}$$

where $\sigma = \left(8V^2+Q^2\right)^{\frac{1}{2}}$.

Then, the ϕ_1 at $z = L$ is

$$\phi_1 = e_{21}\cdot\phi_{inc} = (-2)\frac{V}{\sigma}e^{-i\frac{Q}{4}}\sin\left(\frac{\sigma}{4}\right)\cdot\phi_{inc}. \qquad \text{(A-18)}$$

Therefore, the intensity of the first order mode is

$$I_1 = \phi_1\cdot\phi_1{}^* = 4\frac{V^2}{\sigma^2}\sin^2\left(\frac{\sigma}{4}\right)I_{inc} \qquad \text{(A-19)}$$

For solving e_{31} for $\alpha = 1$, Eq. (A-14) can be reduced as follows

$$e_{31} = \frac{1}{2}\mathcal{L}^{-1}\left[\frac{2C_1^2}{s\left(s^2 - C_2 s + 2C_1\right)}\right] . \tag{A-20}$$

From the table of the Laplace transform, we have the transform pair

$$\frac{w^2}{s\left(s^2 + 2\xi w s + w^2\right)} \Leftrightarrow 1 + \frac{e^{-\xi w t}\sin\left(w\sqrt{1-\xi^2}\,t - \psi\right)}{\sqrt{1-\xi^2}} \tag{A-21}$$

where $\psi = \operatorname{atan}\left(\frac{\sqrt{1-\xi^2}}{-\xi}\right)$.

Let $w^2 = 2C_1^2$ and $2\xi w = -C_2$, then

$$w = \sqrt{2}C_1 = \frac{V}{\sqrt{2}L}$$

$$\xi = -\frac{C_2}{2w} = i\frac{Q}{2\sqrt{2}V}$$

$$\sqrt{1-\xi^2} = \frac{1}{2\sqrt{2}V}\left(8V^2 + Q^2\right)^{\frac{1}{2}} = \frac{1}{2\sqrt{2}V}\sigma$$

$$\psi = \operatorname{atan}\left(\frac{\sqrt{1-\xi^2}}{-\xi}\right) = \operatorname{atan}\left(i\frac{\sigma}{Q}\right)$$

$$\Rightarrow \tan\psi = \left(i\frac{\sigma}{Q}\right)$$

$$\Rightarrow \sin\psi = \left(\frac{\sigma}{2\sqrt{2}V}\right)$$

$$\Rightarrow \cos\psi = (-i)\frac{Q}{2\sqrt{2}V}$$

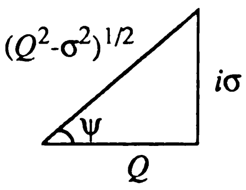

where $\left(Q^2 - \sigma^2\right)^{1/2} = i2\sqrt{2}V$

Substituting w, ψ, ξ, and $\sqrt{1-\xi^2}$ to Eq. (A-20) and Eq. (A-21), we have

$$e_{31} = \frac{1}{2}\left(1 + \frac{2\sqrt{2}V}{\sigma} e^{-i\frac{Q}{4L}z} \sin\left(\frac{\sigma}{4L}z - \psi\right)\right). \tag{A-22}$$

Since $\sin(\alpha \pm \beta) = \sin\alpha \cdot \cos\beta \pm \sin\beta \cdot \cos\alpha$, then

$$\sin\left(\frac{\sigma}{4L}z - \psi\right) = (-i)\frac{Q}{2\sqrt{2}V}\sin\left(\frac{\sigma}{4L}z\right) - \frac{\sigma}{2\sqrt{2}V}\cos\left(\frac{\sigma}{4L}z\right). \tag{A-23}$$

Substituting Eq. (A-23) into Eq. (A-22), e_{31} becomes

$$e_{31} = \frac{1}{2}\left(1 + e^{-i\frac{Q}{4L}z}\frac{2\sqrt{2}V}{\sigma}\left[-i\frac{Q}{2\sqrt{2}V}\sin\left(\frac{\sigma}{4L}z\right) - \frac{\sigma}{2\sqrt{2}V}\cos\left(\frac{\sigma}{4L}z\right)\right]\right). \tag{A-24}$$

Then, the ϕ_2 at $z = L$ is

$$\phi_{31} = e_{31} \cdot \phi_{inc} = \frac{1}{2}\left(1 - e^{-i\frac{Q}{4}}\left(i\frac{Q}{\sigma}\sin\left(\frac{\sigma}{4}\right) + \cos\left(\frac{\sigma}{4}\right)\right)\right) \cdot \phi_{inc}. \tag{A-25}$$

Therefore, the intensity of the second order mode becomes as follows

$$\begin{aligned} I_2 &= \phi_{31} \cdot \phi_{31}^* = e_{31} \cdot e_{31}^* \cdot I_{inc} \\ &= \frac{1}{4}\left(1 - e^{-i\frac{Q}{4}}\left(i\frac{Q}{\sigma}\sin\left(\frac{\sigma}{4}\right) + \cos\left(\frac{\sigma}{4}\right)\right)\right)\left(1 - e^{i\frac{Q}{4}}\left((-i)\frac{Q}{\sigma}\sin\left(\frac{\sigma}{4}\right) + \cos\left(\frac{\sigma}{4}\right)\right)\right). \quad \text{(A-26)} \\ &= \frac{1}{4}\left(1 - \left(2\frac{Q}{\sigma}\sin\frac{Q}{4}\sin\frac{\sigma}{4} - 2\cos\frac{Q}{4}\cos\frac{\sigma}{4} + \left(\frac{Q}{\sigma}\right)^2\sin^2\frac{\sigma}{4} + \cos^2\frac{\sigma}{4}\right)\right)I_{inc} \end{aligned}$$

Since

$$(\cos x - \cos y)^2 + \left(\frac{y}{x}(\sin x - \sin y)\right)^2$$

$$= 1 - 2\frac{y}{x}\sin x \sin y - 2\cos x \cos y + \left(\frac{y}{x}\right)^2 \sin^2 x + \cos^2 x$$

I_2 can be represented as follows

$$I_2 = \frac{1}{4}\left(\cos\frac{\sigma}{4} - \cos\frac{Q}{4}\right)^2 + \left(\frac{Q}{\sigma}\sin\frac{\sigma}{4} - \sin\frac{Q}{4}\right)^2 I_{inc} \,. \tag{A-27}$$

For solving intensity of the zero order mode with $\alpha = 1$, Eq. (A-12) can be reduced as follows

$$\begin{aligned} e_{11} &= \mathcal{L}^{-1}\left[\frac{s^2 - 2C_2 + C_1^2}{s^3 - C_2 s^2 + 2C_1^2 s}\right] = \mathcal{L}^{-1}\left[\frac{\left(s^2 - sC_2 + 2C_1^2\right) - C_1^2}{s\left(s^2 - C_2 s + 2C_1^2\right)}\right] \\ &= \mathcal{L}^{-1}\left[\frac{1}{s}\right] - e_{31} = 1 - e_{31} \end{aligned} \tag{A-28}$$

and

$$\phi_0 = e_{11}\phi_{inc} \,. \tag{A-29}$$

Therefore, the intensity of the second order mode at $z = L$ becomes

$$I_0 = \phi_0 \cdot \phi_0^* = \frac{1}{4}\left[\left(\cos\left(\frac{\sigma}{4}\right) + \cos\left(\frac{Q}{4}\right)\right)^2 + \left(\frac{Q}{\sigma}\sin\left(\frac{\sigma}{4}\right) + \sin\left(\frac{Q}{4}\right)\right)^2\right] I_{inc} \,. \tag{A-30}$$

Finally, we have

$$\begin{aligned} I_0 &= \frac{1}{4}\left[\left(\cos\frac{\sigma}{4} + \cos\frac{Q}{4}\right)^2 + \left(\frac{Q}{\sigma}\sin\frac{\sigma}{4} + \sin\frac{Q}{4}\right)^2\right] I_{inc} \\ I_1 &= \left[\frac{2V}{\sigma}\sin\frac{\sigma}{4}\right]^2 I_{inc} \\ I_2 &= \frac{1}{4}\left[\left(\cos\frac{\sigma}{4} - \cos\frac{Q}{4}\right)^2 + \left(\frac{Q}{\sigma}\sin\frac{\sigma}{4} - \sin\frac{Q}{4}\right)^2\right] I_{inc} \end{aligned} \tag{A-31}$$

where

$$\sigma = \left(8V^2 + Q^2\right)^{\frac{1}{2}}$$

$$\alpha = (-n_0)\frac{k}{k^*}\sin\theta = 1$$

$$Q = \frac{k^{*2}L}{n_0 k\cos\theta}$$

$$V = \frac{kn_1 L}{\cos\theta}$$

A.3 The Derivation of $\frac{dI_2}{dQ}$

From Eq. (A-31), we have

$$I_2 = \frac{1}{4}\left[\left(\cos\frac{\sigma}{4} - \cos\frac{Q}{4}\right)^2 + \left(\frac{Q}{\sigma}\sin\frac{\sigma}{4} - \sin\frac{Q}{4}\right)^2\right]I_{inc}$$

where $\sigma = \left(8V^2 + Q^2\right)^{1/2}$. Let $I_{\text{inc}} = 1$, therefore $\frac{dI_2}{dQ}$ can be represented as follows

$$\frac{dI_2}{dQ} = \frac{2}{4}\left[\left(\cos\frac{\sigma}{4} - \cos\frac{Q}{4}\right)\left(f_1 + \frac{1}{4}\sin\frac{Q}{4}\right) + \left(\frac{Q}{\sigma}\sin\frac{\sigma}{4} - \sin\frac{Q}{4}\right)\left(\frac{1}{\sigma}\sin\frac{\sigma}{4} + Qf_2 - \frac{1}{4}\cos\frac{Q}{4}\right)\right]$$

where $f_1 = \frac{d}{dQ}\cos\frac{\sigma}{4}$

$$f_2 = \frac{d}{dQ}\left(\sigma^{-1}\sin\frac{\sigma}{4}\right).$$

Since σ includes parameter Q, we need take a derivative of σ with Q. Then

$$\frac{d\sigma}{dQ} = \left(8V^2 + Q^2\right)^{-\frac{1}{2}} Q = \frac{Q}{\sigma}$$

With $\frac{d\sigma}{dQ}$, f_1 and f_2 become

$$f_1 = \frac{d}{dQ}\cos\frac{\sigma}{4} = \left(-\frac{1}{4}\right)\sin\frac{\sigma}{4}\frac{d\sigma}{dQ} = \left(-\frac{1}{4}\right)\frac{Q}{\sigma}\sin\frac{\sigma}{4}$$

$$f_2 = \frac{d}{dQ}\left(\sigma^{-1}\sin\frac{\sigma}{4}\right) = \sigma^{-1}\frac{1}{4}\frac{Q}{\sigma}\cos\frac{\sigma}{4} - \frac{1}{\sigma^2}\frac{Q}{\sigma}\sin\frac{\sigma}{4} = \frac{Q}{\sigma^2}\left(\frac{1}{4}\cos\frac{\sigma}{4} - \frac{1}{\sigma}\sin\frac{\sigma}{4}\right)$$

Substituting f_1 and f_2 to $\frac{dI_2}{dQ}$, we have

$$\frac{dI_2}{dQ} = \frac{1}{2}\left[\frac{1}{4}\left(\cos\frac{\sigma}{4} - \cos\frac{Q}{4}\right)\left(\sin\frac{Q}{4} - \frac{Q}{\sigma}\sin\frac{\sigma}{4}\right) + \left(\frac{Q}{\sigma}\sin\frac{\sigma}{4} - \sin\frac{Q}{4}\right)\right.$$
$$\left.\left(\frac{1}{\sigma}\sin\frac{\sigma}{4} + \frac{Q^2}{\sigma^2}\left(\frac{1}{4}\cos\frac{\sigma}{4} - \frac{1}{\sigma}\sin\frac{\sigma}{4}\right) - \frac{1}{4}\cos\frac{Q}{4}\right)\right]$$

$$= \frac{1}{2}\left(\frac{Q}{\sigma}\sin\frac{\sigma}{4} - \sin\frac{Q}{4}\right)\left[\left(-\frac{1}{4}\right)\cos\frac{\sigma}{4} + \frac{1}{\sigma}\sin\frac{\sigma}{4} + \frac{Q^2}{\sigma^2}\left(\frac{1}{4}\cos\frac{\sigma}{4} - \frac{1}{\sigma}\sin\frac{\sigma}{4}\right)\right]$$

BIBLIOGRAPHY

BIBLIOGRAPHY

[1] L. Brillouin, "Diffusion de la lumiere et des rayons X par un corps transparent homogene," Ann. Phys. (Paris), vol.17, pp.88-122,1922.

[2] P. Debye and F. W. Sears, "On the scattering of Light by Supersonic waves," Proc. Nat. Acad. Sci.(u.s.), vol.18, pp.409-414, 1932.

[3] R. Lucas and P.Biguard, "Properties optigues des milieux Solides et liquides aux vibration elastiques ultra sonores," J. Phys. Rad., vol.3, pp.464-477, 1932.

[4] C. V. Raman and N. S. Nath, "The diffraction of Light by high frequency Sound waves," part I, Proc. Indian Acad. Sci., vol.2A pp.406-412, 1935.

[5] C. V. Raman and N. S. Nath, "The diffraction of Light by high frequency Sound waves," part II, Proc. Indian Acad. Sci., vol.2A pp.413-420, 1935.

[6] C. V. Raman and N. S. Nath, "The diffraction of Light by high frequency Sound waves," part III, Proc. Indian Acad. Sci., vol.3 pp.75-84, 1936.

[7] C. V. Raman and N. S. Nath, "The diffraction of Light by high frequency Sound waves," part IV, Proc. Indian Acad. Sci., vol.3 pp.119-125, 1936.

[8] C. V. Raman and N. S. Nath, "The diffraction of Light by high frequency Sound waves," part V, Proc. Indian Acad. Sci., vol.3 pp.459-465, 1936.

[9] C. V. Raman and N. S. Nath, "Generalized theory", Proc. Indian Acad. Sci., vol.4 pp.222-242, 1936.

[10] W. R. Klein, B. D. Cook, and W. G. Mayer, "Light diffraction by ultrasonic gratings," Acustica, Vol.15, pp.57-74, January 1965.

[11] W. R. Klein and B. D. Cook, "Unified Approach to Ultrasonic Light Diffraction," IEEE Tarns. on Sonics and Ultrasonics, su-14, pp.123-135, July 1967.

[12] P. Phariseau, "On the diffraction of Light by progressive supersonic waves," Proc. Indian Acad. Sci., vol.44, pp.165-170, 1956.

[13] A. B. Bhatia and W.S. Noble, "Diffraction of Light by Ultrasonic Waves," Proc. Roy. Soc.(london), vol.220, ser. A, pp.356-385, 1953

[14] A. Korpel, "Acousto-Optics," in Applied Solid state Science, vol.3, edited by R. Wolfe, pp.73-179, (Academic, New York, 1972).

[15] C. S. Tsai, "Experimental Investigation of the Resolution Capability of Microwave Ultrasonic Beam Visualization Techniques Using Bragg Diffraction of a Laser Beam," J. Acou. Soc. V.48, pp.1110-1118, 1970.

[16] D. T. Pierce and R. L. Byer, "Experiments on the Interaction of Light and Sound for the Advanced Laboratory," AJP, vol.41, pp.314-324, 1973.

[17] R. Alder, "Interaction between Light and Sound," IEEE spectrum, pp.42-54, 1967.

[18] T. Poon and A. Korpel, "High efficiency acousto-optic diffraction into the second Bragg order," IEEE Ultrasonics Symp., pp.751-754, 1981.

[19] R. Alferness, "Analysis of propagation at the second order Bragg angle of a thick holographic grating," J. Opt. Soc. Am., vol.66, pp.353-362, 1976.

[20] C. T. Chen,"Linear System Theory and Design," Holt, Rinehard and Winston, pp45-56, 1984.

[21] W. H. Louisell, "Coupled Mode and Parametric Electronics," John Wiley and Sons, Inc., New York 1960.

[22] G. W.Willard, "Criteria for Normal and Abnormal Ultrasonic Light Diffraction Effects," J. Acoust. Soc. of Am. Vol. 21, pp.101-108, March, 1949.

[23] V. Raman and K. S. Venkateraman, "Adiabatic piezo-optic coefficient of liquids," Proc. Roy. Soc. (London), Vol,171, pp.137-147, 1939.

[24] M. T. Wauk and D. K. Winslow, "Determination of acoustic transducer conversion loss by impedance measurements," IEEE Trans. Sonics and Ultrasonics, SU-16, pp.86-88, July 1969.

[25] E. I. Gordon, "A review of acousto optical deflection and modulation devices," Proc. IEEE, vol. 54, pp.1391-1401, Oct.1966.

[26] R. W. Dixon and E. I. Gordon, "Acoustic light modulator using optical heterodyne mixing," Bell system Tech. J., vol.56, p.367, 1967.

[27] E. I. Gordon, "Figure of merit for acousto-optical deflection and modulation devices," IEEE J. of Quantum Electronics (Correspondence), vol. QE-2, pp.104-105, May 1966.

[28] A. Korpel, P. Adler, P. Desmanes and T. M. Smith, "An ultrasonic light deflection system," IEEE J. of Quantum Electronics, vol. QE-1, pp.60-61, Apr. 1965..

[29] E. I.Gordon, "Figure of Merit for acousto-optical deflection and modulation devices," IEEE J. of Quantum Electronics, vol QE-2 pp.104-105, May 1966..

[30] I. C. Chang, and D. L.Hecht, "Second Order Birefringent Acoustic-Optic Deflector with Double Resolution and high Efficiency," IEEE Ultrasonics Symp. pp.130-132, 1975.

[31] A. Korpel, P. Adler, P. Desmanes and W. Watson, "A television display using acoustic deflection and modulation of coherent light," Proc. IEEE, vol 54, pp.1429-1437, Oct.1966.

[32] M. G. Cohen, and E. I. Gordon, "Acoustic beam probing using optical techniques," Bell system Tech. J., vol. 44, p.693, 1965.

[33] G. W. Willard, "Utra Sound Waves Made Visible," Bell Labs, Record, XXV, pp. 194-200, May 1947.

[34] S. Bhagavantan and B. R. Rao, Nature, vol. 161, pp.927, 1948.

[35] H. S. Hatfield,"Ultrasonics," John Wiley and Sons, Inc., New York, 1939.

[36] W. R. Klein, "Light diffraction by Ultrasonic beams of high frequency near Bragg incidence," presented at the 5th Internal Cong. on Acoustic, Belgium, Sep. 1965.

[37] T. M. Reeder and D. K. Winslow, "Characteristics of Microwave Acoustic Transducers for Volume Wave Excitation," IEEE Trans. Microwave theory and Techniques, Vol. MTT-17, No. 11, pp.927-941, Nov. 1969.

[38] H. W. Bode, "Network Analysis and Feedback Amplifier Design," New York: Van Nostrand, pp.360-371, 1945.

[39] R. M. Fano, "Theoretical limitations on the broadband Matching of Arbitrary Impedances," J. Franklin Inst., Vol. 249, pp.57-84, pp.139-154, Jan., Feb. 1950.

[40] The ARRP Handbook for the radio Amateur by the American Radio Relay League, pp.2-51~2-55, 1988.

[41] A. H. Rosenthal, "Application of Ultrasonic Light Modulation to Signal Recording, Display, Analysis and Communication," IRE Trans. Ultras. Eng., Vol. UE-8, pp1-5, Jan. 1961.

[42] W. Liben, "Some Applications of an ultrasonic light modulator," J. Acoust. Soc. Amer. Vol.34, pp.860-861, June 1962.

[43] R. Whitman, A. Korpel, and S. Lotsoff, "Application of Acoustic Bragg diffraction to optical processing techniques," in Proc. Symp. Moderm Optics, pp.243-255, 1967.

[44] A. Kopel, "Acousto-optic Signal Processing," in Optical processing, New York: plenum, ch. 10, pp171-194, 1976.

[45] L. N. Flores and D. L. Hecht, "Acoustp-optic Signal Processors,"in SPIE Conf. Proc., Vol. 118, pp. 182-192. 1977.

[46] T. R. Bader, "Acousto-optics Spectrum analysis," Appl. Opt., Vol. 18, pp. 1668-1672, June 1979.

[47] R. Kingslake and B. J. Thompson, "Acousto-optics," in Applied Optics and Optical Engineering, Vol. 6, New York: Academic Press. ch. 4, pp. 89-136.

[48] A. Kopel, P. Alder, P. Desmaress, and W. Wastson, "A Television Display Using Acoustic Deflection and Modulation of Coherent Light," Appl. Opt., Vol. 5, pp. 1667-1675, Oct. 1966.

[49] L. C. Foster, C. B. Crumley, and R. L. Cohoon, "A high resolution optical scanner using a traveling wave acoustic lens," Appl. Opt., Vol. 9, pp. 2154, 1970.

[50] S. K. Yao, D. Weid, and R. M. Montgonery, "Guided acoustic wave traveling lens for high speed optical scanners," Appl. Opt., Vol. 18, pp. 446-453, Feb. 15, 1979.

[51] C. B. Crumly, L. C. Foster, and M. D. Ewy, "Laser mode locking by an external Doppler cell," Appl. Phys. Letters. Vol. 6, pp.6, 1965.

[52] N. Goto, Y. Kanayama, and Y. Miyazaki,"Integrated Optic matrix-vector multiplier using mult-frequency acousto-optic diffraction" IEEE Ultra. Symp. Proc., pp. 487-490, Oct. 1989.

[53] C. S. Tsai and D. Young, "Magneto static-forward-volume-wave-based quided-wave magneto-optic Bragg cells and application to communications and signal processing," IEEE Trans. an Microwave theory and Techniques, Vol. 38, pp. 560-570, May, 1990.

[54] Z. Y. Cheng and C. S. Tsai, "A novel integrated acousto-optic frequency shifter," j. Lightwave Technology Vol. 7, pp. 1575-1580, Oct. 1989.

[55] D. Y. Zang, P. Le and C. S. Tsai, "Integrated acoustic device modules in LiNbo/sub 3/ for digital data processing," IEEE Ultra. Symp. Proc. pp.451-453, Oct, 1988.

[56] A. Korpel and D. J. Mehrl, "Bragg diffraction Imaging with predominantly spherical lens," IEEE Ultra. Symp. Proc., pp. 735-737, Oct, 1988.

[57] M. S. Wu, T. Shiosaki, and A. Kawabata, "Electro-optic diffraction modulation in Zn O film on sapphire," IEEE J. Quantum Electronics, pp. 252-256. Mar. 1989.

[58] Xin Cheng and C. S Tsai., "Electo optic Bragg diffraction modulators in GaAs ? AlGaAs heterostructure wave guides," J. Light Wave Tech. Vol. 6, pp. 809-817, June, 1988.

[59] J. P. Powers, K. Y. Wang, and G. Wade, "Use of Bragg diffraction imaging for Acoustic velocity measurement," J. Acoust. Soc. Amer., pp. 1593-1597, Nov, 1972.

[60] J. Landry, J. Powers, and G. Wade, "Ultrasonic imaging of internal structure by Bragg diffraction," Appl. Phys. Letter 15, pp. 186-188, Sep. 1969.

[61] A. Korpel, "Visualization of the cross section of a sound bean by Bragg diffraction of light ," Appl. Phys. Letter 9, pp. 425-427. Dec. 1966.

[62] A. Korpel, "Acoustic Imaging by diffracted light, I. two-dimensional Interaction," IEEE. Trans. Sonics and Ultrasonics su-15, pp. 153-157, 1968.

[63] A. Korpel, "Spatial imaging of sound field by Bragg diffraction of light," Int'l J Nondestructive Testing 1, pp. 337, 1970.

[64] A. Korpel, "Astihmatic Imaging properties of Bragg diffraction," J. Acoust. Soc. Amer., pp. 1059-1061, 1971.

[65] C. S. Tsai and H. V. Hance, "Optical Imaging of the cross section of a Microwave Acoustic Beam in Rutile by Bragg diffraction of a laser Beam," J. Acoustic. Soc. Amer. Vol. 41, pp. 1345-1347. 1967.

[66] C. S. Tsai and H. V. Hance, "Experimental Investigation of the resolution capability of microwave ultrasonic beam visualization Technique using Bragg diffraction of a laser beam," J. Acoust. Soc. Amer. Vol. 48, pp. 1110-1118, 1970.

[67] H. V. Hance, J. K. Parks, and C. S. Tsai, "Optical imaging of complex ultrasonic field by diffraction of laser beam," J. Appl. Phys., pp. 1981-1984, 1967.

[68] G. Wade, C. J. Landry, and A. A, Desouza, "Acoustical transparencies for optical imaging and ultrasonic diffraction," Acoustical Holography, Vol. 1, Plenum, New York, pp. 159-172, 1969.

[69] R. A. Smith, G. Wade, J. Pevers, and J. Landry, "Studies of resolution in a Bragg imaging system," J. Acoust. Soc. Amer., Vol. 49, pp. 1062-1068, 1971.

[70] L. W. Kessler, "A pulsed Bragg diffraction method of ultrasonic visualization," IEEE Trans. Sonics and Ultra., su-19, pp.425-427, Oct 1972.

[71] F.E. Nixon, "Handbook of Laplace Transformation, Fundamentals, Applications, Tables, Examples, " Prentice-Hall, 1965.